This is to certify that the

dissertation entitled

Three Dimensional Dynamic Analysis of the Human Hand for Predicting Tendon, Ligament and Nerve Wear in the Carpal Tunnel During Typing

presented by

Wendy Sue Reffeor

has been accepted towards fulfillment
of the requirements for

Doctoral degree in Philosophy

Major professor

Date 6/27/01

Three Dimensional Dynamic Analysis of the Human Hand for Predicting Tendon, Ligament and Nerve Wear in the Carpal Tunnel During Typing

By

Wendy Sue Reffeor

AN ABSTRACT OF A DISSERTATION

Submitted to
Michigan State University
in partial fulfillment of the requirements
for the degree of

DOCTOR OF PHILOSOPHY

Materials Science and Mechanics

2001

Professor Robert W. Soutas-Little

ABSTRACT

Three Dimensional Dynamic Analysis of the Human Hand for Predicting Tendon, Ligament and Nerve Wear in the Carpal Tunnel During Typing

By

Wendy Sue Reffeor

The hand is one of the most complex parts of the human body. The hands contain forty percent of the bones and fifty percent of the muscles in the human body. In addition, the opposable thumb is one of two features that separates primates from other animals.

This study develops a three dimensional, dynamic mathematical model that may be used to predict the relative tendency of an activity to cause carpal tunnel syndrome. The model can be used to calculate both the forces in and the motion of the tendons in the hand. The forces and the deflections of the tendons are combined to determine a measure of the energy lost in the carpal tunnel because of the friction between the tendons and the tunnel itself.

An analysis is performed on the index finger for the typing of one sentence. The purpose of this analysis is to

determine if the model provides valid results. In addition, in providing this analysis, the accuracy of the measuring system is determined and shown to be adequate for measuring the motion and forces on the hand.

Char

Kehc

work

DEDICATION

I dedicate this manuscript to my family: Bruce and Charlotte Reffeor and Cindy, Patrick, Stephanie and Annette Kehoe. Without their constant and unfailing support, this work would not have been possible.

thro

Sout

enco

degr

focu

know

woul

sect

Dr.

time

stud

with

compl

ACKNOWLEDGEMENTS

I take this opportunity to thank those who helped me through this project.

First and foremost, I'd like to thank Dr. Robert Soutas-Little. Thank you for your constant support and encouragement. You not only helped me to finish this degree, but also helped with my teaching and kept me focused on what is important. Thank you for sharing your knowledge and more importantly, your wisdom.

Without Patricia Soutas-Little and Claudia Angeli, I would have been unable to complete the experimental sections of this work. Thank you both.

To my committee--Dr. Gary Cloud, Dr. Melissa Crimp, Dr. Thomas Pence, and Dr. Vorro—thank you for all of your time and assistance.

I'd also like to thank all of my fellow graduate students and colleagues at Grand Valley State University, without whose support I would not have been able to complete this work.

To the ladies in the department office, JoAnn Peterson, Iris Taylor, Lorna Coulter, and Debbie Conway, your help is priceless. You are very appreciated and make it possible for everyone in the department to succeed.

TABLE OF FIGURES

TABLE OF TABLES

LIST OF ABBREVIATIONS

ADD	Adductor Pollicis
APB	Abductor Pollicis Brevis
APL	Abductor Pollicis Longus
CMC	Carpometacarpal
CTS	Carpal Tunnel Syndrome
DIP	Distal Interphalangeal
EDC	Extensor Digitorum Communis
EMG	Electromyographic
EMI	Electromagnetic Imaging
EPB	Extensor Pollicis Brevis
EPL	Extensor Pollicis Longus
ES	Extensor Slip
FP	Flexor Digitorum Profundus
FPB	Flexor Pollicis Brevis
FPL	Flexor Pollicis Longus
FS	Flexor Digitorum Superficialis
IO	Interosseous
IP	Interphalangeal
LE	Long Extensor
LU	Lumbrical
MCP	Metacarpophalangeal
OPP	Oppponens Pollicis
PCSA	Physiological Cross Sectional Area
PIP	Proximal Interphalangeal
RB	Radial Band of Extensor
RI	Radial Interosseous
TE	Terminal Extensor
UB	Ulnar Band of Extensor
UI	Ulnar Interosseous

For cen

the human ha

mechanisms kn

is one of the

remainder of

of nineteen b

large number

serve redunda

function of s

allows humans

motions that r

caps to crushi

ripeness of a

Within the

variations. H

over (fibers of

different muscl

Leijnse et al.,

from one tendon

addition to the

CHAPTER 1–INTRODUCTION

For centuries, scientists and physicians have studied the human hand, one of the most complex biological mechanisms known. Scientists believe that hand development is one of the factors that helped humans develop beyond the remainder of the animal kingdom. The human hand consists of nineteen bones and forty-six muscles in addition to a large number of ligaments. Many of the muscles in the hand serve redundant functions and physicians still debate the function of some of the muscles. This complexity is what allows humans to utilize the opposable thumb and to control motions that range from grasping and turning pill bottle caps to crushing small objects to gently testing the ripeness of a fruit.

Within the range of normal human hands, there are many variations. Humans have different degrees of muscle cross-over (fibers of one muscle inserting into the tendon for a different muscle) (Leijnse, 1997b; Leijnse et al., 1992; Leijnse et al., 1993) and tendon junctions (tendon fibers from one tendon crossing over into another tendon) in addition to the anatomical variations required by size and shape diffe

increases th

human hand f

Abnorma

challenges t

diseases com

arthritis and

focuses on CT

CTS cost

dollars annua

qualitatively

CTS (Billi, C

Serina, & Re

France, 1994

However, compa

that potentia

Cobb, An, Co

Keir, Bach,

and actually

CTS (Armstro

Moore, Wells,

Ayland, 1997a

women than me

tasks such as

shape differences among people. Each of these variations increases the difficulty of modeling and understanding human hand function.

Abnormal or diseased hands present even greater challenges to the understanding of hand function. Hand diseases commonly studied include rheumatoid and osteo-arthritis and carpal tunnel syndrome (CTS). This study focuses on CTS.

CTS costs corporations and individuals millions of dollars annually and much work has been done to qualitatively assess the potential of an activity to cause CTS (Billi, Catalucci, Barile, & Masciocchi, 1998; Smutz, Serina, & Rempel, 1994a; Smutz, Miller, Eaton, Bloswick, & France, 1994b; Sommerich, Marras, & Parnianpour, 1998). However,comparatively little work has been done to assess that potential mathematically (Bay, Sharkey, & Szabo, 1997; Cobb, An, Cooney, & Berger, 1994; Cobb, Cooney, & An, 1996; Keir, Bach, & Rempel, 1998a; Keir, Bach, & Rempel, 1998b) and actually predict the potential of an activity to cause CTS (Armstrong & Chaffin, 1979; Miller & Freivalds, 1995; Moore, Wells, & Ranney, 1991; Werner, Armstrong, Bir, & Ayland, 1997a). The disease occurs more frequently in women than men and is generally associated with repetitive tasks such as typing. Although the disease affects only one tenth of

affect as ma

in repetitiv

CTS is

carpal tunne

increased pre

Keir et al.,

Owens, 1995)

et al., 1997;

Mackinnon, 19

frictional co

can cause the

on the media

al., 1994b).

done by Arms

Chaffin, 197

Tachibana, 1

This st

CTS based up

Although oth

for the hand

in the carpa

into a singl

task to caus

one tenth of a percent of the entire population, it may affect as many as fifteen percent of those people involved in repetitive tasks and manual labor.

CTS is caused by irritation of the median nerve in the carpal tunnel. This irritation is believed to result from increased pressure in the carpal tunnel (Cobb et al., 1994; Keir et al., 1998a; Keir et al., 1998b; Seradge, Jia, & Owens, 1995) or from direct wear on the median nerve (Bay et al., 1997; Nakamichi & Tachibana, 1995; Novak & Mackinnon, 1998). Wear on the flexor tendons due to frictional contact with the carpal tunnel and each other can cause these tendons to swell and increase the pressure on the median nerve (Miller & Freivalds, 1995; Smutz et al., 1994b). This study combines the two theories as was done by Armstrong, Miller and Nakamichi (Armstrong & Chaffin, 1979; Miller & Freivalds, 1995; Nakamichi & Tachibana, 1995).

This study develops the first ever model to predict CTS based upon the input forces and the motion of the hand. Although other studies have provided equations of motion for the hand and models for determining the friction force in the carpal tunnel, none have combined the information into a single model capable of predicting the tendency of a task to cause CTS. In addition, none have analyzed the motion of t

the inertial

done to ver

trends to ca

situation.

Althoug

focused on t

abnormalities

1954; Chao &

Little, 1969;

Rutledge, 197

1949; Landsme

Lin, Amadio,

Schwarz, 1955

attempts to m

predict its b

prosthetics a

An, Chao, Coo

Kawai, & Chao

Berglund, Uch

Linscheid, 19

Brook, Mizrah

Armstrong, 19

Meyers, & Hol

motion of the hand using infrared camera systems or studied the inertial effects on the motion. Further work must be done to verify that the model indeed agrees with known trends to cause CTS and that it can be used in a clinical situation.

Although many of the earlier studies of the hand focused on the anatomical construction of the hand and abnormalities thereof (Backhouse, 1968; Backhouse & Catton, 1954; Chao & Cooney, 1977; Close & Kidd, 1969; Eaton & Little, 1969; Eyler & Markee, 1954; Fischer, 1969; Harris & Rutledge, 1972; Kaplan, 1965; Kaplan, 1966; Landsmeer, 1949; Landsmeer, 1955; Landsmeer, 1961; Landsmeer, 1976; Lin, Amadio, An, & Cooney, 1989; Stack, 1962; Taylor & Schwarz, 1955; Tully, 1995), recent studies have included attempts to model the hand mathematically in order to predict its behavior and assist in the development of prosthetics and muscle relocation surgeries (Amis, 1987; An, Chao, Cooney, & Linscheid, 1979; An, Himeno, Tsumura, Kawai, & Chao, 1990; An, Kwak, Chao, & Morrey, 1984; An, Berglund, Uchiyama, & Coert, 1993; An, Chao, Cooney, & Linscheid, 1985; Armstrong, 1982; Boozer et al., 1994; Brook, Mizrahi, Shoham, & Dayan, 1995; Buchholz & Armstrong, 1991; Buchholz & Armstrong, 1992; Buford, Meyers, & Hollister, 1990; Chao, 1980; Chao & An, 1978a;

Chao, Opgra

Cooney, 197

Daube, & As

Brand, 1981

Masset, & Ma

Mass, 1994;

Landsmeer, 1

1997b; Leijn

Kalker, 1995

Hoger, 1978,

Spoor & Lan

Giurintano,

Berglund, A

Many o

have focuse

muscles (Ba

et al., 1994

1994; Harris

Duffy, 1992;

al., 1989; M

Spoor, 1983;

1968; Thomps

& Sharkey, 1

et al., 1979;

Chao, Opgrande, & Axmear, 1976; Chao & An, 1978b; Chao & Cooney, 1977; Chevallier & Payandeh, 1998; Cooney, An, Daube, & Askew, 1985; Cooney & Chao, 1977; Crowninshield & Brand, 1981; Dennerlein, Diao, Mote, & Rempel, 1998; Duque, Masset, & Malchaire, 1995; Greenwald, Shumway, Allan, & Mass, 1994; Hazelton, Smidt, Flatt, & Stephens, 1975; Landsmeer, 1962; Leijnse, 1996; Leijnse, 1997a; Leijnse, 1997b; Leijnse, 1997c; Leijnse et al., 1992; Leijnse & Kalker, 1995; Leijnse et al., 1993; Micks, Reswick, & Hoger, 1978; Small, Bryant, & Pichora, 1992; Spoor, 1983; Spoor & Landsmeer, 1976; Tamai et al., 1988; Thompson & Giurintano, 1989; Toft & Berme, 1980; Uchiyama, Coert, Berglund, Amadio, & An, 1995).

Many of the mathematical studies of the human hand have focused on the function and uniqueness of individual muscles (Backhouse & Catton, 1954; Close & Kidd, 1969; Cobb et al., 1994; Dennerlein et al., 1998; Greenwald et al., 1994; Harris & Rutledge, 1972; Kerr, Griffis, Sanger, & Duffy, 1992; Leijnse, 1997c; Leijnse & Kalker, 1995; Lin et al., 1989; Micks et al., 1978; Shewsbury & Kuczynski, 1974; Spoor, 1983; Srinivasan, 1976; Thomas, Long, & Landsmeer, 1968; Thompson & Giurintano, 1989; Zissimos, Szabo, Yinger, & Sharkey, 1994) and the static functions of the hand (An et al., 1979; An et al., 1984; An et al., 1985; Armstrong, 1982; Buchh

1985; Chao,

Close & Kid

Miller, Dum

Leijnse, 199

al., 1992; L

Micks et al.,

1983; Spoor

the knowledg

dynamic moti

Buchner, Hin

which is nec

activity to

In orde

typing, a th

hand is form

model include

link, six deg

kinematic and

modeled as a w

limit the size

Although much

the incorporati

a dynamic syste

1982; Buchholz & Armstrong, 1992; Buchner, Hines, & Hemami, 1985; Chao, 1989; Chao et al., 1976; Chao & An, 1978b; Close & Kidd, 1969; Cooney & Chao, 1977; Hirsch, Page, Miller, Dumbleton, & Miller, 1974; Keir et al., 1998b; Leijnse, 1996; Leijnse, 1997a; Leijnse, 1997b; Leijnse et al., 1992; Leijnse & Kalker, 1995; Leijnse et al., 1993; Micks et al., 1978; Shewsbury & Kuczynski, 1974; Spoor, 1983; Spoor & Landsmeer, 1976). These works have led to the knowledge base necessary to facilitate the study of the dynamic motion of the human hand (Brook et al., 1995; Buchner, Hines, & Hooshang, 1988; Esteki & Mansour, 1997) which is necessary in order to predict the tendency of an activity to cause CTS.

In order to better understand the link between CTS and typing, a three-dimensional, dynamic model of the human hand is formulated. The theoretical development of this model includes all four fingers and the thumb as three link, six degrees of freedom bodies and includes both kinematic and kinetic analyses. Although the hand could be modeled as a whole, each finger is modeled independently to limit the size of the system of equations being solved. Although much of this modeling is based upon earlier works, the incorporations of all fingers and the thumb, the use of a dynamic system accounting for the accelerations of the fo

mo

th

ou

se

are

thro

liga

the

tendo

energy

fingers and the three-dimensional model are formulated in this work.

The fingers of the hand act essentially independently because each has its own dedicated muscles. Since the system of equations created by the model is inherently underdetermined (muscle function in the hand is redundant), both muscle grouping and system optimization will be used to reduce the degrees of freedom in the system. Here, the initial optimization criterion utilized is taken from earlier work, however, the secondary criterion and the optimization algorithm used are new. In addition, no previous model has been formulated which includes both the forces and excursions simultaneously. Outputs from the model include the muscle forces and tendon excursions for the entire course of the motion being observed. These outputs are calculated in a piecewise manner with each data set being analyzed independently.

The forces and excursions determined using the model are used to determine the energy lost in the carpal tunnel through the tendons rubbing on the transverse carpal ligament and the carpal bones that form the tunnel. Both the means of calculating the friction force between the tendons and the carpal tunnel and the definition of the energy criterion are defined in this work. Energy lost will be calculated as the work required to move the tendons over the tunnel assuming that the coefficient of kinetic friction is as demonstrated in the literature (Linn, 1968), (Shih, Ju, Rowlands, An, & Chao, 1993), (Armstrong & Chaffin, 1979).

One trial was conducted to collect experimental data to validate the model. This trial consisted of a single activity conducted a single time. These data in no way can be used to draw conclusions about the tendency of typing to cause CTS and was collected solely for the purpose of model validation. However, the method of collecting the data was never used previously. Motion analysis systems based upon infrared light such as the BTS system used in this work have not been applied to measuring the motion of small body segments such as the finger.

Although the model was formulated for the entire hand and data were collected for the entire hand during one trial of the experimental procedure, only the index finger was analyzed. This analysis is representative of that which can be done for the other fingers and the entire hand. When used in a clinical setting, the procedures developed to implement the model can be followed to draw conclusions about hand function and causes of CTS.

I

the re

total

that f

activ

devel

the d

accur

segme

reso

the

to d

the

to th

is to

In the future, this model can be utilized to determine the relative tendency of two activities to cause CTS. The total energy generated by an activity can be compared to that from other activities (or positions during an activity) to conclude which is more likely to cause CTS.

In the course of analyzing the data from the trial and developing the data collection techniques used to gather the data, additional studies were done to determine the accuracy of the rigid body assumption for the finger segments, the ability of the BTS motion analysis system to resolve 3 mm markers, and the resolution and linearity of the keyboard force transducers. In addition, work was done to determine the necessity of including inertial terms in the equations of motion. Note that this work applies only to the typing task and should be reevaluated if this model is to be used to analyze other tasks.

T

been s

for m

the f

devel

of Ha

the

of t

move

the

effe

expe

physi

physi

of ea

the st

contri

of eac

CHAPTER 2–LITERATURE REVIEW

The human hand is a very complex mechanism which has been studied by physicians, biomechanists and ergonomists for most of this century. Physicians are still debating the functions of some of the muscles in the hand and have developed entire journals (Journal of Hand Surgery, Journal of Hand Therapy and The Hand to name a few) to the study of the hand. Biomechanists are developing mathematical models of the hand in order to better understand and describe its movement and functionality, and ergonomists are studying the effect of workplace habits on the function of the hand.

In order to form a model of the hand to study the effects of typing on the tendons in the carpal tunnel, expertise must be drawn from the fields of anatomy, physiology, biomechanics and ergonomics. Anatomy and physiology yield the details of the functions and locations of each of the muscles and ligaments in the hand as well as the structure of the carpal tunnel. Biomechanics contributes a means of modeling the origins and insertions of each of the muscles as well as modeling the structure of th

as

ma

op

ha

in

co

th

gi

Fig
of

the fingers and the hand. It also contributes information as to the function of the hand as understood from mathematical models. The proper application of optimization theory to biological systems. Ergonomicists have studied the effects of carpal tunnel syndrome on individuals and populations. Each of these fields has contributed considerable knowledge to the current study of the hand.

For clarity, diagrams of the muscles of the hand are given in Figure 3-5.

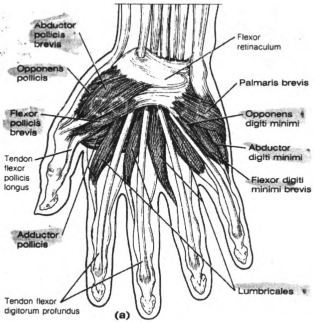

Figure 1--Palmer View of the Superficial Intrinsic Muscles of the Hand. Taken From Spence(Spence, 1990), pg. 223.

Flexor
carpi u

Extens
carpi u

Tendons
extensor
radialis b
and longu

Figure
Poster
Right
Taken
1990),

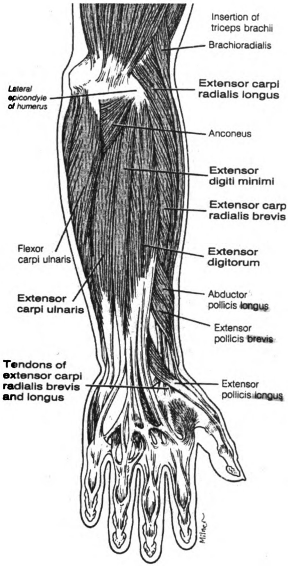

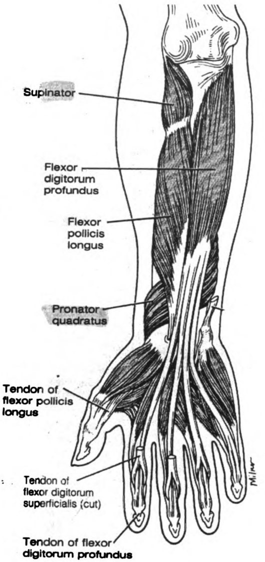

Figure 2--Superficial Posterior Muscles of the Right Forearm and Hand. Taken From Spence(Spence, 1990), pg. 220.

Figure 3--Deep Anterior Muscles of the Right Forearm. Taken From Spence(Spence, 1990), pg. 220.

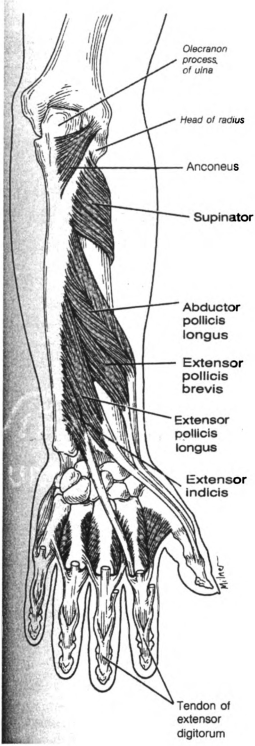

Figure 4--Deep Posterior Muscles of the Right Forearm and Hand. Taken From Spence(Spence, 1990), pg. 223.

Fig
Har

thi

BIO

mode

Kine

rece

func

join

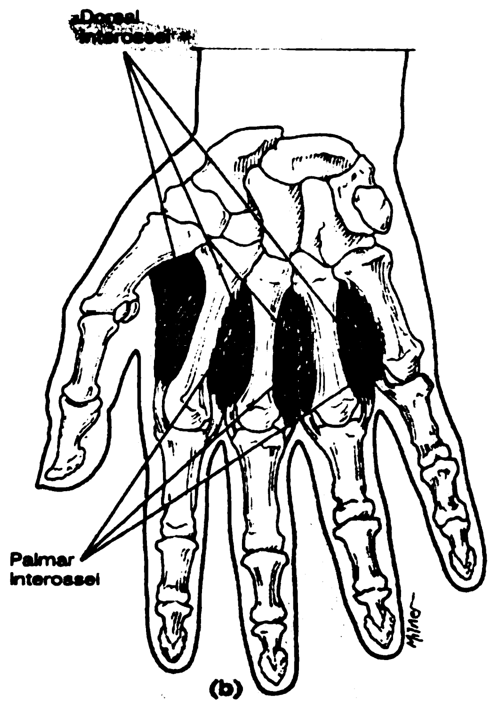

Figure 5-- Palmer View of the Interossei Muscles of the Hand. Taken From Spence(Spence, 1990), pg. 223.

As this study focuses on the biomechanics of the hand, this field will be reviewed first.

BIOMECHANICAL CONTRIBUTIONS TO THE STUDY OF HAND FUNCTION

Biomechanists have developed two forms of mathematical models to explain the function of the human hand. Kinematic modeling has been used to determine the muscles necessary to maintain balanced motion, to understand muscle function and to depict anatomical relationships between the joints. Kinetic modeling has been used to determine the

forces in each of the muscles during particular motions, the reactions at the joints, and the muscles active during certain activities.

Kinematic Modeling

Kinematic modeling has been used extensively to enhance the understanding of the function of the human hand. Kinematic models have been used to develop relationships between the motion of the proximal interphalangeal (PIP) and distal interphalangeal (DIP) joints, to determine the limits on motion of the finger, to describe the redundancy of the muscles in the hand, and to describe the function of the lumbricales muscle.

Since the motion of the PIP and DIP joints are coupled in most people, a relationship that allows the two joints to be modeled as a single joint was developed by Spoor and Landsmer in 1976 (Spoor & Landsmeer, 1976) as a portion of the study by the authors of the zig-zag motion of the finger. The zig-zag motion is described as the motion that allows the metacarpophalangeal joint to be extended while the interphalangeal joints are flexed. The authors showed that the zig-zag motion could be predicted using either kinematic or kinetic models and that the two models provide comparable results.

det
fin
the
et a
lum
tem
supe
inte
ban
con
tem
for
pos
con
gen
The
exc
exc
FS,
In
alt
inde

Leijnse and his associates used a kinematic model to determine the limits on the possible lifting motions of the finger (Leijnse et al., 1992), to determine the coupling of the motions of multiple fingers on the same hand (Leijnse et al., 1993), and to describe the function of the lumbricales muscle (Leijnse & Kalker, 1995). From a six tendon--flexor digitorum profundus (FP), flexor digitorum superficialis (FS), extensor digitorum communis (EDC), interosseus (IO), radial band of extensor (RB), and ulnar band of extensor (UB)--model in which slack variables (a constant--zero if the tendon is taut and positive if the tendon is slack--subtracted from the displacement equation for the tendon) were used to describe the inactive tendon positions, Leijnse (Leijnse et al., 1992) drew multiple conclusions about the possible constraints on the muscles generating the lifting motion of a single human finger. The following constraint combinations were allowed: 1) zero excursion of the ED, active FS, inactive FP, 2) zero excursion EDC, active FP, inactive FS, 3) zero excursion FS, FP active, 4) zero excursion FP, 5) zero excursion IO. In this paper, Leijnse and his associates showed that although many of the muscles of the fingers are coupled, independent motion of the fingers can be achieved through a limit

muscl

in tw

the

of t

Leij

show

inex

rela

the

that

bon

(FF

(ED

(LJ

Kal

of

FF

on

to

se

wh

limited range of motion due to the redundancy of the finger muscle system.

The motion of the fingers on a given hand are coupled in two ways—muscle fiber cross-over and interconnections of the tendons. The coupling effects of the interconnections of tendons upon the fingers of the hand were studied by Leijnse in 1993 (Leijnse et al., 1993). The model created showed the interconnections as two dimensional, inextensible cords. These interconnections limit the relative motion between two fingers because of coupling of the two motions.

The lumbrical muscle is different from most muscles in that it both originates and inserts at tendons rather than bones. Its origin is on the flexor digitorum profundus (FP) and its insertion is on extensor digitorum communis (EDC). In order to study the function of the lumbricales (LU) muscle in the hand, Leijnse and Kalker, (Leijnse & Kalker, 1995) created a five tendon, two dimensional model of the finger. Since the lumbrical muscle originates on the FP, the FP is taken as being in two segments in the model; one proximal to the origin of the lumbrical and one distal to the origin. The proximal segment is modeled as being in series with both the distal segment and the lumbricals which are in turn parallel with each other. Since the FP

is inserted on the anterior side of the hand and the LU is inserted on the posterior side, the FP and the LU work against each other when both are active and create a "locking" of the DIP and the PIP. This "locking" allows these joints to be controlled by the LU and the FP independently of the position of the MCP joint. When the LU is slack and the distal FP is taut, the FP acts to flex the DIP-PIP. When the LU is taut and the distal segment of the FP is slack, the FP acts to extend the DIP-PIP.

From these three two dimensional models, Leijnse and his associates were able to explain many functions of the human hand. They were able to show which motions are possible given certain muscular constraints, describe the coupling of finger motions and develop a greater understanding of the function of the lumbricales muscle. Further, Spoor and Landsmeer developed a model, that helped describe the coupling of the PIP and DIP joints, of the zig-zag condition of the finger using only kinematic inputs.

Kinetic Models

Although some work has been done on developing purely kinematic models of the hand, most work includes both kinematic constraints and an analysis of the forces

[illegible]

involved in the motion. These models are referred to as kinetic models. Kinetic models can be broken into two catagories, static or quasi-static and dynamic.

Static models refer to those in which there is no motion. Examples are pinching a key or grasping an object. Since many of the tasks done by the hand is, in fact, static, many people have studied static models of the hand. Quasi-static models analyze dynamic motions by looking at them in a piecewise manner. Quasi-static models do not take into account the inertial effects of the mass of the bodies involved, but do not take into account the speed of the muscle contraction. Since muscle behavior is rate dependent, this is a significant distinction.

Dynamic models take into account the inertial effects of the bodies involved and the speed of the muscles. These models are the most complete models used to analyze motion, however, they are also very complex and are, therefore, seldom used.

Static and quasi-static models

Since many of the actions performed by the hand are related to gripping or grasping an object, and so are static functions, models which describe the static fun

in

1965

orde

This

pass

used

The c

base

exten

and i

muscl

with

exten

Hirsc

simpl

a met

to re

elect

inact

intere

conclu

functions of the hand give insight into the forces involved in many of the normal daily functions of the hand.

In 1968, Thomas and his associates (Thomas et al., 1968) performed a static analysis of the human finger in order to study the contribution of the lumbrical muscle. This model included both the active (contraction) and passive (elastic response) contributions of the muscles and used both kinetic and kinematic analysis of the system. The conclusion reached was that the equivalent IP segment (based on coupling of the PIP and DIP joints) cannot be extended without the presence of the intrinsics (lumbrical and interosseus muscles). Specifically, the lumbrical muscle allows the extension of the IP joint to be performed with lower all-around force in the muscles than if the extension were to be performed by the interosseus alone.

Two more models were proposed between 1968 and 1976. Hirsch and his associates (Hirsch et al., 1974) proposed a simple static model of the thumb to evaluate the forces in a metacarpophalangeal (MCP) joint of the thumb. In order to reduce the underdetermined system of equations, electromyographical (EMG) data were used to eliminate inactive muscles during the particular activities of interest ("wine jug" or open and "key" or flat pinch). The conclusion reached was that the maximum reaction force at the MCP joint of the thumb during the two described activities was ten times the load applied at the tip of the thumb. Spoor and Landsmeer (Spoor & Landsmeer, 1976) described the zig-zag motion of the MCP joint using a static kinetic model as well as the kinematic model described earlier. They found that the results of the kinetic model compared well with those of the kinematic model.

The first substantial three-dimensional work was performed by a group of researchers, lead by Edmond Chao, at the Mayo Clinic in the mid to late 1970s and into the 1980s. Although this work was for static analysis of the hand, it is the groundbreaking work in the field of biomechanics of the hand. In 1976, a three dimensional static analysis of the kinetics of the hand in four actions—tip pinch, lateral pinch, ulnar pinch and grasp—was performed (Chao et al., 1976). The model was formulated using two coordinate systems per joint and allowing the positions of the tendons to be accurately represented without having to account for the joint angle. Euler angles were used to define the position of the joint in all positions. The first rotation, ϕ (representing flexion/extension), was performed about the fixed (more proximal of two bodies being considered) Z-axis; the second rotation, θ (representing abduction/adduction), about the line of nodes which corresponds to a y-axis and the final rotation, ψ (representing axial rotation), was about the moving (more distal of two bodies being considered) x-axis. The model assumed that the distance between the two coordinate systems defining a joint was fixed. A direct consequence of this assumption is that there can be no translations at the joint. The statically indeterminate system was reduced by systematically eliminating four of the nine unknowns in the equations. The system was solved using each of the 126 possible combinations of active and inactive forces, and inadmissible solutions were eliminated. Solutions were considered inadmissible if any of the tendons was carrying a compressive load, any of the joint reaction forces was tensile, any of the results were unreasonably high, or the extensors exceed the limit for being defined as passive elements. All of these conditions would violate the basic assumptions of the model. The conclusions drawn in the study were: 1) in pinch, the tendons have force magnitudes that obey the following FP>FS>RI and UI>LU; 2) in grasp, the intrinsic muscles are responsible for a greater load than the flexors; 3) the extensors are passive during grasp and active during pinch; 4) pinch creates higher contact and forces which cause hypere

functi

higher

radia

joint

Chao,

give

publ

ana

act

use

max

ima

ele

all

spe

ter

of

dete

inva

prom

tomo

hyperextension at the DIP and PIP than does the grasp function; 5) the normal contact force at the MCP joint is higher in grasp than in any other hand function; and 6) radial deviation and axial twisting are greatest at the MCP joint in all actions studied. In a later work, (Cooney & Chao, 1977) the quantitative results of the model above are given.

In 1978, An and his associates (including Chao) published a paper that reported the results of a detailed anatomical study to determine the locations and lines of actions of the finger and thumb tendons in the hand. They used various techniques including X-ray analysis of metal markers placed in the tendons (invasive) , ultrasonic imaging, tomographic xerography technique and electromagnetic imaging (EMI) body scanner (last three are all non-invasive). Based upon results from ten cadaveric specimens, they established the unit vectors for all of the tendons in the hand and the normalized locations for each of the tendons at each joint. These locations were all determined using the X-ray images. Of the three non-invasive techniques used, the only one that showed any promise was the EMI body scanner which utilizes computer tomography.

In 1977, Berme and his associates (Berme, Paul, & Purves, 1977) studied the effects of the ligamentous structures of the MCP joint. This study showed that during tap turning and pinching, the ligaments do carry a load. In general, this load is described by the moments at the joints and is not explicitly assigned to ligaments.

Toft and Berme (Toft & Berme, 1980) developed a three-dimensional model of the thumb. This model included the ligamentous structures and predicted the forces in the ligaments, tendons and joints for squeeze and squeeze and pinch activities. Two conclusions can be drawn from the data presented: 1) the collateral ligaments at the IP joint of the thumb do not carry load during the activities observed, however, the collateral ligaments at the MCP joint do carry a significant load; 2) the minimum reaction forces at the IP joint were approximately two times the applied force and at the MCP joint were three times the applied force. However, these results did not include the effects of antagonistic muscles which would act to increase the joint reactions.

In 1988, Buchner and his associates (Buchner et al., 1988) developed a model of the human hand that included inertial effects due to the motion of the body segments. This model introduced a method for determining the tendon di

we

ba

re

of

wo

ex

re

di

mo

in

co

ef

th

eq

mo

Th

li

yi

me

asp

displacement based upon joint angles. In addition, a weighting factor was introduced to the lateral and central bands of the extensor in order to explain variations in the relative positions of the PIP and DIP joints. The results of the model are smooth force and displacement curves which would be expected in a normal hand.

In 1995, Brook and his associates (Brook et al., 1995) expanded upon the work of Buchner and developed a relationship between angular position of the joints and the displacement of the tendons. In addition, in their modeling, they modified the constraint relationships on the intrinsic muscles and the portions of the extensor communis. This expansion of the constraints allowed the effect of the uneven approach of the two lateral bands of the extensor communis to be accounted for in the model.

An innovative approach to determine the equilibrium equations was proposed in 1979 by Storace and Wolf. The model developed was based on the principle of virtual work. This is the only example of such a development in the literature for modeling of the human hand. This model yielded the equilibrium equations in a simple, easy to use method.

Other models have been developed to study various aspects of the hand. In 1995, Giurintano and his assoc

Myers

both

two

mode

hing

rota

of

of

nor

de

mo

At

Fig

the o

the o

they d

it yiel

associates (Giurintano, Hollister, Buford, Thompson, & Myers, 1995) modeled the thumb as a five-link chain. Since both the carpal joint and the MCP joint in the thumb have two non-perpendicular non-concurrent axes, the authors modeled the joints as links connected at each end by a hinge joint rather than point contact joints. The axes of rotation for these hinges are not perpendicular to the axis of the thumb. See Figure 6 for an illustration of the use of the intermediate link. Therefore, this model featured non-orthogonal coordinate systems (Euler angles) to describe the rotations and translations of the links. The model agreed very well with experimental results.

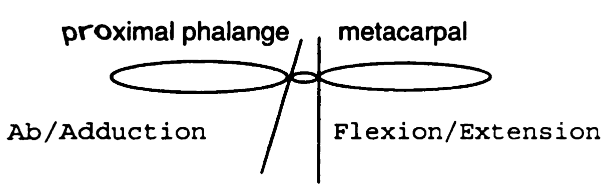

Figure 6—Joint Modeling Using Intermediate Link

Seirig and Arvikar (Seirig & Arvikar, 1989) presented the only full hand model found in the literature. All of the other models modeled one finger at a time. Although they did not give any details on how the model was formed, it yielded results for each of the muscles and each of the

joint
paper
relat
the w

kine
(Lei
cont
thi
add
par

th
tr
co
coa
ten
conc
tend
Leijn
types
the mod
and har
experim

joints in the hand for pulling and pinch activities. Their paper also included locations of the tendons and ligaments relative to the joint centers and a description of each of the muscles of the hand and their functions.

Leijnse published four papers describing different kinetic models of the human hand. In 1996, Leijnse (Leijnse, 1996) proved that a bi-articular chain cannot be controlled by two parallel antagonistic muscles. Thus, a third muscle is required to control the chain. In addition, if the lines of action of the two muscles are not parallel, the chain cannot be held in equilibrium.

In a later paper, Leijnse (Leijnse, 1997b) described the effect of intertendinous force transfers. These force transfers are the result of two anatomical constructs—coactivation and tendon cross-overs. In the case of muscle coactivation, fibers from one muscle body insert into the tendon of another muscle body, thereby causing some concurrent activation. The second, cross-overs in the tendons themselves is referred to as passive connection. Leijnse presented a detailed model which includes both types of interconnection. He then experimentally verified the model by eliminating the cross-overs in both the model and hand and showed that the model described the experimental results very well. This model is twodime

inex

199

lum

act

Fin

sho

ana

th

e

d

de

fo

of

the

(pin

paper

devel

conclu

dimensional and assumes that the cross-overs are inextensible and one dimensional (of zero length).

In the third paper in the series, Leijnse (Leijnse, 1997a) showed through a simple kinetic model that the lumbrical is never the limiting muscle in unloaded activities and thus is correctly sized anatomically. Finally, in the fourth paper, Leijnse (Leijnse, 1997c) showed that the flexor profundus is better positioned anatomically than the flexor superficialis for control of the biarticular finger.

Dynamic Modeling

Dynamic modeling includes the effects of the rate of extension on the muscles. There is only one example of dynamic modeling in the literature.

In 1997, Esteki and Mansour (Esteki & Mansour, 1997) developed a dynamic model of the human hand that included force-velocity and length-tension parameters in the muscles of the hand. Although the muscle parameters were dynamic, the model was used to study inherently static conditions (pinch and grasp). From the information given in the aper, it is very difficult to determine how the model was eveloped and therefore, difficult to understand the nclusions drawn.

the

driv

have

lumb

inte

func

the

CON

da

as

i

c

d

tw

pl

fi

both

the

the v

data

Kinetic models have led to a greater understanding of the functions of the human hand and the muscle forces which drive the hand in order to perform various functions. They have been used to better understand the function of the lumbrical muscle, the reaction forces in the MCP joint, the internal muscle forces in pinch, grasp and squeeze functions, the forces in the ligaments of the fingers, and the effects of interconnections between the tendons.

COLLECTION OF POSITION DATA

Until recently, no one has actually collected position data on moving fingers. In December, 1999, Rash and his associates (Rash, Belliappa, Wachowiak, Somia, & Gupta, 1999) published a paper in which they describe a study comparing motion data collected using a three camera, three dimensional video motion analysis to data collected using two dimensional lateral view fluoroscopy. Markers were placed on each of the joints of the index finger and the finger was flexed and extended while recording data with both systems simultaneously. The researchers found that the two systems agreed well and therefore concluded that the video motion analysis systems are capable of collecting data for motion of the fingers.

OPTIMIZATION OF BIOLOGICAL SYSTEMS

As in all biological systems, the human hand is a redundant system. This redundancy allows the hand to continue to function in case of injury and also allows for the hand to perform high force, low frequency tasks such as grasping an object as well as low force, high frequency tasks such as typing. For the investigator, this redundancy presents a problem. The redundant systems cause the system of equations formed when modeling the hand to be underdetermined. Thus, in order to solve the system of equations some form of system reduction must be used.

There are many methods found in the literature to reduce the underdetermined system of equations created when modeling biological systems. Most of these methods use some physiological reasoning to justify the reduction.

Physiological reduction is the result of reasoning based upon the function of the body. In each method, sound reasoning is used to develop the optimization criteria, however, because of the difficulty in performing in vivo testing, little direct experimental evidence has been found to support one line of physiological reasoning over another. However, there are facts about the hand which lead to criteria for evaluating the various optimization methods. For example, it is known that antagonistic muscles act during most motions of the hand. These antagonistic muscles allow the hand to move in a variety of ways as well as lending stability to the joint. Another criterion for judging the validity of a given optimization criteria is the smoothness of the force-time curves. It is unlikely that the normal hand or any other biological system has discontinuous force-time curves during any activity.

Of the criteria which have been proposed in the literature, some are linear and others are nonlinear. The linear criteria all favor the muscle with the largest moment arm (Tsirakos, Baltzopoulos, & Bartlett, 1997). Some of the criteria will allow this muscle to be loaded up to a predetermined limit, at which time the other muscles are required to take the remainder of the load. In addition, linear criteria do not ever predict antagonistic muscle activity and thus do not realistically determine the muscle forces in the hand. Nonlinear criteria, on the other hand, allow for muscles other than those with the greatest mechanical advantage to begin load sharing at lower levels. In addition, many nonlinear criteria predict antagonistic muscle forces.

m

e

i

d

l

m

l

to

Gr

Gi

cho

met

di

of

comb

resu

simu

Linear Optimization Criteria

Many linear optimization criteria have been proposed in the literature. The most frequently used are force minimization, stress minimization and weighted force and/or stress minimization.

The principle behind stress minimization is that the muscles will attempt to minimize the total stress in all or each of the muscles involved in a given activity. Stress in a muscle is defined as the force generated by the muscle divided by the physiological cross sectional area (PCSA). There are two approaches to utilizing the stress minimization principle. An and his associates (An et al., 1984; An et al., 1985) and Leijnse (Leijnse, 1997c) chose to minimize the stress in each individual muscle. Crowninshield and Brand (Crowninshield & Brand, 1981) and Giurintano and his associates (Giurintano et al., 1995) chose to minimize the total stress in the system. Both methods yield results although the results were somewhat different.

Cooney and Chao utilized EMG data to reduce the number of unknowns in their model (Cooney & Chao, 1977). They combined the flexor brevis and opponens pollicis due to EMG results that show the two muscles are active simultaneously. Also Hirsch and his associates (Hirsch et al., 1974) utilized EMG reduction to eliminate the flexor and extensor pollicis longus and the extensor brevis in their model of the thumb. Toft and Berme (Toft & Berme, 1980) used EMG data to reduce their thumb model. However, they also pointed out the fact that EMG data are difficult to use for any activity other than isometric contraction because as motion progresses in a dynamic activity, some of the muscles which were initially inactive become active and vice versa. There are some very large disadvantages to using EMG data. First, using EMG is limited to those activities where EMG data exist. In addition, noninvasive EMG data can be obtained only for surface muscles. Finally, continuous models cannot be created because muscles activate and deactivate over the course of a motion.

Seirig and Arvikar (Seirig & Arvikar, 1989) described an optimization criterion they called the merit criterion in which a linear combination of the muscle forces, constraint forces and constraint moments was used as the optimization criterion. They were able to obtain results for all of the internal forces using this optimization riterion; however, since the criterion was linear, they ere not able to predict antagonistic muscle activities.

In 1978, Chao and An (Chao & An, 1978b) suggested many optimization criteria based upon: 1) minimum force in a given muscle, 2) minimum reaction moment at a given joint in a given direction, 3) minimum sum of forces, minimum sum of reaction moments in each of the coordinate directions, and 4) minimum sum of reaction moments in the y and z coordinate directions. From the thirty linear optimization criteria described in the paper, only six acceptable solutions arose. Penrod and his associates (Penrod, Davy, & Singh, 1974) also used a weighted total force optimization criterion.

In Chao and An's 1978 paper (Chao & An, 1978a) , based upon the fact that there is little verification that any of the physiological methods is the correct one, the authors utilized a method in which a number of muscles equal to the degree of indeterminancy was set equal to zero. All such combinations (a total of one hundred twenty) were calculated and those solutions that met the basic criteria were retained as feasible solutions. A solution space was constructed and overlaps in the space were said to be viable solutions.

In conclusion, although many linear optimization criteria have been utilized to predict hand forces, few can allow any muscle other than the one with the largest moment arm to carry load and none are able to predict antagonistic muscle activity.

Nonlinear Optimization Criteria

There are as many nonlinear optimization criteria as there are linear optimization criteria in the literature. These criteria allow the forces in biological systems to be more accurately estimated. Most importantly, nonlinear criteria predict antagonistic forces where linear criteria do not. Since antagonistic forces are present in almost all human motions, the fact that linear optimization criteria do not predict antagonistic forces has been an overriding concern with the linear optimization criteria. Nonlinear criteria have also been introduced which take into account dynamic muscle characteristics such as force-velocity and force-displacement characteristics. Taking these characteristics into account tends to smooth the force-time curves.

The first nonlinear optimization criterion to be used was the sum of the square of the muscle forces. This criterion was introduced by Pedotti and his associates in 1978 (Pedotti, Krishnan, & Stark, 1978). Although this criterion keeps the muscle forces low, thereby limiting muscle energy consumption, it does not take into account

physiological limits on the muscles and will allow a small muscle to carry a large load. Pedotti and his associates compared the results of minimizing the sum of the squares of the muscle forces to the results from three other criteria. The other criteria were the sum of the muscle forces, the sum of the muscle forces normalized by the maximum muscle force and the sum of the squares of the muscle forces normalized by the squared maximum muscle force. When they compared the temporal patterns for each of the optimization criteria to those from EMG for each of the muscles used, they found that the linear criteria did not yield results which compared well with EMG data. In addition, they found that summing the squares of the muscle forces was not accurate. Therefore, they concluded that the best choice of those criteria examined was the normalized muscle stress squared.

Energy minimization is an attempt to minimize the amount of energy used by the muscles to perform a given task. This method was utilized by Nubar and Contini in 1961 (Nubar & Contini, 1961) and is based on the Lagrange multiplier method in dynamics. The mathematical equations of the model were derived for the dynamic case but solved for a static example.

Muscle stress limits were introduced in a criterion based upon a least squares approach that minimizes the sum of each of the individual muscle stresses squared. This criterion is believed to minimize the energy used by the entire system of muscles and was used by Buchner and his associates (Buchner et al., 1988) and by Brook and his associates (Brook et al., 1995). This method does take into account the relative sizes of the muscles, but still it does not incorporate physiological criteria such as muscle speed and elongation.

In 1981, Crowninshield and Brand (Crowninshield & Brand, 1981) introduced a criterion that incorporated the physiological properties of muscles. This criterion is based upon the force-endurance relationship originally proposed by Grosse-Lordemann and Muller (Grosse-Lordemann, 1937). This relationship stated that the endurance of the muscle is related to the muscle force raised to a power, n. Thus, the criterion proposed by Crowninshield and Brand is to minimize the sum of the muscle forces raised to the same power, n. Since n is an experimentally determined constant that varies from individual to individual, this criterion allows for flexibility depending on the individual being tested. However, Crowninshield and Brand analyzed the effects of changing n on the results of the optimization and found that although there is a large difference in the results of the optimization between n = 1 and n = 2, there is little comparative change between n =2 and n = infinity. Experimentally, n falls between 2.54 and 3.14. Since there is such a small change in the optimization criterion based upon the power, Crowninshield and Brand chose n = 3 as an average value and used that for all subsequent calculations. Using Crowninshield and Brand's optimization criterion incorporates physiological criteria into the optimization as well as predicting active antagonistic muscles. The only remaining disadvantage is that the model does not enforce smoothness in the muscle force-time curves. Since it is not likely that the body operates in a discontinuous manner, the muscle force-time curves should be smooth.

ERGONOMIC CONSIDERATIONS IN THE WRIST

Considerable work has been done to determine the causes of carpal tunnel syndrome (CTS). It is believed that there are two possible causes for CTS; either the median nerve is compressed because of increased pressure in the carpal tunnel or movement of the median nerve is restricted causing stretching of the nerve. Proposed causes of the increased pressure in the carpal tunnel are frictional wear on the tendons in the carpal tunnel causing fraying of the tendons, edema, incursion of the lumbrical muscle into the tunnel, and position variations. It is also believed that the median nerve can be compressed by direct pressure from the tendons in the carpal tunnel.

In 1995, Seradge and his associates (Seradge et al., 1995) published the results of a study of the in-vivo carpal tunnel pressure. They concluded that the average carpal tunnel pressure in individuals with CTS is higher than that in individuals without CTS. This could lead to the conclusion that higher carpal tunnel pressure is a symptom of CTS rather than a cause. However, they also concluded that certain postures—making a power fist and grasping a small object firmly followed by wrist extension, wrist flexion and isometric flexing of the fingers to a much lesser degree--resulted in higher pressures in both individuals with and without CTS. Therefore, activities that include these types of motions could cause CTS through increased carpal tunnel pressure.

Werner and his associates (Werner, Armstrong, Bir, & ylard, 1997b) also studied the effects of hand, wrist, and inger positions in causing increased carpal tunnel ressure. They agreed with previous researchers as to the sitions that increased carpal tunnel pressure.

Keir and his associates (Keir et al., 1998b) showed that loading the fingertip by both pinching and pressing caused increases in carpal tunnel pressure, although the pinching task showed a much greater increase. They (Keir et al., 1998a) also showed that finger position affects carpal tunnel pressure. They concluded that as the MCP angle increased from neutral in either flexion or extension, carpal tunnel pressure decreased. They also showed that for all angles of MCP tested, the minimum carpal tunnel pressure occurred at a wrist angle of approximately twenty degrees flexion and maximized at maximum extension. Although there is a variation in carpal tunnel pressure with MCP joint angle, the pressures in the postures tested in this study are significantly lower than those found during making a fist or grasping an object. Therefore, it is possible that for typing, increased carpal tunnel pressure is not the main factor in causing CTS.

A second proposed cause of carpal tunnel syndrome is direct pressure on the median nerve by the flexor tendons. Investigators (Armstrong & Chaffin, 1979; Miller & Freivalds, 1995; Moore et al., 1991) have developed models based upon the model of a belt on a pulley to determine the normal force on the median nerve imposed by the flexor tendons passing over it under load. Armstrong's model

(Armstrong & Chaffin, 1979) gave a linear relationship between the tendon force and the reaction force on the median nerve. The force on the median nerve was also linearly related to the sine of the wrist flexion/extension angle divided by two. Figure 7 illustrates the model used to determine this relationship.

Therefore, the reaction force can be described by nearly linear lines radiating out from zero degrees and zero tendon force. Figure 8 is a graph of median nerve reaction force versus flexion/extension angle for various values of tendon force. From this model he was able to predict that the tendency to develop CTS was related to the wrist flexion/extension angle and the tendon force during an activity. This agreed with observations although the model was very simple.

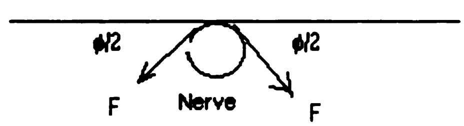

Figure 7—Model of Interaction of Tendon Force and Median Nerve

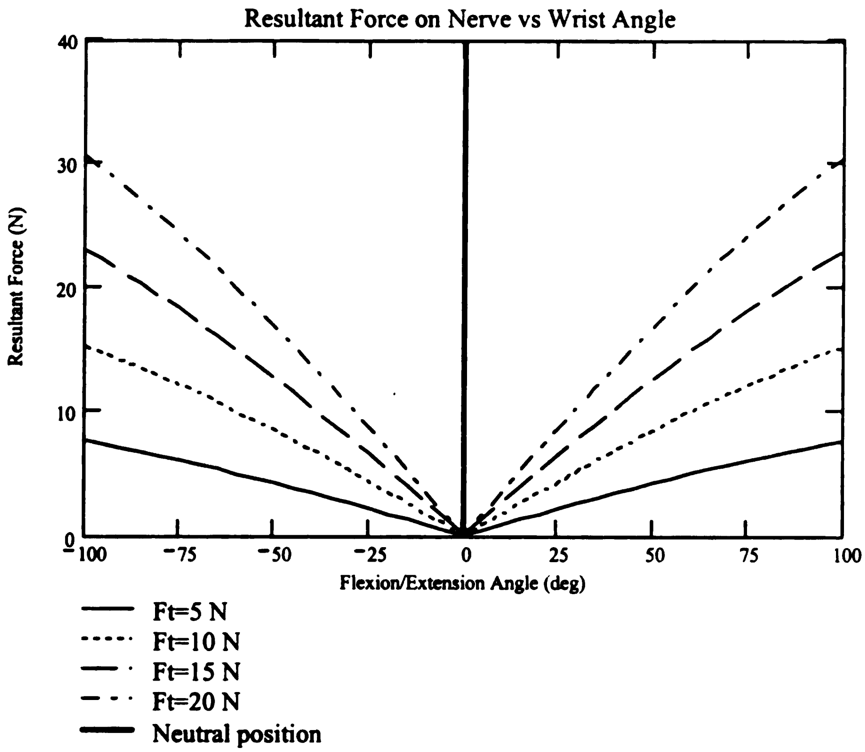

Figure 8—Graph of Reaction Force on Median Nerve Versus Tendon Force

Moore and his associates (Moore et al., 1991) developed a more complicated model in which the tendon radius for the wrist is a function of the angle of contact between the tendon and the wrist, the excursion of the tendon with respect to the proximal end of the wrist joint required to achieve the current wrist joint angle in reference to the neutral, and the moment arm of the tendon when the wrist angle is zero degrees. The angle of contact is a simple angle based only upon flexion and extension of the wrist. The pressure on surrounding tissues caused by a given tendon is then a function of the tendon radius, the force in the tendon, the coefficient of friction, the width of the tendon and the angle of contact. The pressure relationship is developed from the relationship for friction of a belt on a pulley. See Figure 7 for a schematic of the belt and pulley model. Externally applied forces were measured using transducers and then scaled using relationships developed by An (An et al., 1985) for grasping to determine the tendon forces. In the conclusions, the authors reported that the tendon force in the equation caused the model to predict CTS due to high force activities and the excursions of the flexor tendons predicted CTS due to high repetition. It was concluded that the work from friction best described the total influence of an activity in causing CTS. This is because the frictional work incorporates both the excursion of the tendon and the force in the tendon in a multiplicative manner.

In 1995, Miller and Freivalds (Miller & Freivalds, 1995) used a model very similar to that described by Moore and his associates to predict total cumulative damage in a tendon. Using this model, they predicted that women, because of having sharper wrist radii, would be more likely to develop CTS than men. In addition, they noticed an increa

and wr

agree

Althou

the nu

of CTS

I

1994b

force

signs

to the

decrea

propos

in the

be cau

by dir

durati

primate

wrist,

observe

Ar

pressur

muscle

investi

increase in the stress in the tendons from both grasp force and wrist deviation from neutral. This is in general agreement with statistics of CTS in the general population. Although the model predicted the general trends expected, the numerical incidences did not compare well with reports of CTS.

In 1994, Smutz and his associates (Smutz et al., 1994b) studied the relationship between repetitive low force activities and tendon fraying. Although no visible signs of fraying existed after testing, tendon force distal to the wrist decreased significantly with no corresponding decrease in force proximal to the wrist. The authors proposed three explanations for the apparent lack of change in the tissue: 1) compression of the median nerve may not be caused by fraying of the tendons themselves, but instead by direct compression of the median nerve, 2) the test duration may not have been long enough, 3) the nonhuman primate used in the test may not adequately model the human wrist, and 4) tendon damage may have occurred, but was not observed.

Another possibility for a cause of the increased pressure in the carpal tunnel is incursion of the lumbrical muscle into the carpal tunnel. This possibility was investigated by Cobb and his associates (Cobb et al., 1994). By placing wires into cadaveric lumbrical muscles on intact hands, they discovered that incursion of the lumbrical muscle into the carpal tunnel is a normal occurrence. However, the mass of the lumbrical muscle varied greatly from individual to individual. Therefore, in hands with larger lumbrical muscles, increased pressure in the carpal tunnel could occur. The incursion of the lumbrical into the carpal tunnel is consistent with studies that show that carpal tunnel pressure increases with finger flexion.

In 1997, Bay (Bay et al., 1997) and his associates performed a cadaveric study in which they concluded that a probable cause of CTS is stretching of the median nerve. They concluded that this stretching could be caused by two mechanisms—direct stretching of the nerve caused by increasing the distance over which it must act and shear from the tendons sliding over the nerve. Their study showed that the greatest elongation of the nerve occurred in extension of the wrist and this agrees with studies of the causes of CTS.

CHAPTER 3—DEVELOPMENT OF DYNAMIC HAND MODEL

The dynamic hand model for predicting the tendency of typing to cause carpal tunnel syndrome utilizes three steps. These are the kinetic model, which is a study of the forces acting on the hand, the kinematic model, which is the study of the motion of the hand, and finally the combination of the two in a simple pulley model to determine the energy lost in the wrist due to the friction of the flexor tendons on the transverse carpal ligament and carpal bones.

KINETIC MODEL DEVELOPMENT

The hand is an extremely complex mechanism consisting of nineteen bones and 46 muscles in addition to numerous tendons, ligaments and flesh. In order to adequately model such a complex mechanism, simplifying assumptions must be made. In addition, methods of analysis from engineering mechanics must be utilized in determining the equations of motion and modeling the wear of the tendons in the wrist. A three-dimensional model is developed and all of the assumptions incorporated in that model are described.

In this model, it is assumed that all of the bones act as rigid bodies, the tendons act as inextensible cords, and the joints were idealized. All interphalangeal joints and thumb metacarpophalangeal joints are treated as hinges allowing only flexion/extension and the finger metacarpophalangeal and thumb carpometacarpal joints are treated as universal joints allowing flexion/extension and abduction/adduction. Although the metacarpophalangeal joints and thumb carpometacarpal joint do not have active (voluntarily muscle controlled) axial rotation, this is left as a degree of freedom because of the strong coupling of abduction/adduction and axial rotation from the joint geometry (saddle shaped).

A list of muscles considered in this model and their abbreviations, taken from the work of An and Chao (An et al., 1979) is shown in Table 1.

In addition to the general assumptions made about the modeling of the tissues in the hand—those given above in addition to neglecting the ligaments and motion of the flesh (skin and fatty tissue)—some assumptions were made about the individual muscles involved in the modeling. The extensor indicis and extensor minimi muscles were grouped with the extensor communis for their respective fingers, thus eliminating two unknowns. Since in each case the specialized extensor muscles act along a line similar to that of the extensor communis for their respective fingers,

Table 1–Tendons and muscles involved in hand function

Hand Element	Joint	Unknown Tendon and Intrinsic Muscle Forces
Fingers	DIP	Terminal Extensor (TE) Flexor Profundus (FP)
	PIP	Extensor Slip (ES) Radial Band (RB) Ulnar Band (UB) Flexor Subliminus (FS)
	MCP	Long Extensor (LE) Radial Interossseous (RI) Ulnar Interosseous (UI) Lumbrical (LU)
Thumb	IP	Flexor Pollicis Longus (FPL) Extensor Pollicis Longus (EPL)
	MCP	Abductor Pollicis Brevis (APB) Flexor Pollicis Brevis (FPB) Adductor Pollicis (ADD) Extensor Pollicis Brevis (EPB)
	CMC	Opponens Pollicis (OPP) Abductor Pollicis Longus (APL)

although without the branching at the individual joints, this assumption will yield a combined total extensor force rather than individual forces for each muscle. In addition to combining the extensor muscles, Chao (Chao & An, 1978a) proposed four constraint equations based upon the geometry of the extensor tendon complex and the origin and insertion of the lumbical muscles. These are given below:

$$
\begin{aligned}
TE &= RB + UB \\
RB &= \frac{2}{3}LU + \frac{1}{6}LE \\
UB &= \frac{1}{3}UI + \frac{1}{6}LE \\
ES &= \frac{1}{3}LU + \frac{1}{6}LE + \frac{1}{3}RI + \frac{1}{3}UI
\end{aligned} \tag{1}
$$

The Newton-Euler equations of motion for the hand were derived by analyzing each of the finger segments separately beginning with the distal segment and working proximally. There are two coordinate systems utilized in this derivation.

The first is the global system relative to the laboratory in which the input data for the model were gathered. This system is composed of a y-direction which is perpendicular to the floor pointing upward, a z-direction which points from left to right on the keyboard, perpendicular to the y-axis and the x-axis which can be oriented by crossing the y and z axes. This system is illustrated below in Figure 9.

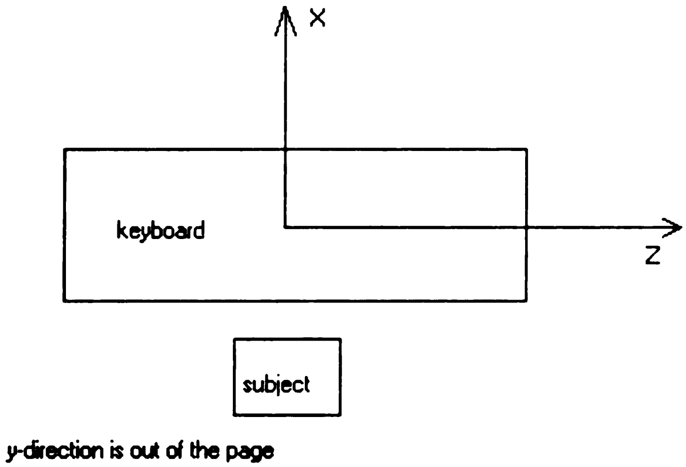

Figure 9—Global Coordinate System

The second coordinate system is actually a series of coordinate systems called segmental systems. There is one segmental system on each finger segment. In these systems, the x-direction is along the long axis of the finger segment pointing proximally, the y-direction is normal to the finger segment pointing dorsally, and the z-direction is in accordance with the right hand rule. The base of this system is the proximal joint center for each segment. This system is illustrated below in Figure 10.

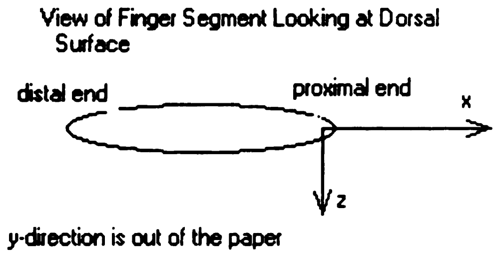

Figure 10—Segmental Coordinate System

In the equations of motion, **a** is the absolute acceleration and $\dot{H}$ is the angular momentum of the segment being considered. $\dot{H}$ is defined according to the Newton-Euler equations of motion as:

$$\dot{\overline{H}} = \overline{\overline{I}} \cdot \overline{\alpha} + \overline{\omega} \times \overline{\overline{I}} \cdot \overline{\omega} \qquad (2)$$

where $\overline{\overline{I}}$ is the inertia matrix for the body. Since the coordinate system used for the equilibrium equations is chosen to be the principal axes of the body and is located at the center of mass of the body, all of the product moment of inertia terms in the inertia matrix are zero. The time derivative of the angular momentum reduces to:

$$\dot{H}_x = I_{xx}\alpha_x + (I_{zz} - I_{yy})\omega_y\omega_z \qquad (3)$$
$$\dot{H}_y = I_{yy}\alpha_y + (I_{xx} - I_{zz})\omega_x\omega_z \qquad (4)$$
$$\dot{H}_z = I_{zz}\alpha_z + (I_{yy} - I_{xx})\omega_x\omega_y \qquad (5)$$

The moments of inertia and the mass of the finger segment were determined assuming the finger segment can be modeled as a cylinder with an elliptical cross section. This shape was chosen because it closely approximates the shape of the finger segment. Although an ellipsoid appears to model the segment more accurately, it was shown by Buchholz (Buchholz & Armstrong, 1991; Buchholz & Armstrong, 1992) that ellipsoids do not accurately model the finger segments mathematically. In addition, the ellipsoids add unnecessary complexity to the model. The mass is determined as:

$$m = \rho\pi abh \qquad (6)$$

In this equation, ρ is the mass density of the finger and is estimated as 1.1 g/cm^3 (Esteki & Mansour, 1997) (Brand(Brand & Mosby, 1985) used 1.02 g/cm^3). The dimensions of the elliptical cylinder are *a*, the width of the segment at the center; *b*, the thickness of the segment at the center; and *h*, the length of the segment. See Figure 11 for how these dimensions were defined.

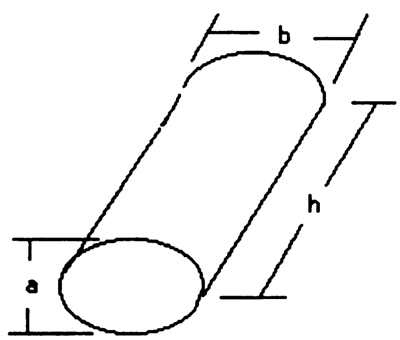

Figure 11–Dimensions for Moment of Inertia and Mass Calculations

The moments of inertia were calculated using the following formulas for the moments of inertia of an elliptical cylinder:

$$I_{xx} = \frac{m}{4}(a^2 + b^2) \tag{7}$$

$$I_{yy} = m\left(\frac{b^2}{4} + \frac{h^2}{12}\right) \tag{8}$$

$$I_{zz} = m\left(\frac{a^2}{4} + \frac{h^2}{12}\right) \tag{9}$$

The unit vectors for the tendon forces were defined using the method developed by Chao (Chao et al., 1976). One point on the tendon is taken on the distal side and another on the proximal side of the joint at the ends of the synovial sheaths in a neutral position. Since each point is specified in the local segmental coordinate system, these points will remain relatively stationary during motion. However, the unit vector formed by taking one point on each of the two attached segments will change. Figure 7 illustrates this point. Note also the change of length of the tendon from the motion can be seen in this illustration.

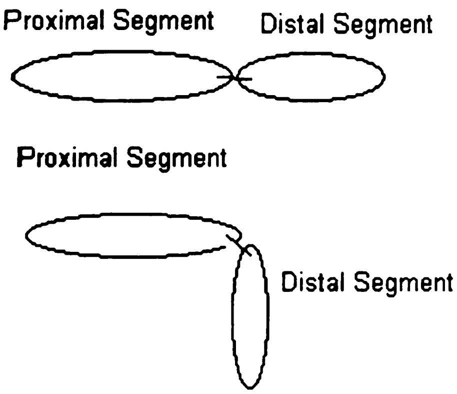

Figure 12–Rotation of Tendon Vector Connecting Two Points at Ends of Synovial Sheaths as Finger Segments Rotate Relative to Each Other (Arrows Represent Vector)

A table containing the points, taken from Chao (Chao et al., 1976), is found in Appendix A. These values are based on an average of fifteen specimens. Each point is defined in its respective coordinate system and therefore, in order to calculate the unit vector for the tendon, the proximal point must be transformed into the distal coordinate system according to the following equation:

$$\overline{P}_D = \overline{\overline{R}} \cdot \overline{P}_P + \overline{L} \tag{10}$$

where $\overline{P}_D$ is the vector representing the proximal point expressed in the distal system, $\overline{\overline{R}}$ is the Euler angle transformation matrix between the two systems being examined, $\overline{P}_P$ is the vector representing the proximal point expressed in the proximal system, and $\overline{L}$ is the vector representing the distance, expressed in the distal system, between the proximal system and the distal system.

Once all points were expressed in the distal coordinate system, a unit vector for each force is constructed using the following equation:

$$\hat{f} = \frac{\bar{P}_D - \bar{D}}{\left|\bar{P}_D - \bar{D}\right|} \qquad (11)$$

where $\hat{f}$ is the unit vector for the force under consideration, $\bar{D}$ is the column vector representing the distal point on the tendon and $\overline{P}_D$ is as defined before.

All position vectors, $\bar{r}$ for the moment equations, were defined by the following equation:

$$\bar{r} = \bar{D} - c\bar{g} \qquad (12)$$

where cg is the vector representing the location of the center of gravity of the segment in the distal coordinate system. Since the finger segment is being represented by an elliptical cylinder, $c\bar{g} = \left[-h/2,0,0\right]^T$.

For the distal finger segment, the free body diagram is given in Figure 13:

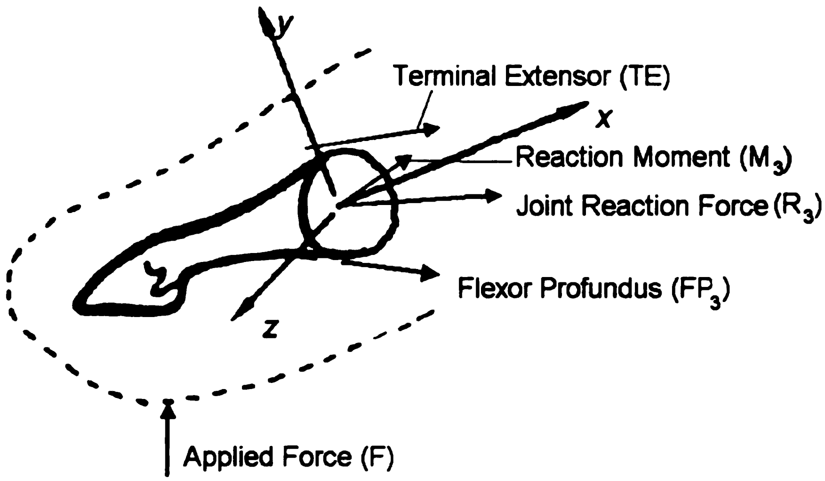

Figure 13—Free Body Diagram of Finger Distal Phalanx

In both the free body diagrams of the finger and thumb segments and in the equations of motion, the numeric subscripts signify the joint at which the force is applied (e.g. 1 = metacarpophalangeal joint, 2 = proximal interphalangeal joint and 3 = distal interphalangeal joint). From the free body diagram above of the distal segment, the Newton-Euler equations of motion are:

$$\sum \vec{F} = \vec{F} + \vec{TE} + \vec{FP}_3 + \vec{R}_3 + m_3\vec{g} = m_3\vec{a}_3 \tag{13}$$

$$\sum \vec{M} = r_F \times \vec{F} + r_{TE} \times \vec{TE} + r_{R3} \times \vec{R}_3 + \vec{M}_3 = \dot{\vec{H}}_3 \tag{14}$$

Although the reaction, R, and the moment, M, at the joint are shown as being general, three dimensional vectors, due to the specification of the joint as a hinge joint, the component of the moment vector in the z direction is zero. In addition, $\omega_x, \omega_y, \alpha_x$ and α_y are all zero and therefore, $\dot{H}_{3x} = 0, \dot{H}_{3y} = 0$ and $\dot{H}_{3z} = I_{zz}\alpha_z$. The applied force, $\bar{F}$, and the weight of the segment are in the global y direction. This assumption is definitely true for the weight, and is an approximation for the force $\bar{F}$. Since typing is the activity being studied, this approximation should be fairly accurate.

Each of the remaining two finger segments will be handled in a similar manner. The free body diagram of the finger middle phalanx is:

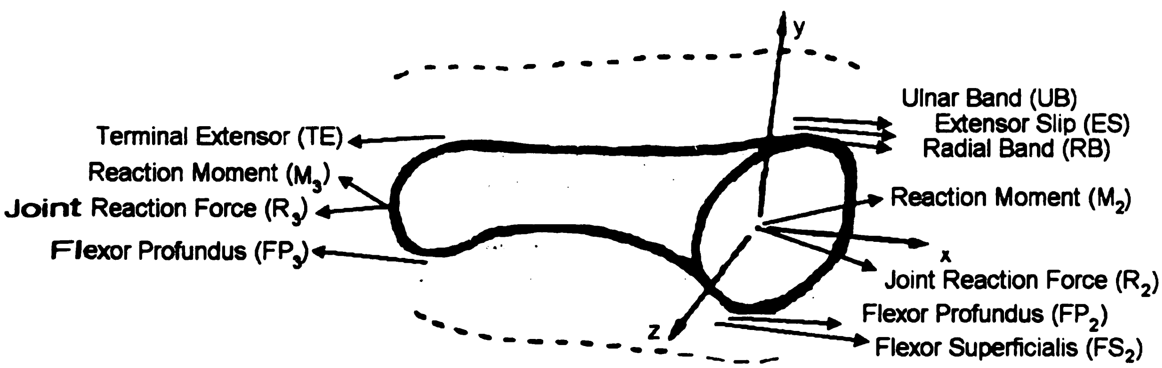

Figure 14–Free Body Diagram of Finger Middle Phalanx

The equations of motion for the middle phalange are:

$$\sum \bar{F} = \bar{R}_3 + T\bar{E} + F\bar{P}_3 + E\bar{S} + R\bar{B} + U\bar{B} + F\bar{P}_2 + F\bar{S}_2 + \bar{R}_2 + m_2\bar{g} = m_2\bar{a}_2 \tag{15}$$

$$\sum \bar{M} = \bar{r}_{R3} \times \bar{R}_3 + \bar{r}_{TE} \times T\bar{E} + \bar{r}_{FP3} \times F\bar{P}_3 + \bar{r}_{ES} \times E\bar{S} + \bar{r}_{RB} \times R\bar{B} + \bar{r}_{UB} \times U\bar{B} + \bar{r}_{FP2} \times F\bar{P}_2 + \bar{r}_{FS2} \times F\bar{S}_2 + \bar{r}_{R2} \times \bar{R}_2 + \bar{M}_2 + \bar{M}_3 = \dot{\bar{H}}_2 \tag{16}$$

The components of the reaction moment and time derivative of the angular velocity for the middle phalange are simplified in precisely the same manner as those for the finger distal phalange.

The free body diagram of the finger proximal phalange is:

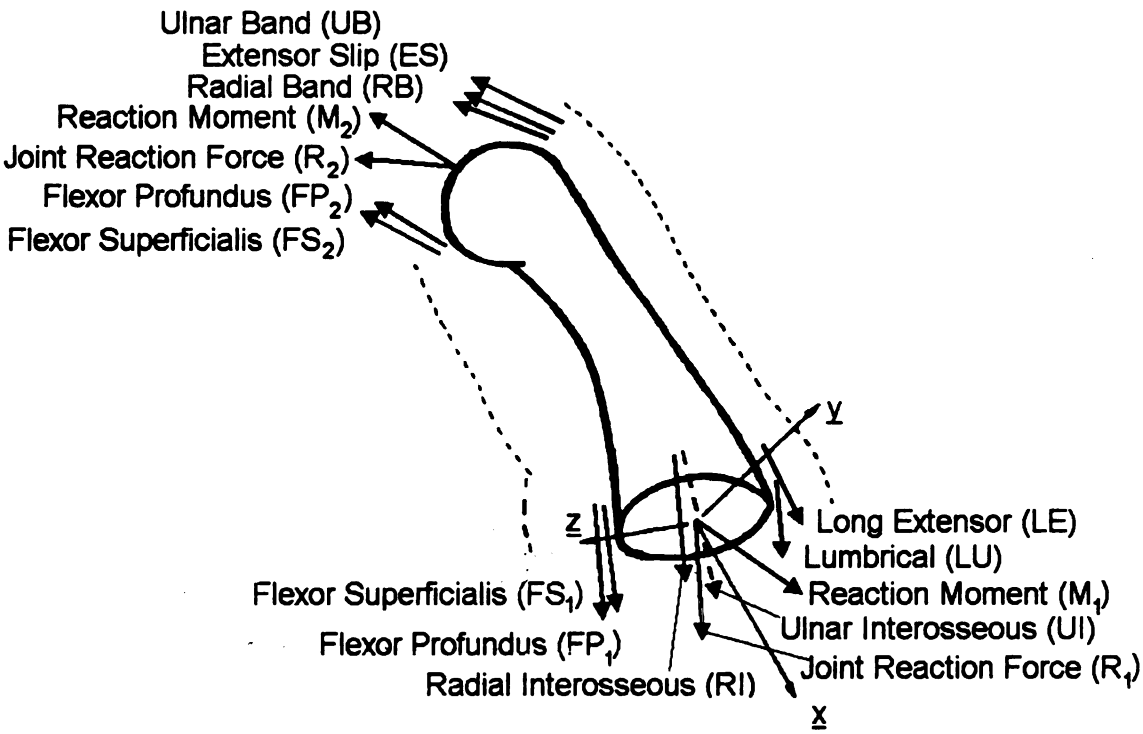

Figure 15—Free Body Diagram of Finger Proximal Phalanx

The equations of motion for the proximal phalange are:

$$\begin{aligned}\sum \vec{F} = &\vec{R}_2 + \vec{ES} + \vec{RB} + \vec{UB} + \vec{FP}_2 + \vec{FS}_2 + \vec{LU} + \vec{RI} + \vec{UI} + \vec{FS}_1 + \vec{FP}_1 \\ &+ \vec{LE} + \vec{R}_1 + m_1\vec{g} = m_1\vec{a}_1\end{aligned} \quad (17)$$

$$\begin{aligned}\sum \vec{M} = &\vec{r}_{R2} \times \vec{R}_2 + \vec{r}_{ES} \times \vec{ES} + \vec{r}_{RB} \times \vec{RB} + \vec{r}_{UB} \times \vec{UB} + \vec{r}_{FP2} \times \vec{FP}_2 \\ &+ \vec{r}_{FS2} \times \vec{FS}_2 + \vec{r}_{LU} \times \vec{LU} + \vec{r}_{RI} \times \vec{RI} + \vec{r}_{UI} \times \vec{UI} + \vec{r}_{FP1} \times \vec{FP}_1 \\ &+ \vec{r}_{FS1} \times \vec{FS}_1 + \vec{r}_{LE} \times \vec{LE} + \vec{r}_{R1} \times \vec{R}_1 + \vec{M}_2 + \vec{M}_1 = \dot{\vec{H}}_1\end{aligned} \quad (18)$$

For the proximal phalange, the reaction moments about both the y and z directions are zero. Unlike the previous two segments, none of the angular velocities or angular accelerations is zero and therefore, the full equations for the time derivative of the angular velocity must be used.

Although the system of equations above consists of eighteen scalar equations, only four of the equations can be used to solve for the unknown muscle forces. The remainder of the equations were used to solve for the reaction forces and moments at the joints. The constraints presented earlier, based upon the geometry of the extensor complex and lumbrical muscle, provide four more equations to solve the system. Therefore, since there are ten unknown tendon forces, the degree of indeterminacy of the system is two.

The equations for the thumb were derived in a similar manner. There are three free bodies to be considered when examining the thumb—the distal segment, the proximal segment and the metacarpal bone.

The free body diagram of the distal thumb segment is shown in Figure 16:

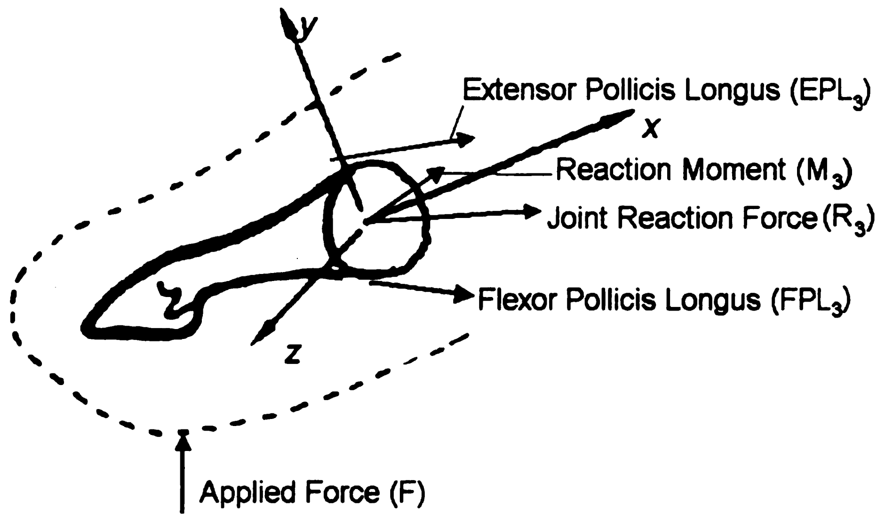

Figure 16–Free Body Diagram of Thumb Distal Segment

From this free body diagram, the following equations of motion are derived:

$$\sum \vec{F} = \vec{F} + \vec{E}PL_3 + FP\vec{L}_3 + \vec{R}_3 + m_3\vec{g} = m_3\vec{a}_3 \qquad (19)$$

$$\sum \vec{M} = r_F \times \vec{F} + r_{EPL3} \times \vec{E}PL_3 + r_{FPL3} \times FP\vec{L}_3 + r_{R3} \times \vec{R}_3 + \vec{M}_3 = \vec{H}_3 \qquad (20)$$

The thumb proximal segment can be modeled as shown in Figure 17:

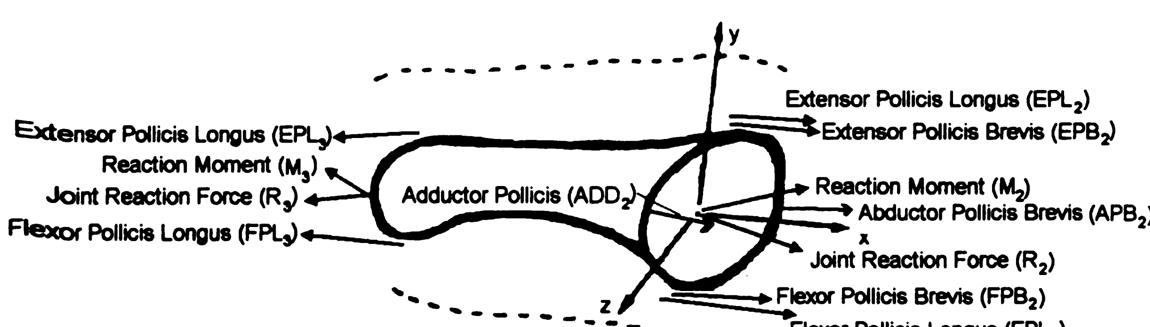

Figure 17–Free Body Diagram of Thumb Proximal Segment

From this free body diagram, the equations of motion are:

$$\sum \vec{F} = \vec{EPL}_3 + \vec{FPL}_3 + \vec{EPL}_2 + \vec{FPL}_2 + \vec{ADD}_2 + \vec{EPB}_2 + \vec{FPB}_2 + \vec{APB}_2 + \vec{R}_3 + \vec{R}_2 + m_2\vec{g} = m_2\vec{a}_2 \quad (21)$$

$$\sum \vec{M} = r_{EPL3} \times \vec{EPL}_3 + r_{FPL3} \times \vec{FPL}_3 + r_{EPL2} \times \vec{EPL}_2 + r_{FPL2} \times \vec{FPL}_2 + r_{ADD2} \times \vec{ADD}_2 + r_{EPB2} \times \vec{EPB}_2 + r_{FPB2} \times \vec{FPB}_2 + r_{APB2} \times \vec{APB}_2 + r_{R3} \times \vec{R}_3 + r_{R2} \times \vec{R}_2 + \vec{M}_3 + \vec{M}_2 = \vec{H}_2 \quad (22)$$

The thumb metacarpal is modeled as shown in Figure 18:

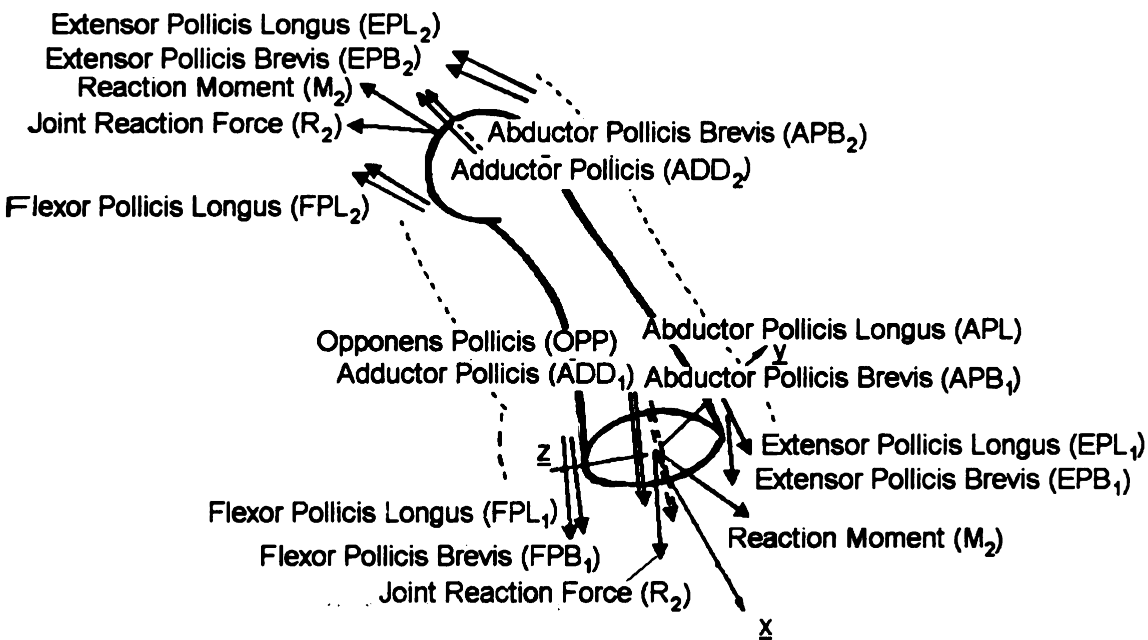

Figure 18—Free Body Diagram of Thumb Metacarpal

From this free body diagram, the equations of motion are:

$$\sum \vec{F} = \vec{EPL}_2 + \vec{FPL}_2 + \vec{ADD}_2 + \vec{EPB}_2 + \vec{FPB}_2 + \vec{APB}_2 + \vec{EPL}_1 + \vec{FPL}_1 + \vec{ADD}_1 + \vec{EPB}_1 + \vec{FPB}_1 + \vec{APB}_1 + \vec{OPP} + \vec{APL} + \vec{R}_2 + \vec{R}_1 + m_1\vec{g} = m_1\vec{a}_1 \quad (23)$$

$$\sum \vec{M} = r_{EPL2} \times \vec{EPL}_2 + r_{FPL2} \times \vec{FPL}_2 + r_{ADD2} \times \vec{ADD}_2 + r_{EPB2} \times \vec{EPB}_2 + r_{FPB2} \times \vec{FPB}_2 + r_{APB2} \times \vec{APB}_2 + r_{EPL1} \times \vec{EPL}_1 + r_{FPL1} \times \vec{FPL}_1 + r_{ADD1} \times \vec{ADD}_1 + r_{EPB1} \times \vec{EPB}_1 + r_{FPB1} \times \vec{FPB}_1 + r_{APB1} \times \vec{APB}_1 + r_{OPP} \times \vec{OPP} + r_{APL} \times \vec{APL} + r_{R2} \times \vec{R}_2 + r_{R1} \times \vec{R}_1 + \vec{M}_2 + \vec{M}_1 = \vec{H}_1 \quad (24)$$

Note that again in the case of the thumb, only four of these eighteen equations were useful for determining the unknown muscle forces. Since there were eight unknown muscle forces in the thumb, this leaves a system that is undetermined by a degree of four. Unlike with the fingers, there have been no relationships developed in the literature to reduce the degree of indeterminacy in the system of equations of motion for the thumb.

In addition to the constraint equalities provided by the equations of motion, the following inequalities will be applied when solving for the muscle forces.

$$0 \leq F_i / PCSA_i \leq 0.2\,Mpa \qquad (25)$$

where F_i is the force in the i^{th} muscle and PCSA is the physiological cross sectional area. The PCSA is defined as the volume of the muscle divided by the mean fiber length. A table of the PCSAs for the muscles in the hand, taken from Chao and his associates (Chao, 1989), is found in Appendix B. Equation 25 constrains the muscle stresses, and therefore forces, to be tensile and to not exceed the maximum possible muscle stress as reported in the literature (Burke, 1973; Esteki & Mansour, 1997).

Given this set of inequalities, the system is then optimized using two optimization criteria:

$$Minimize \sum_i (F_i / PCSA_i)^3 \quad (26)$$

$$Minimize \sum_j \left[F(t_j) - F(t_{j-1})\right]^2 \quad (27)$$

The first inequality, equation 26, is the criterion developed by Crowninshield and Brand (Crowninshield & Brand, 1981) to optimize biological systems. As was pointed out in the literature review, this criterion is based upon muscle fatigue and yields results that include active antagonistic muscles.

The second inequality is being introduced in this research. The purpose of this inequality is to force smoothness of the force-time curves. It minimizes the sum of the squares of the differences between the force at the current time increment and the force at the previous time increment for each muscle. It has been pointed out in the literature (Siemienski, 1992) that the force-time curves should be smooth as it is unlikely that the body changes its choices of muscles during a motion. In most cases, a change in muscle selection would be the only explanation for a discontinuity in the force-time curves.

KINEMATIC MODEL DEVELOPMENT

Accelerations

The accelerations of each segment of the finger were found using numerical differentiation of the position data obtained through laboratory testing (described in the experimental procedure section of this document). For this, a five-point central difference formula is used (Mathews, 1987). This formula is given below in equation 28.

$$f'' = \frac{-f(t_{i+2}) + 16f(t_{i+1}) - 30f(t_i) + 16f(t_{i-1}) - f(t_{i-2})}{12\Delta t^2} \tag{28}$$

As will be described in the experimental procedure section, $\Delta t = 0.01$ s. f is the value of the function at the increment given in the subscript. Although two data points are lost at both the beginning and end of the data file, this did not cause a loss of useful data. As the hand was moved into position to begin typing, data were recorded. These data were not used in the model. Also, at the end of the file, data were recorded as the subject rested. This data assured that the entire motion was included in the data file. These resting data were also not needed for the model.

In addition, the angular velocities and angular accelerations for each body were found by numerically differentiating the Euler angles for the relative position of two adjacent finger segments using the same central difference formula.

Tendon Displacement

There have been a number of means to determine the displacement of tendons mentioned in the literature. These methods served different purposes depending upon the needs of the model being presented. Landsmeer introduced the first of these methods (Landsmeer, 1961). He developed three different models for determining the length of the tendon.

The first and simplest is the model, shown below in Figure 19, that Landsmeer chose to use for extensor tendons in which the change in length of the tendon is equal to the change in arc length at the joint. This change in arc length is calculated using the simple formula

$$\Delta = r\theta \tag{29}$$

Landsmeer considered this model to be accurate for extensor tendons because these tendons rest on the bones of the joint and the radius of curvature for the joints can be estimated fairly accurately.

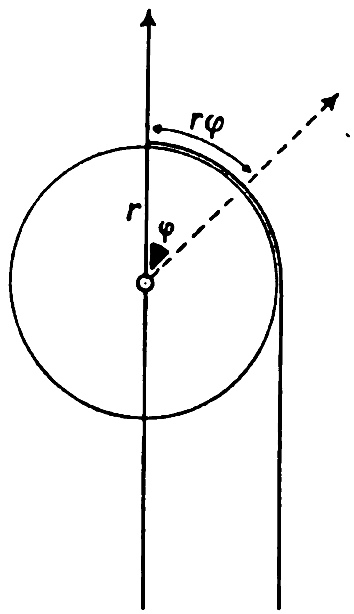

Figure 19--Landsmeer's Extensor Tendon Model. Taken from Landsmeer.(Landsmeer, 1961)

The second model Landsmeer recommended, shown below in Figure 20, was for use with flexor tendons. Because these tendons would tend to bowstring without the synovial sheaths and the sheaths are free to rotate around the joint, Landsmeer assumed that the synovial sheath would remain stationary at the midpoint of the joint. Given this assumption, the change in arc length is given by

$$\Delta = 2r\sin(1/2\ \theta) \tag{30}$$

Note that for small angles, this reduces to the first model (Using $\sin \gamma = \gamma$ for small angles).

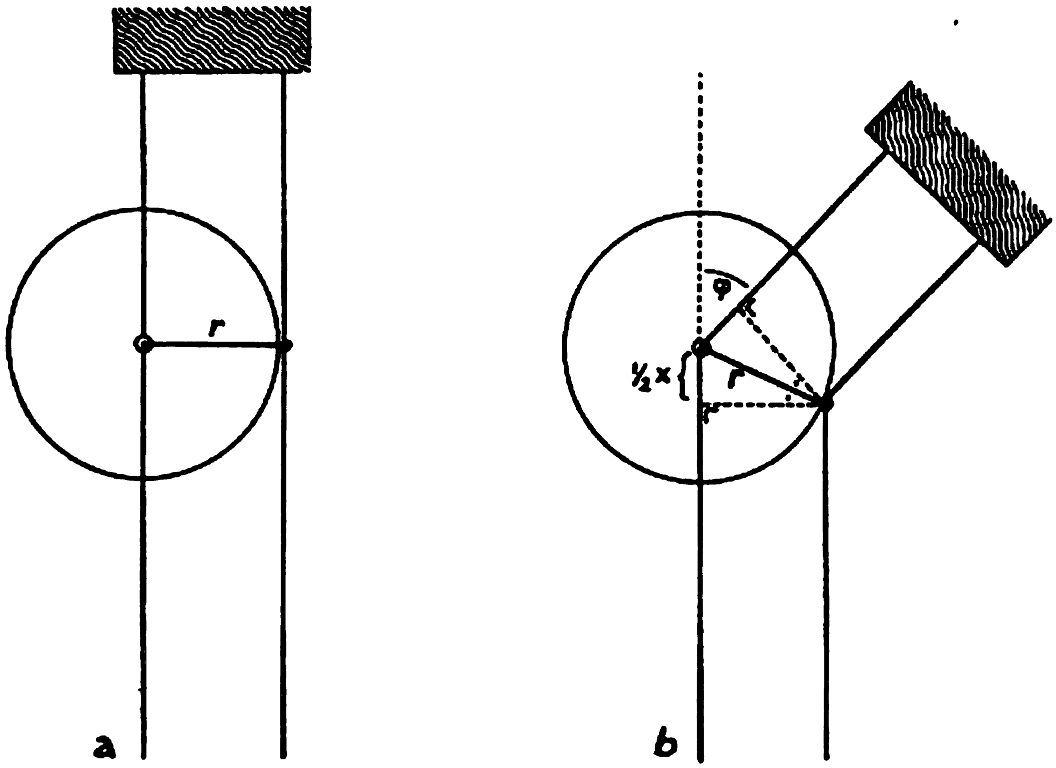

Figure 20--Landsmeer's Second Model. Taken from Landsmeer.(Landsmeer, 1961)

The third model, shown in Figure 21, is much more complex than the first two. It allows for bowstring of the tendon in a flexible sheath that is fixed to each of the bones comprising the joint. The change in length of the tendon in this case is

$$\Delta = \theta D + y\{2-\theta/\tan(\theta/2)\} \qquad (31)$$

where y represents the distance from the point of attachment of the synovial sheath to the bone and d represents the distance from the center of the finger bone to the tendon. The larger the value of y, the more this model varies from the other two. This is a result of the fact that bowstring will increase with greater distance between the joint and the attachment of the synovial sheaths to the bone. If d, y and r are held constant, the variation between each of the models with angle of flexion can be determined.

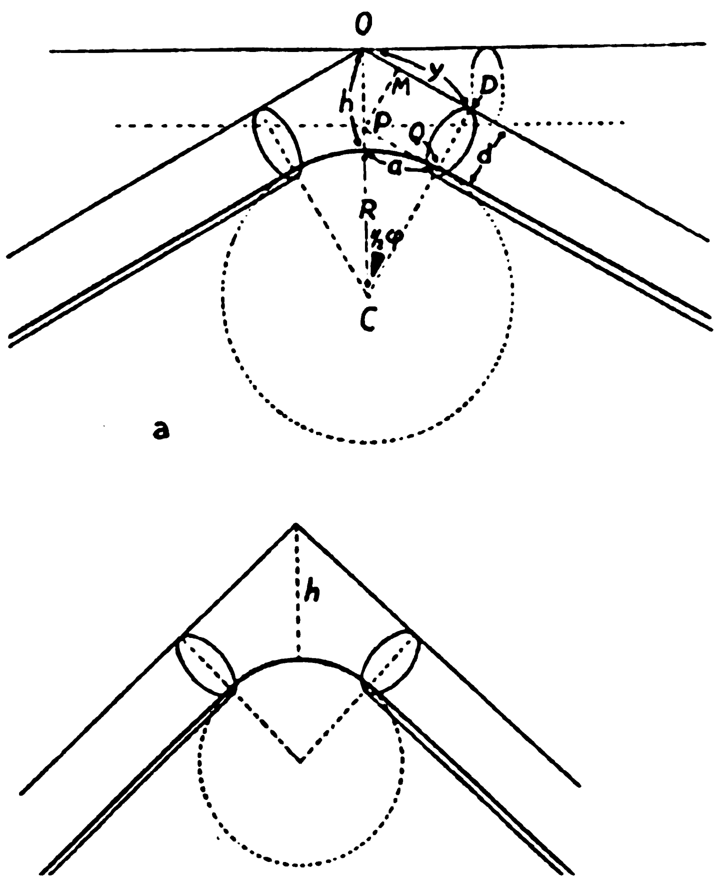

Figure 21--Landsmeer's Third Model. Taken from Landsmeer.(Landsmeer, 1961)

In order to compare Landsmeer's three methods of calculating tendon displacement, each was used to calculate the FS tendon displacement for the distal interphalangeal joint of the index finger. Values for the constants, r, d and y, were taken from An(An, Ueba, Chao, Cooney, & Linscheid, 1983) in order to make the comparison. Figure 22 illustrates the percent difference between each of Landsmeer's models. Note that the first model always yields a larger displacement than the second. The third model has lower displacements at small angles than either of the other two models, however at larger angles, the third model yields higher displacements. In each case, the percent difference was calculated assuming that the later model was the standard.

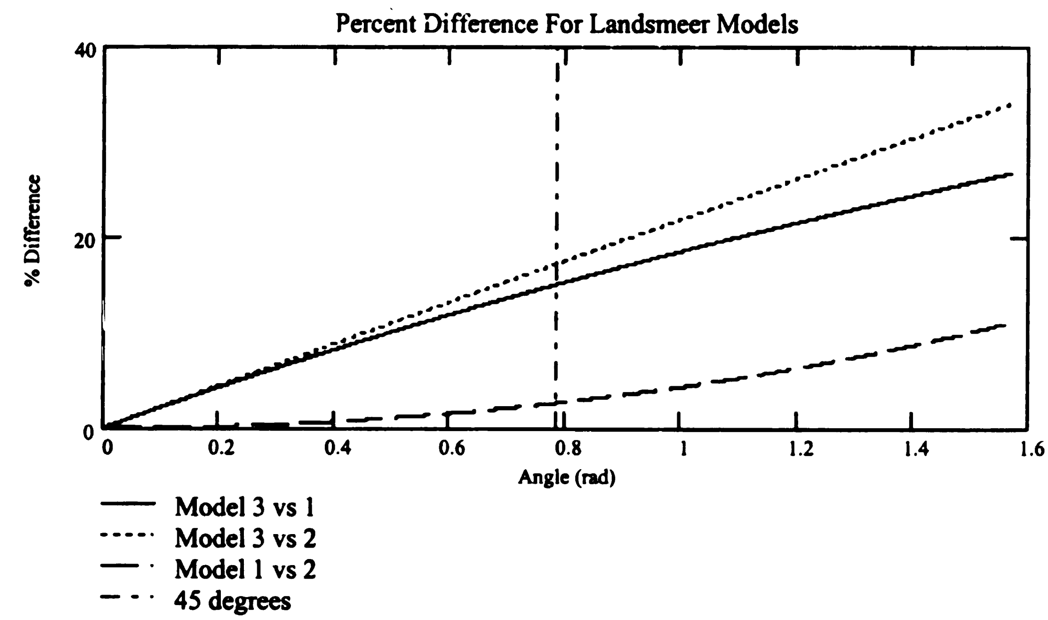

Figure 22–Percent Difference Between Three Landsmeer Models for Tendon Excursion

As can be seen in Figure 22, the maximum difference between the first two models is 11.1% at the extreme of the motion. Although this is a considerable error, if the motion is constrained to act in the range of rotation of less than forty-five degrees that is generally true for typing with the normal hand, this error reduces to 2.6%. Given that each of these models is an approximation, a 2.6% difference would tend to suggest using the simpler of the two. The percent difference between the third and second models is 34.0% at 90 degrees and 17.2% at 45 degrees. Also, the percent difference between the third and first models is 26.7% at 90 degrees and 15.0% at 45 degrees. This large deviation can be explained by the large amount of bowstringing of the flexor tendons that is accounted for in the third model and not accounted for in either of the first two models.

In 1978, Armstrong and Chaffin (Armstrong & Chaffin, 1978) developed an empirical model based upon the joint thickness and the joint angle for the wrist and fingers. Although the finger model predicted the displacement values very well, it was only based upon four hands and did not account for variations in the size of hands. There is no apparent advantage to choosing this model over one of the three proposed by Landsmeer. The model for the wrist, however, is the only one found in the literature and will, therefore, be used and is described below.

Following is the equation taken from Armstrong and Chaffin (Armstrong & Chaffin, 1978) as modified by Miller and Freivalds (Miller & Freivalds, 1995) and subsequently modified to use the angle in radians and give the wrist displacement in mm.

$$E_W = (0.9181\phi_i + 0.1745\phi_i\, t + 3.700\phi_i\, t\, i_1 - 0.03351\phi_i\, t\, i_2)x10^{-3} \qquad (32)$$

where:

ϕ_i = wrist flexion/extension angle in radians at the i^{th} time interval

t = thickness of the wrist

$$t = \sqrt{\left(\frac{2}{\pi^2}c^2 - b^2\right)} \qquad (33)$$

i_1 = 0 for extension, 1 for flexion

i_2 = 0 for the superficialis tendon, 1 for the profundus tendon

c = wrist circumference

b = wrist breadth

In 1995, Brook and his associates (Brook et al., 1995) derived equations for the excursion of each of the tendons in the hand based upon Landsmeer's models. Although they derived equations for each of the tendons in the hand, the current model only uses the excursions of the flexor tendons and, thus, only those excursions will be described herein. Using Brook's notation modified to label joints as described in this work, the excursions of the flexor tendons were:

$$E_i^{FDP} = \phi_{3i} d_3^{FDP} + 2y_3^{FDP}\left\{1 - \frac{\phi_{3i}/2}{\tan\left(\phi_{3i}/2\right)}\right\} + \phi_{2i} d_2^{FDP} + 2y_2^{FDP}\left\{1 - \frac{\phi_{2i}/2}{\tan\left(\phi_{2i}/2\right)}\right\}$$
$$+ \phi_{1i} d_1^{FDP} + 2y_1^{FDP}\left\{1 - \frac{\phi_{1i}/2}{\tan\left(\phi_{1i}/2\right)}\right\} + \left(b_a^{FDP} + h_a^{FDP}\theta_i\right)\theta_i \quad (34)$$

$$E_i^{FDS} = \phi_{2i} d_2^{FDS} + 2y_2^{FDS}\left\{1 - \frac{\phi_{2i}/2}{\tan\left(\phi_{2i}/2\right)}\right\} + \phi_{1i} d_1^{FDS} + 2y_1^{FDS}\left\{1 - \frac{\phi_{1i}/2}{\tan\left(\phi_{1i}/2\right)}\right\} \quad (35)$$
$$+ \left(b_a^{FDS} + h_a^{FDS}\theta_i\right)\theta_i$$

In the above equations, ϕ_i is the flexion/extension angle at the i^{th} time interval and θ_i is the abduction/adduction angle at the i^{th} time interval. This is consistent with the choices of Euler angles used throughout this work. The subscripts used in the equations represent the joints with 1 being the metacarpophalangeal joint, 2 the proximal interphalangeal joint and 3 the distal interphalangeal joint. d and y were as defined by Landsmeer and were approximated for the index finger in Table 2 below. Finally b_a and h_a were constants based upon the modification of Landsmeer's model III as a second order polynomial. This modification was published by Buchner

(Buchner et al., 1988) based upon data from Fischer (Fischer, 1969). b_a and h_a can be found in Table 2 which is modified from Brook (Brook et al., 1995). The coefficients in Table 2 were calculated from data collected by An (An et al., 1983).

Table 2—Coefficients of Excursion Models (Index finger) (mm)

Joint	Tendon	d	y	b_a	h_a
DIP	FP	2.97	3.96		
PIP	FS	4.13	6.73		
	FP	5.76	7.5		
MCP	FS	9.56	8.14	1.1	0.68
	FP	8.32	8.32	0.52	0.66

By summing the excursion for the finger motion and that for the wrist motion, the total excursion of the FP and FS for the index finger can be found. Since the values for the constants to use Brook's model were only available for the index finger, a different way of determining the excursions for the other fingers must be used.

In order to determine those other tendon excursions, the distance between the distal and proximal points on the tendon, Chao (Chao et al., 1976), is used to determine the tendon length at the joints. This assumes that the tendon bowstrings between the two points (one on each side of the joint). The difference between this model and Landsmeer's third model is the difference between the arc length connecting two points on the hypothetical circle and the ray connecting the same two points. This difference is linearly dependent upon the radius of the circle; however, the percent error between the two models is only dependent upon the angle. The difference increases with the angle of flexion as illustrated in Figure 22.

The distance between the two tendon points was already obtained in order to form the unit vectors for the tendon for the kinematic model. By summing the distances at each joint, the tendon length for each of the tendons can be determined. From this length, the incremental change in length can be determined. The equation for the total tendon length is:

$$
\begin{aligned}
E(t_i) &= L_2(t_i) + L_1(t_i) + L_0(t_i) + J_3(t_i) + J_2(t_i) + J_1(t_i) + E_W(t_i) \\
J_3(t_i) &= \left|\vec{P}_{D2}(t_i) - \vec{D}_3(t_i)\right| \\
J_2(t_i) &= \left|\vec{P}_{D1}(t_i) - \vec{D}_2(t_i)\right| \\
J_1(t_i) &= \left|\vec{P}_{D0}(t_i) - \vec{D}_1(t_i)\right|
\end{aligned}
\qquad (36)
$$

The distances are as shown below in Figure 23. Since L_1, L_2 and L_3 are constant and ΔE is obtained by subtracting the length at t_i from that at t_{i+1}, when calculating the instantaneous change in tendon length, they cancel out. Thus the equation for the instantaneous change in tendon length becomes:

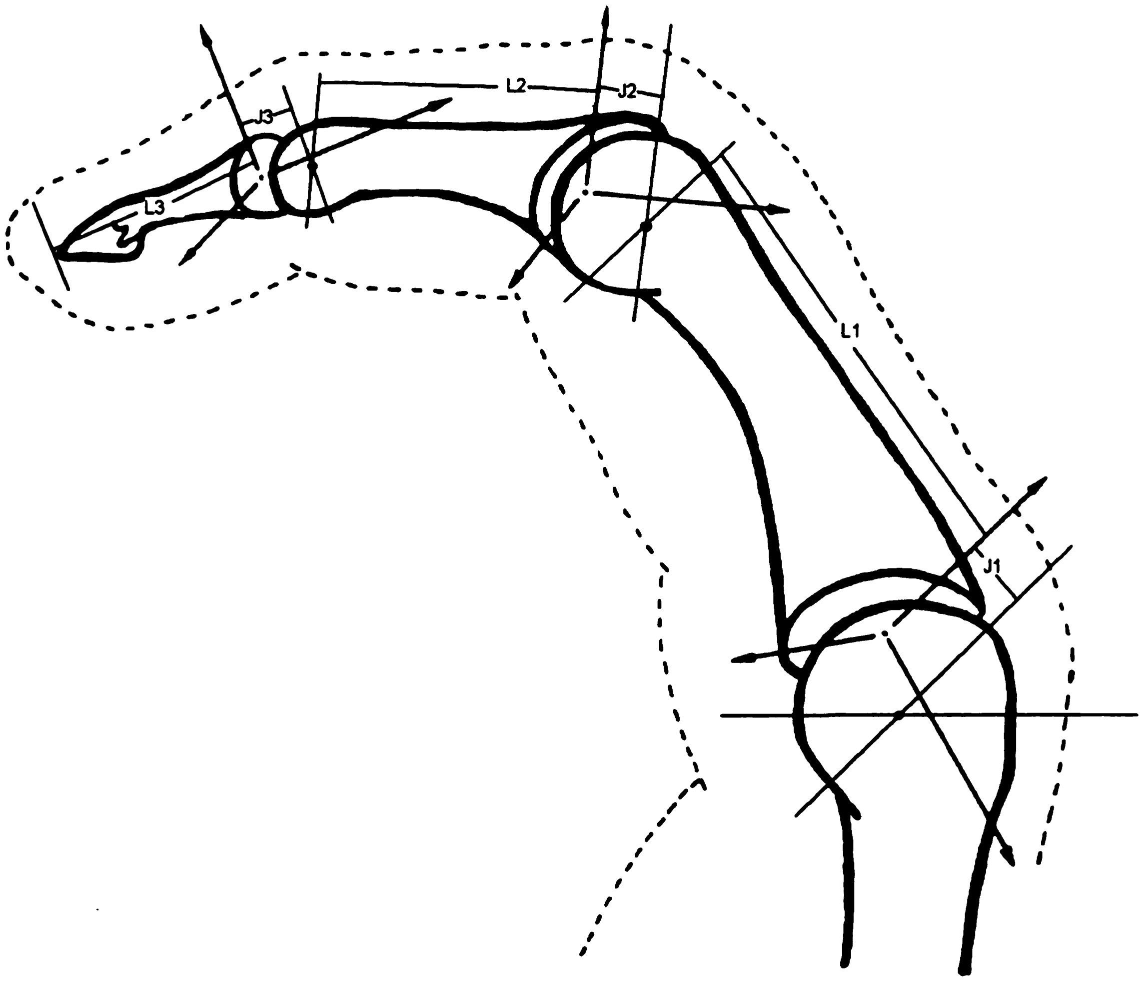

Figure 23--Lengths of Tendon Shown on Finger

$$\Delta E(t_i) = \Big[\Big(\left|\vec{P}_{D2}(t_i) - \vec{D}_3(t_i)\right| + \left|\vec{P}_{D1}(t_i) - \vec{D}_2(t_i)\right| + \left|\vec{P}_{D0}(t_i) - \vec{D}_1(t_i)\right|\Big) + E_W(t_i)\Big] - \Big[\Big(\left|\vec{P}_{D2}(t_{i+1}) - \vec{D}_3(t_{i+1})\right| + \left|\vec{P}_{D1}(t_{i+1}) - \vec{D}_2(t_{i+1})\right| + \left|\vec{P}_{D0}(t_{i+1}) - \vec{D}_1(t_{i+1})\right|\Big) + E_W(t_{i+1})\Big] \qquad (37)$$

PULLEY MODEL

According to the principal of conservation of energy, the heat energy dissipated into the carpal tunnel by the tendons rubbing on the carpal tunnel is equal to the frictional work done by those tendons.

Therefore, in order to determine the amount of heat energy dissipated in the carpal tunnel during a given activity, the instantaneous displacement of the tendon is multiplied by the frictional force of the tendon acting on the carpal tunnel. Since the displacements have already been determined, only the development of the equations for the frictional force need be described.

The model used to determine the frictional force generated by the tendons rubbing on the carpal tunnel is similar to the model of a belt on a pulley developed in most statics texts. The relationship between the tension in the belt at the end leading into the motion and that trailing the motion is

$$\frac{T_1(t_i)}{T_2(t_i)} = e^{\mu\alpha(t_i)} \qquad (38)$$

In this equation, T_1 is the leading edge tension, T_2 is the trailing edge tension, μ is the coefficient of static friction and α is the angle of contact between the belt and the pulley. The friction force can be obtained using the following

$$f(t_i) = T_1(t_i) - T_2(t_i) \qquad (39)$$

Finally, simplifying these two equations yields an equation for the friction, one in terms of T_2 and the other in terms of T_1.

$$f(t_i) = T_2(t_i)(e^{\mu\alpha(t_i)} - 1)$$
$$f(t_i) = T_1(t_i)(1 - e^{-\mu\alpha(t_i)}) \tag{40}$$

For the wrist, the situation is somewhat complicated by the fact that the direction of tendon motion changes. Since the tendon forces have been calculated for the hand side of the wrist and are unknown for the forearm side, the hand side forces must always be used to compute *f*. For flexion, the hand side forces are equivalent to T_1 in the above equations and for extension, the hand side forces are equivalent to T_2. Also, the instantaneous extension given above is positive for flexion and negative for extension. Therefore, the friction force *f* can be written, using the Heaviside step function as

$$f(t_i) = H\langle \Delta E(t_i) \rangle T_2(t_i)(e^{\mu\alpha(t_i)} - 1) + H\langle \Delta E(t_i) \rangle T_1(t_i)(1 - e^{-\mu\alpha(t_i)}) \tag{41}$$

All other variables in equation 41 are as described before. The coefficient of friction used in this model is 0.01 as it is the only value which is contained in each of the ranges for the coefficient of friction in a joint found in the literature (Linn, 1968), (Shih et al., 1993), (Armstrong & Chaffin, 1979).

The angle of contact, α, is defined as the flexion/extension angle of the wrist. Since the transverse carpal ligament runs perpendicular to the long axis of the forearm and the tendons run predominantly along that axis, the primary contact of the tendons on the ligament is along the angle defined by flexion/extension. Pronation and suppination of the wrist will cause the tendons to slide across the ligament slightly and will not significantly influence the angle of contact. Figure 24 and Figure 25 show the anatomy of the wrist and can be utilized to visualize the motion of the tendons in the carpal tunnel. Although axial rotation of the wrist may cause a small change in the contact angle, the change will not be significant.

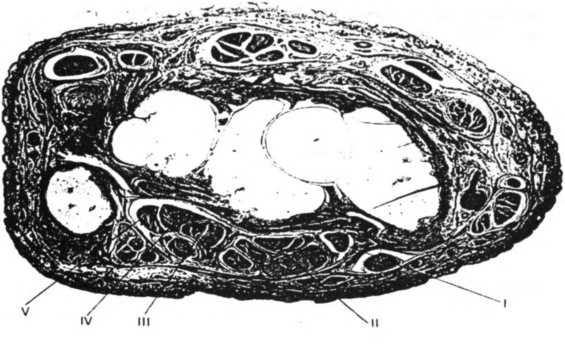

Figure 24--Cross-section of Wrist Showing Locations of Tendons in the Carpal Tunnel. The deep tendons are marked with their respective roman numerals. Taken from Landsmeer(Landsmeer, 1976), pg. 14.

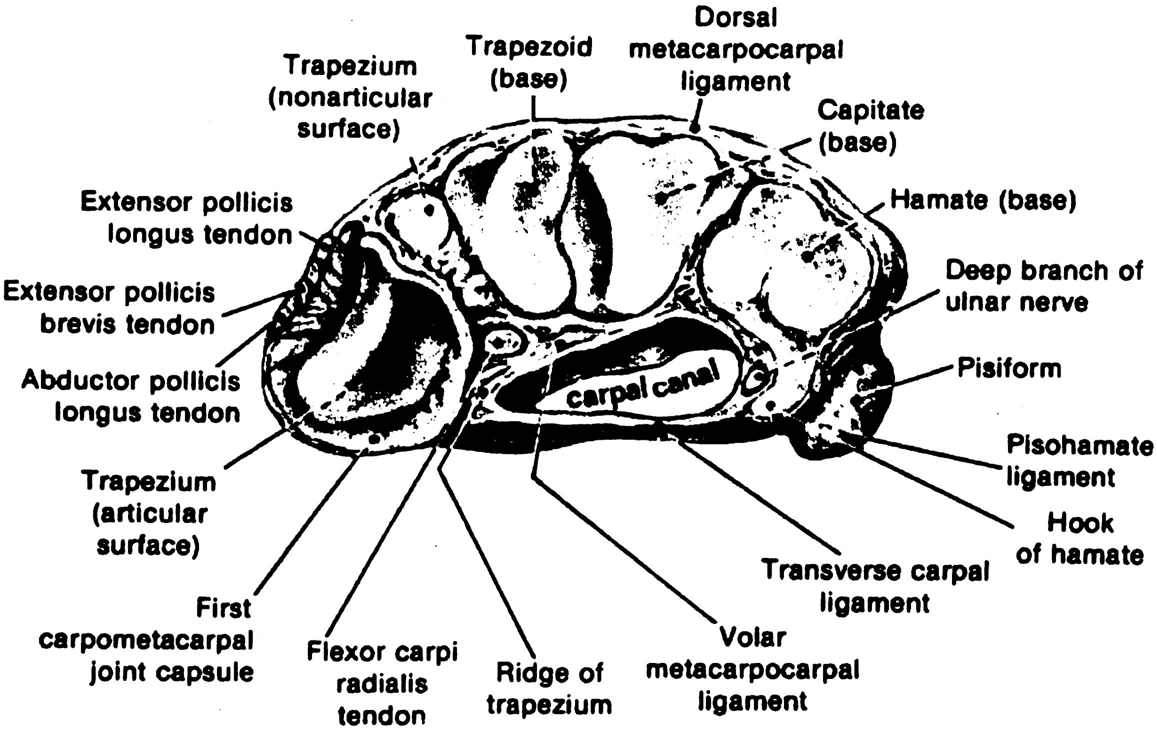

Figure 25--Cross-section of the Wrist Showing the Location of the Carpal Canal. Taken from Kaplan(Kaplan, 1965), pg. 103.

The frictional force between the tendons and the transverse carpal ligament or bones of the wrist can be calculated using the approach outlined above. The instantaneous energy dissipated can be calculated by multiplying the instantaneous frictional force by the instantaneous displacement of the tendon. For a particular activity, the total energy dissipated is equal to the sum of the instantaneous energies over the entire activity and over each of the tendons flexor tendons.

$$Energy = \sum_i \sum_j \Delta E(t_i)_j f(t_i)_j \tag{42}$$

where $\Delta E(t_i)_j$ is the instantaneous change in the extension of tendon j at time interval i and $f(t_i)_j$ is the instantaneous friction force in tendon j at time interval i.

By calculating the force in each of the tendons in the hand and using those data to determine the frictional force in the tendons passing over the transverse carpal ligament and then multiplying that force by the instantaneous displacement of the tendons, a total energy dissipated in the wrist from a given activity can be calculated. This value can be compared to values generated by activities to give a relative tendency of an activity to cause carpal tunnel syndrome.

CHAPTER 4—EXPERIMENTAL PROCEDURE

In order to verify the validity of this model, experimental position and force data were taken during the typing of a trial sentence. Once all of the data were accumulated, it was analyzed for use in the model and the model was verified.

In addition, tests were run on both the force and position measurement systems in order to verify the measurement systems were capable of sufficient resolution to gather data for use in the model.

TESTING PROTOCOL

One set of data was acquired according to the procedure to follow. These data were solely for the purpose of validating the model and were not intended as a clinical test from which major conclusions could be drawn. Testing was conducted under UCRIS approval, IRB # 93580.

Ideally, data would be gathered for the entire hand during a single test. The BTS camera system was incapable of resolving markers on the entire hand simultaneously due to the proximity of the markers on the hand. This proximity caused the markers to be superimposed with respect to the cameras during the test. When two markers are superimposed, the camera cannot differentiate between the two markers and therefore the system cannot resolve each target.

Since the system was unable to resolve markers on the entire hand, each finger was targeted and tested individually. Although this does not allow the hand as a whole to be modeled as precisely as if a single test were used, the fingers do act independently with the exception of a small degree of interconnectedness(Leijnse, 1997b; Leijnse et al., 1992; Leijnse et al., 1993). The independent motion of the fingers combined with the fact that this model assesses cumulative effects, allows test data acquired for each finger independently to accurately model the behavior of the entire hand when combined.

A test sentence was composed that would provide the most keystrokes by the fingers of the right hand in a short period of time (preferably about 10 seconds with an average typist). The test sentence was, "A kind, jolly person helps bumpkins." This sentence included each of the keys on the right hand side at the following frequencies: Y-1,

U-1, I-2, O-2, P-3, H-1, J-1, K-2, L-3, Semi-colon-0, N-3, M-1, Comma-1, Period-1.

The test sentence was typed three times for each finger. The tests for a given finger were conducted consecutively and the hand was retargeted for the next finger immediately following the third test. When retargeting, the markers on the hand and wrist were not moved. Since the time required to complete all of the tests resulted in only 165 seconds of total typing time over a six-hour testing period, muscle fatigue was not considered to be a problem. Given the redundancy of the test, however, the skill level and familiarity of the test subject with the sentence, did result in improved typing times as the tests progressed. This improved typing speed could skew the results versus a single test, as force generated in a muscle is a function of the speed of motion (Bigland & Lippold, 1954).

During the typing trials, the subject was seated in a comfortable typing chair that was adjusted to the subject's liking. The positioning of the subject in the workspace can be seen in Figure 26. In addition, the subject was asked if there was any difference between the feel of the instrumented keys and the non-instrumented ones. Keys were adjusted until the subject felt no difference. This allowed the testing to accurately imitate an actual typing situation.

At the start of the test, in order for the BTS system to allow tracking of the data points, the subject was asked to lift the right hand and angle it toward cameras 3 & 4. Although the motion analysis system recorded the position data as the subject moved from this position to the typing position, this was not considered part of the test for data analysis.

Between tests, the test subject was asked to relax. This period was only approximately five minutes between tests of a single finger. Changing of the markers to a different finger required approximately fifteen to twenty minutes.

Position and force data were synchronized using the maximum force and minimum global y coordinate for the first keystroke. Since the minimum global y coordinate corresponds with the bottom of the keystroke, it was assumed to also correspond to the maximum key force. The validity of this assumption will be discussed in the results section.

MEASUREMENT SYSTEM

Both motion and force data were needed to verify the accuracy of the model generated in this work. A BTS four-camera 100 Hz motion analysis system was used to collect the position data for each of the tests. The force exerted on the keyboard keys was measured using a standard computer keyboard with strain gages mounted on each key under the keycap. The laboratory setup can be seen in Figure 26.

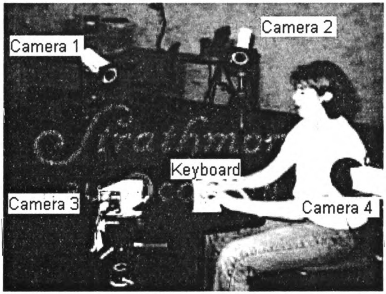

Figure 26—Laboratory Setup for Testing

Position Measurement

During each test, the hand was targeted with eleven retroreflective markers. Three markers were used to define each wrist, hand and proximal finger segment. The remaining two finger segments were each defined using two markers because it was assumed that these segments were only free to flex and extend and therefore remain in plane with the proximal segment. Analysis was performed to verify this assumption.

A targeting schematic is shown in Figure 27. In this figure, each target is identified by its anatomical position on the body segment and, in the case of the finger segments, a number indicating which segment it is on (2-proximal segment, 3-middle segment, 4-distal segment). In addition, the targets are numbered to facilitate identifying them later in this document. Although only the targeting schematic for the index finger is shown, the targeting system was consistent for each of the remaining digits.

During testing, position and force data were recorded at 100 Hz. This frequency is well over the actual frequency of controlled human movement, generally considered to be below 8 Hz(Winter, 1987).

In order for the camera system to determine the three-dimensional location of any given target, two cameras must be capable of "seeing" that target. In some of the frames of data, this criterion was not met for target 1. In those cases, that target was replaced mathematically in the following manner.

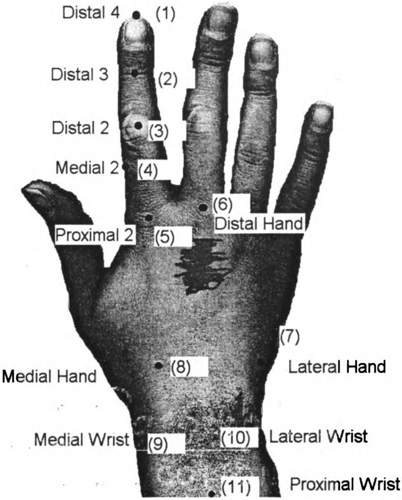

Figure 27—Targeting Schematic for Fingers

A relationship was determined between the flexion/extension angle for the PIP joint and that for the DIP joint. The assumption that there is a relationship between these two angles and that the DIP joint is not capable of fully independent motion is supported in the literature (Buchner et al., 1988; Harris & Rutledge, 1972; Thomas et al., 1968). Both the EDC and the FP muscles cross both the DIP and PIP joints and are the only two muscles controlling the distal finger segment, therefore, with no other muscles to allow independent motion of the distal segment, its motion is dependent upon the motion of the PIP joint. The relationship developed between the two angles was used to determine the DIP joint angle for the missing markers. The location of the marker 1 was then calculated using the average length of the distal segment and the calculated DIP joint angle using the equation

$$\{Position1\} = \{Position2\} + [R_m] \cdot \lfloor R_{\phi 4} \rfloor \cdot \{length4\} \qquad (43)$$

In Equation 43, $\{Position1\}$ is the position of target 1 in the global coordinate system, $\{Position2\}$ is the position of target 2 in the global coordinate system, $[R_m]$ is the rotation matrix between the global coordinate system and the middle segment coordinate system, $\lfloor R_{\phi 4} \rfloor$ is the rotation matrix between the middle segment coordinate system and the distal segment coordinate system and $\{length4\}$ is the vector between targets 2 and 1 expressed in the distal segment coordinate system.

Once the missing markers were reconstructed, the file containing the three dimensional position of all eleven markers throughout the motion was complete.

Force Measurement

Forces were measured using a specially designed keyboard (see

Figure 28). Each of the keys on the right hand of the keyboard was instrumented using a strain gage. A picture of one such key is shown in Figure 30. The strain gages were calibrated immediately after the testing to determine the force versus output voltage relationship.

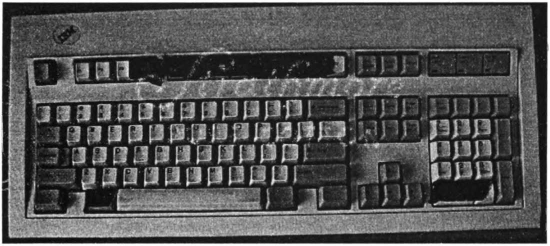

Figure 28–Instrumented Keyboard used for Measuring Finger Force on Keys during Testing

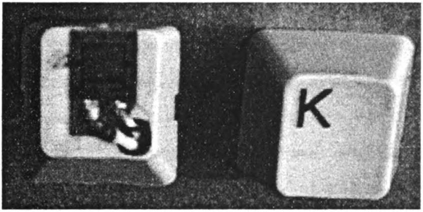

Figure 30—Instrumented Key used for Measuring Finger Force on Keys during Testing

Each key was produced by removing the key cap and sanding down the surface of the key. This was to allow the strain gage to be mounted on the top of the key without increasing the overall height of the key. In addition, the key was then much weaker making it deflect more under the applied loads and thus giving larger strain readings. Once the key was sanded, a hole was drilled in the key for the strain gage wires. Finally, the strain gage was mounted on the key.

Output from the strain gages was recorded using a National Instruments strain indicator and Labview. Data were taken at 100 Hz so that the force and position data could be synchronized.

DATA ANALYSIS

In order to utilize the position and force data in the model, they first had to be filtered and differentiated to provide the inputs necessary for the model—centroidal accelerations, angular velocities, angular accelerations, tendon displacements and external forces were calculated from measured data.

Filtering

Both the position and the force data were filtered to reduce the effects of electronic noise. All position data were filtered using a single pass 10^{th} order, Chebychev filter with a pass frequency of 8 Hz, a stop frequency of 8.5 Hz and an attenuation factor of 1000. The frequency domain response of this filter is shown in Figure 31. Although the frequency domain response of this filter is quite good, there is a time domain shift in the filtered data. This shift was calculated and final data use accounted for it.

Filtering was attempted at 6 Hz and 10 Hz to determine the effects of changing the cutoff frequency on the filtered data. It was found that there was not a significant difference between the signals output by the three filters.

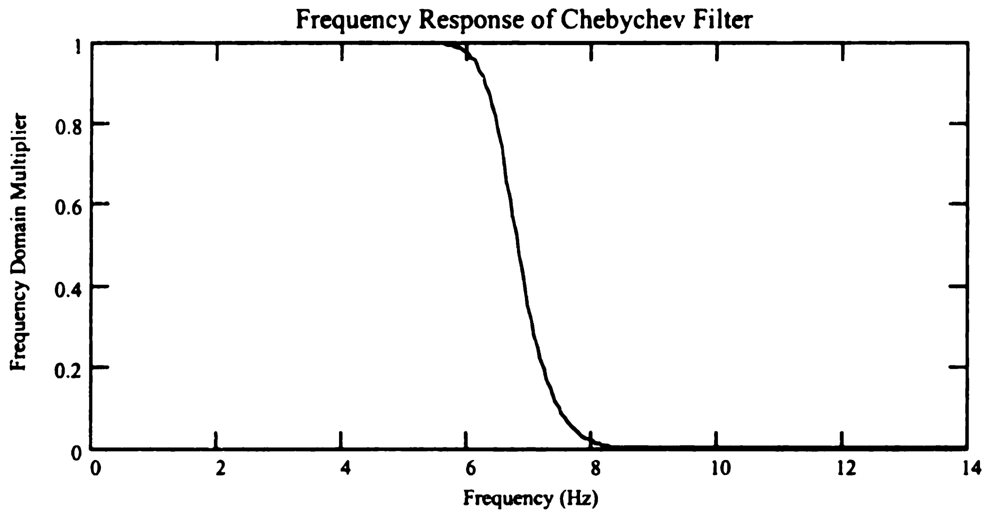

Figure 31—Frequency domain response of the Chebychev filter

The force data were edited rather than filtered. The signal to noise ratio in the force data was over 10 to 1 and therefore, those data points which fell below a certain threshold were forced to equal zero. For the x-component of the applied force, this threshold was o.2 N. For the y-component the threshold was 0.175 N; and for the z-component, it was 0.1 N.

Segment Lengths

The filtered position data were used to determine the lengths for each segment. These lengths were determined by using the distance between the distal and proximal markers and were later used to verify the accuracy of the rigid body assumption and to reconstruct markers which were lost because of obstructed camera views. For example, the length of the distal segment was calculated using equation 44. All others were calculated similarly.

$$length4 = \left|\{position1\} - \{position2\}\right| \tag{44}$$

Here, *length*4 is the length of the distal finger and the other variables are as defined previously.

Segment Unit Vectors

The filtered position data were also used to calculate the unit vectors for each segment. Since the markers were placed in the center of the joint in the local z-direction, the unit vector in the x-direction, $\hat{i}_d$, could be calculated using equation 45.

$$\hat{i}_d = \frac{\{position2\} - \{position1\}}{\left|\{position2\} - \{position1\}\right|} \tag{45}$$

The unit vectors in the x-direction for the middle and proximal finger segments were calculated using a similar equation.

The unit vector of the z-axis of the proximal two segments of the finger was then found by taking the cross product of $\hat{i}_p$ and $\hat{i}_m$, as shown below in equation 46. The order assured correct orientation of the z-axis in accordance with the right hand rule. This method would result in a singularity only in the case that $\hat{i}_p$ and $\hat{i}_m$ are collinear. During the course of typing with the normal hand, this does not occur as the finger is naturally arched to position the fingertip over the keys.

$$\hat{k}_p = \hat{k}_m = \frac{\hat{i}_p \times \hat{i}_m}{\left|\hat{i}_p \times \hat{i}_m\right|} \tag{46}$$

The unit vector for the z-axis of the distal segment was found by correcting the $\hat{k}_p$ to be perpendicular to $\hat{i}_d$. This was done by subtracting that portion of $\hat{k}_p$ that was parallel to $\hat{i}_d$ from $\hat{k}_p$ and dividing by the magnitude of that vector. This is shown mathematically in equation 47.

$$\hat{k}_d = \frac{\hat{k}_p - \left(\hat{k}_p \cdot \hat{i}_d\right)\hat{i}_d}{\left|\hat{k}_p - \left(\hat{k}_p \cdot \hat{i}_d\right)\hat{i}_d\right|} \tag{47}$$

Finally, the unit vectors for the y-axes were calculated by taking the cross product between each segments' unit vectors for the x and z-axes. This procedure was used for all of the finger segments and an example is given in equation 48.

$$\hat{j}_d = \hat{k}_d \times \hat{i}_d \tag{48}$$

In order to form the coordinate systems for the hand, the x-axis was first formed to lie along the third metacarpal. This was accomplished by subtracting coordinates of target 6 from the mean of the coordinates of targets 7 and 8 and then dividing by the magnitude of the vector formed. See equation 49 for the procedure.

$$\hat{i}_h = \frac{\frac{\{position7\}+\{position8\}}{2} - \{position6\}}{\left|\frac{\{position7\}+\{position8\}}{2} - \{position6\}\right|} \tag{49}$$

A second axis in the plane of the hand was then formed by subtracting the coordinates of target 7 from those of target 8 and dividing by the magnitude of that vector.

$$\hat{v}_h = \frac{\{position8\}-\{position7\}}{\left|\{position8\}-\{position7\}\right|} \tag{50}$$

$\hat{v}_h$ was then crossed with the $\hat{i}_h$ and that vector was divided by its magnitude to form $\hat{j}_h$ (it was necessary to divide the cross product by its magnitude since the two unit vectors being crossed were not necessarily perpendicular).

$$\hat{j}_h = \frac{\hat{v}_h \times \hat{i}_h}{\left|\hat{v}_h \times \hat{i}_h\right|} \tag{51}$$

Finally, the unit vector for the z-axis was formed by crossing $\hat{i}_h$ with $\hat{j}_h$.

$$\hat{k}_h = \hat{i}_h \times \hat{j}_h \tag{52}$$

A similar procedure to the above was used for the forearm. The unit vector of the x-axis was formed by subtracting the mean of the coordinates target 9 and target 10 from the coordinates of target 11.

$$\hat{i}_w = \frac{\{position11\} - \frac{\{position9\} + \{position10\}}{2}}{\left|\{position11\} - \frac{\{position9\} + \{position10\}}{2}\right|} \tag{53}$$

A second axis in the plane of the wrist was then formed by subtracting the coordinates of target 10 from those of target 9 and dividing by the magnitude of the vector obtained.

$$\hat{v}_w = \frac{\{position9\} - \{position10\}}{|\{position9\} - \{position10\}|} \tag{54}$$

The $\hat{v}_w$ was crossed with the $\hat{i}_w$ and that vector was divided by its magnitude to form $\hat{j}_w$.

$$\hat{j}_w = \frac{\hat{v}_w \times \hat{i}_w}{|\hat{v}_w \times \hat{i}_w|} \tag{55}$$

Finally, $\hat{k}_w$ was formed by crossing $\hat{i}_w$ with $\hat{j}_w$.

$$\hat{k}_w = \hat{i}_w \times \hat{j}_w \tag{56}$$

Joint Angles

Once the unit vectors for the segmental coordinate systems were formed, the joint angles (Euler angles) were determined. For the DIP and PIP joints, since these were assumed to only allow flexion and extension, the rotation angle was calculated by taking the arc cosine of the dot product between the two adjacent segments' local x-unit vectors. An example of this for the DIP joint is shown below in equation 57. Although, this method does not yield the sign of the angle, hyperextension of these joints in a normal person is not expected and therefore, the negative angle should not occur.

$$\phi 4 = a\cos\left(\hat{i}_m \cdot \hat{i}_d\right) \tag{57}$$

For the MCP and wrist joints, a slightly more complicated procedure was necessary due to the unrestricted rotation of those joints. To calculate the rotations of these joints, rotation matrices were formed using the unit vectors for each segment expressed in the global system. Then the joint rotation matrix was formed by multiplying the distal segment rotation matrix by the transpose of the proximal segment rotation matrix. The Euler angle rotation matrix for this system is

$$\begin{pmatrix} \cos(\theta)\cdot\cos(\phi) & \cos(\theta)\cdot\sin(\phi) & -\sin(\theta) \\ -\cos(\gamma)\cdot\sin(\phi) + \sin(\gamma)\cdot\sin(\phi)\cdot\cos(\theta) & \cos(\gamma)\cdot\cos(\phi) + \sin(\gamma)\cdot\sin(\phi)\cdot\sin(\theta) & \sin(\gamma)\cdot\cos(\theta) \\ \sin(\gamma)\cdot\sin(\phi) + \cos(\gamma)\cdot\cos(\phi)\cdot\sin(\theta) & -\sin(\gamma)\cdot\cos(\phi) + \cos(\gamma)\cdot\sin(\phi)\cdot\sin(\theta) & \cos(\gamma)\cdot\cos(\theta) \end{pmatrix} \tag{58}$$

The first rotation, ϕ (representing flexion/extension), was performed about the fixed (more proximal of two bodies being considered) Z-axis; the second rotation, θ (representing abduction/adduction), about the line of nodes which corresponds to a y-axis and the final rotation, ψ (representing axial rotation), was about the moving (more distal of two bodies being considered) x-axis.

This matrix was set equal to the joint rotation matrices and the joint angles were obtained for each joint.

Center of Gravity

The filtered raw data were also used to compute the center of gravity for each of the finger segments. The center of gravity was assumed to be located midway between the proximal and distal markers in the local coordinate system x and z directions. In the local y-direction, the center of gravity was assumed to be half the thickness measurement for the relevant section below the two markers. See equation (59 for an example of the computation of the center of gravity for the distal finger segment.

$$\{cg4\} = \frac{\{position1\} - \{position2\}}{2} + [R4] \cdot \{offset\} \tag{59}$$

Here, $\{cg4\}$ is the location of the center of gravity of the distal segment in the global coordinate system, $[R4]$ is the transformation matrix from the local distal coordinate system to the global system and $\{offset\}$ is a vector in the local coordinate system allowing the center of gravity to be shifted from the surface of the segment to the center of the segment with respect to the thickness.

Differentiation

Once the angles and centers of gravity were known, each was filtered using the same Chebychev filter as was used on the raw data. In gait analysis, the filter is applied to the raw data and then again to the data after each numerical differentiation. In this research, the second derivatives of the data were obtained directly and, therefore, it is not necessary to apply the filter after the first differentiation. Since both differentiation and filtering are considered to be linear operators, the order of operation is theoretically irrelevant.

The data obtained from the second filter are differentiated using the following five-point central difference formula for the second derivative.

$$f'' = \frac{-f_{i+2} + 16f_{i+1} - 30f_i + 16f_{i-1} - f_{i-2}}{12\Delta t^2} \tag{60}$$

Once the data were differentiated, it was again filtered using the same Chebychev filter.

Local Coordinates

All of the previous work was done with the data in the global coordinate system. In order to utilize the data in the equations of motion, they were transformed into the local coordinate systems. This was achieved by multiplying the vectors in the global system by the rotation matrix from the global system to the local system.

For the angular acceleration data of the proximal finger segment, a somewhat different approach needed to be used. Since the angles, angular velocities and angular accelerations are based upon the non-orthogonal Euler angle directions, transformation equations for the above-mentioned quantities were developed. These are

$$\alpha 2_x = \ddot{\gamma}2 + \ddot{\phi}2 \cdot \sin(\phi 2)\sin(\gamma 2) \quad (61)$$

$$\alpha 2_y = \ddot{\theta}2 \cdot \cos(\gamma 2) + \ddot{\phi}2 \cdot \sin(\theta 2)\cos(\gamma 2) \quad (62)$$

$$\alpha 2_z = -\ddot{\theta}2 \cdot \sin(\gamma 2) + \ddot{\phi}2 \cdot \cos(\theta 2)\cos(\gamma 2) \quad (63)$$

In these equations, the angular accelerations about the x, y, and z-axes for the local proximal finger segment coordinate system are calculated by multiplying the Euler angle angular accelerations by functions of the Euler angles for the proximal finger segment. The angular velocities were then transformed into the correct coordinate system using the same transformations as were used on the angular accelerations.

Masses and Moments of Inertia

The masses, moments of inertia and tendon unit vectors were calculated in accordance with the procedure outlined in Chapter 3.

MODEL IMPLEMENTATION

All of the inputs-unit vectors, accelerations and forces-were input into the system of equations formed by the equations of motion and the constraints due to the extensor mechanism. These equations, as well as the optimization criteria and the stress limits on the muscles, were used to solve for the forces in the tendons.

Optimization

A Quasi-Newtonian linear search method was utilized to solve the underdetermined system of equations. MATLAB automatically selected this search because all of the constraint equations were linear. Because of the inherent instability of optimization, the results obtained from the optimization were highly dependent upon the initial conditions supplied. Therefore, a fairly elaborate set of initial conditions was supplied to the optimization routine.

It was assumed that the joints would absorb the majority of the applied force since the tendons are unable to support a compressive force and the applied load was compressive.

The moment about the z-axis was assumed to be constrained by the tendons since there is no applied moment constraint. Since F_y (y-component of the applied force) is responsible for the majority of the moment about the z-axis, all tendon initial conditions were based upon it. If F_y is positive, this indicates that the angle between the palmer side of the distal finger segment and the vertical is less than ninety degrees. If it is negative, that same angle is greater than ninety degrees. When the angle is less than ninety degrees, depressing the key causes a moment that extends the finger if unrestricted. Therefore, a larger flexor force is necessary to maintain equilibrium. However, when the angle is greater than ninety degrees, the moment caused by depressing the key tends to flex the DIP and perhaps even the PIP joints depending on the magnitude of the angle while still extending the MCP joint. Therefore, the extensor muscle must be used to maintain equilibrium of the distal two segments, but flexor muscles must be used to maintain equilibrium of the proximal segment. In order to maintain this complex condition of equilibrium, the LU, RI and UI muscles must be activated.

These assumptions led to the initial conditions described below:

Case 1, applied force is zero--all forces and moments are set to zero.

Case 2, applied forces are non-zero, angle between distal finger segment and keyboard is less than ninety degrees:

1. Rxdip, Rxpip and Rxmcp were set equal to F_x.
2. Rydip, Rypip and Rymcp were set equal to F_y.
3. Rzdip, Rzpip and Rzmcp were set equal to F_z.
4. All moments (Mxdip, Mydip, Mxpip, Mypip and Mxmcp) were set equal to zero.

5. The tendon forces were assigned the following values:
   a. FP = FS = F_y*10
   b. TE = LU = F_y/6*10
   c. RB = UB = ES = F_y/12*10
   d. LE = F_y/2*10
   e. RI = UI = F_y/30*10

Case 3, applied forces are non-zero, angle between distal finger segment and keyboard is less than ninety degrees:

1. Rxdip, Rxpip and Rxmcp were set equal to F_x.
2. Rydip, Rypip and Rymcp were set equal to F_y.
3. Rzdip, Rzpip and Rzmcp were set equal to F_z.
4. All moments (Mxdip, Mydip, Mxpip, Mypip and Mxmcp) were set equal to zero.
5. The tendon forces were assigned the following values:
   a. FP = FS = F_y/12
   b. TE = 2F_y/3
   c. RB = UB = ES = RI = UI = LU = F_y/3
   d. LE = F_y

Energy Calculation

Once the equations of motion were solved to determine the tendon forces, the tendon forces were utilized to determine the friction force between each flexor tendon and the transverse carpal ligament. Each friction force was then multiplied by the respective tendon displacements to calculate the energy dissipated in the carpal tunnel due to friction between the tendon and the transverse carpal ligament. The total energy dissipated was then calculated by summing the energies for the independent tendons.

CALIBRATION

The BTS system was calibrated using a custom calibration stand with 4 rows and 7 columns of 5 mm retroreflective markers in a 50 mm by 50 mm grid. Four planes each separated by 150 mm were used for the standard calibration procedure including calibrating the cameras for both position and distortion. The cameras were placed in a relatively symmetric pattern to maximize convergence of the system when obtaining marker positions. Actual calibration parameters and camera locations are given in Appendix D.

Calibration of the BTS camera system allows the eleven unknown transformation constants to be found. There are only two direct linear transformation equations used in finding these transformation constants, one for each coordinate direction in camera space (a two-dimensional space). Therefore, a minimum of six markers must be used to determine the eleven constants. If six are used, the system is overdetermined. The method of least squares is used to solve the overdetermined system. This method becomes more accurate as more known points are used. With the before stated number of rows, columns and planes used in the calibration, a total of 112 known points was used to solve for the transformation constants.

The keyboard used to measure force data was also calibrated. Immediately following the tests, each key was loaded in 1-ounce increments to 6 ounces and the electrical response of the strain gages on the keys was recorded. The weights were then removed one at a time while the strain gage response was again recorded. A curve was fitted to the force-voltage data to obtain the slope and the intercept of the data. These values were then applied to the test voltages to yield the force time curves. The calibration curve for the j key is shown in

Figure 32. The calibration curves for all other keys can be found in Appendix F.

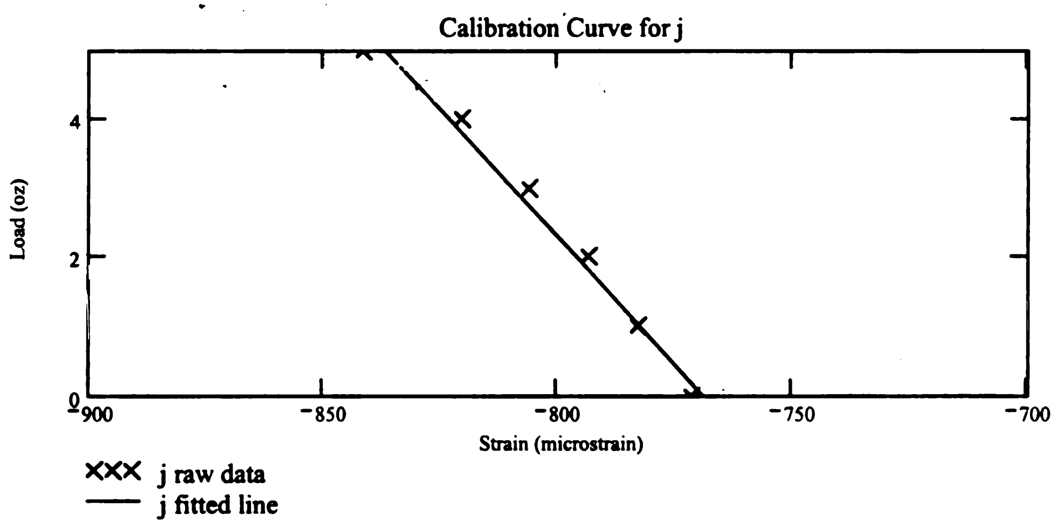

Figure 32—Calibration Curve for j Key

QUALIFYING TESTS

Since this model depends upon obtaining accurate position and force data, the accuracy and repeatability of both the BTS camera system and the keyboard were measured in order to assure the validity of the final test results. An additional concern with the position data was soft tissue motion. The effects of this were also determined using the test data.

In order to verify accuracy and repeatability of the BTS camera system, two 3-mm retroreflective markers were set at a fixed distance of 17.38 mm from each other. These were then moved about in the calibrated space for 2 seconds yielding two hundred data points with which to verify the accuracy of the space. These data were then analyzed to determine the variation in the distance between the two markers. In addition, the entire file was tracked using every combination of two cameras (a total of six combinations) to determine the location of the markers so that any bias to a particular camera or set of cameras could be detected.

In order to verify the accuracy of the keyboard keys, each key was tested using calibrated weights. The keys were loaded from zero to 16.68 N (60 ounces) in 1.39 N (5-ounce) increments. This range was chosen because previous research suggested that the maximum force generated when depressing a key in normal typing is 5.3 N (Rempel, Dennerlein, Mote, & Armstrong, 1994). The weights were then removed one at a time. This procedure was repeated three times for each key. During this testing, data were taken at 10 Hz. This allowed for averaging of the force values at each step without having an unnecessarily large amount of data. Averaging the data was necessary because of slight motion of the weights on the keys causing variation of the gage readings.

In order to verify that soft tissue motion was not significant, the length of the finger segments was assumed to be constant throughout the test. If, in fact, the finger segments are rigid bodies as is being assumed, the length of each segment should be constant. Any variation in the length can be attributed to two causes—inaccuracy of the measurement system and soft tissue motion. Under the forces involved, it is safe to assume that the bones themselves do not deflect significantly. The inaccuracy of the system itself was evaluated utilizing the constantly spaced markers. Although there is no way to isolate the soft tissue motion from the system inaccuracy, some conclusions can be drawn about soft tissue motion by comparing the magnitudes of the errors in the test with the two constantly spaced markers and the errors in the calculation of the length of the finger segments.

CHAPTER 5—RESULTS AND DISCUSSION

In addition to formulating and testing the model for predicting CTS, the test data were examined to determine the necessity of modeling the typing task utilizing inertial terms as well as the stability of the optimization technique. The accuracy of the BTS motion analysis system in tracking position data for the hand and the keyboard used for measuring force data was tested to determine their capabilities in acquiring position and force data respectively for the hand.

ANALYSIS METHODS

In order to simulate the positions for which the markers were not visible to two cameras, a relationship was developed between the PIP and the DIP. This was used in conjunction with the average length of the distal segment to determine the position of the distal target on the distal finger segment as outlined in the experimental procedures section. The relationship between the PIP and DIP angles was determined first by using a first order regression algorithm. In addition, coefficients were calculated for polynomials of up to fifth order. Note, that there is not a significant increase in the correlation values as the order of the polynomial increases. Also, the performance of the higher order polynomials at higher values of φ4, the flexion/extension angle of the PIP joint, is not better than that for the first order polynomial. Below, in Table 3, the coefficients and R^2 correlation values for each of the polynomials tested are listed.

Table 3—Polynomial Coefficients for Relationship Between φ3 and φ4

	C_0	C_1	C_2	C_3	C_4	C_5	R^2
1	0.894	-0.277	--	--	--	--	0.952
2	0.508	0.196	-0.051	--	--	--	0.964
3	-0.93	2.414	-1.043	0.202	--	--	0.966
4	-1.016	1.841	-0.319	0.105	0.03	--	0.966
5	-40.893	139.83	-186.572	121.633	-37.948	4.592	0.969

Although the R^2 correlation for the first order equation is 0.952, a relatively strong correlation, the equation was weakest when ϕ4 was the greatest. ϕ4 was the greatest at those points that needed to be replaced and therefore, this was not the best equation to use. The equation was modified to get better correlation at those points where the angle was the greatest. This was done manually and the R^2 value was calculated. The resulting equation was

$$\phi 4 = 0.9\phi 3 - 0.25 \quad \textbf{(64)}$$

This equation also yielded an R^2 correlation of 0.952, however, it gave a smaller deviation from the actual values at large angles.

Figure 34 below shows the values of the three curves (original, generated using linear regression values and generated using modified values) over time. Figure 35 is a graph of $\phi 3$ versus $\phi 4$ for the actual data (shown as +'s) and the two lines created by linear regression (solid line) and the modified linear equation chosen (dashed line). Note that the modified curve gives better results at higher flexion values of the angle.

Once the equation for the relationship between the PIP and DIP joint angles was determined and the points for the distal target were reconstructed, the Euler angles for each joint were calculated as well as the positions for the center of gravity for each segment. The Euler angles for the entire test are shown below in Figure 36 -

Figure 38. In addition, the ranges of motion for the test are given in Table 4.

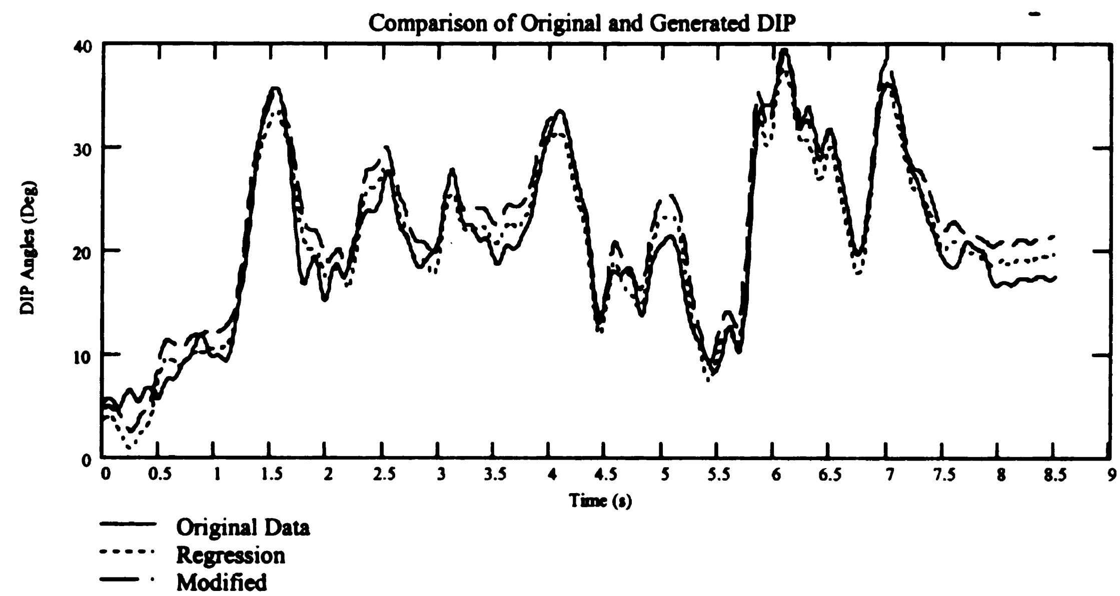

Figure 34—Graph of Comparison of Original, Regressed, and Modified Curves for the DIP Angle

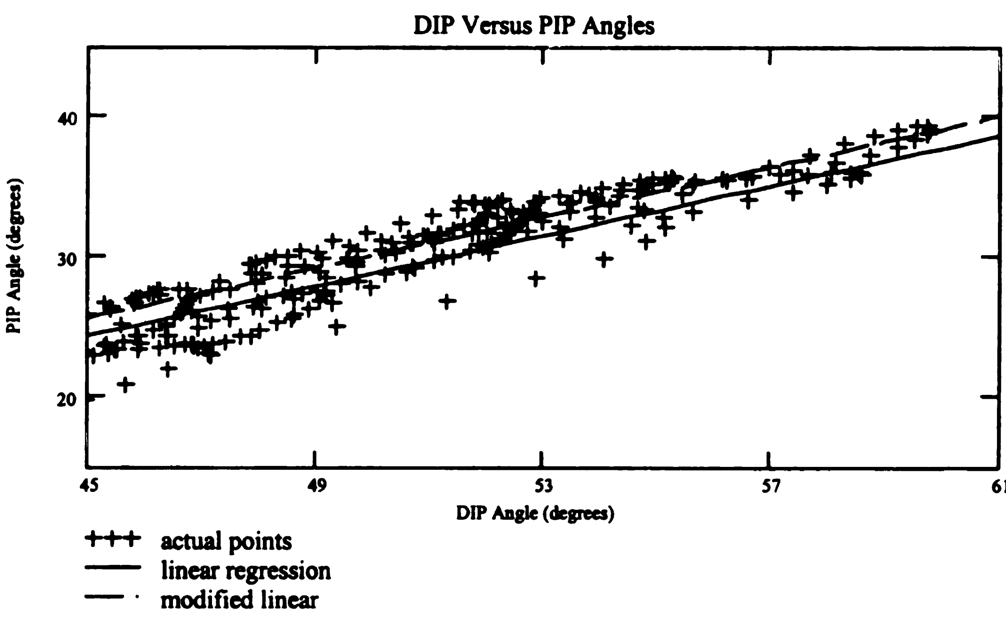

Figure 35—Graph of the DIP versus PIP Angles Showing Actual Points, Linear Regression and Modified Linear Curve

The orientation for the hand and wrist coordinate systems is not initially aligned with those of the finger. Therefore, the absolute values of these angles cannot be compared with the positions of the finger, however, the ranges of motion for abduction/adduction and axial rotation of the MCP joint and all motion of the wrist joint are valid since these ranges do represent the total motion of the joints.

Table 4—Range of Motion for Joints During Test

Joint	Flexion/ Extension (deg)	Range	Abduction/ Adduction	Range	Axial Rotation (Pronation/ Suppination)	Range
DIP	-5 to 39	44	-------	-----	--------	
PIP	20 to 60	40	-------	-----	--------	
MCP	7 to 53	46	-9 to 11	20	11 to 29	18
Wrist	32 to 64	32	-23 to -5	18	-8 to 6	14

Note that the range of motion of the MCP joint and the wrist is much larger for flexion/extension than for either abduction/adduction or axial rotation. This is because the motion of the fingers in typing is primarily to depress the keys, which is achieved through flexion of the finger. Abduction/adduction provides fine control to relocate the fingers over the chosen keys while gross control is supplied by the wrist and forearm. Therefore, the necessary range of motion for abduction/adduction is considerably smaller than that for flexion/extension.

As noted earlier, there is a close correlation between the PIP and DIP flexion/extension angles. This is clearly shown in Figure 36. Although the correlation is not exact ($R^2 = 0.952$ for the linear coefficients described above), there is a very close relationship between the two angles.

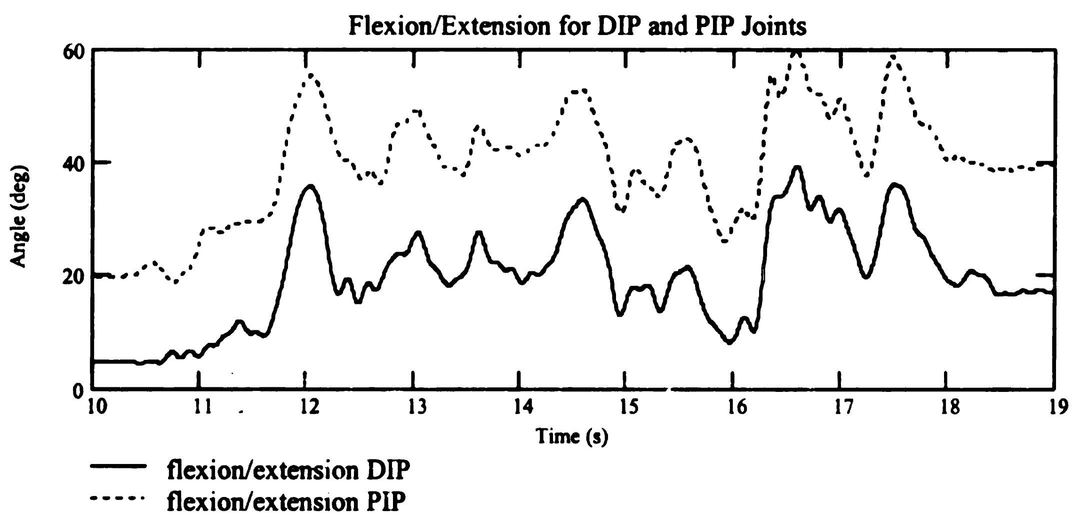

Figure 36—Flexion/Extension Angles for the DIP and PIP Joints

Figure 35 shows the relationship between the Euler angles of the MCP joint. The MCP joint is saddle shaped which causes some degree of coupling between abduction/adduction and axial rotation at the joint. Note that although the relationship is not as strong as that for the flexion/extension angles in the DIP and PIP joints, the abduction/adduction angle and the axial rotation angle follow similar trends. Also, the flexion/extension angle appears to be independent of the other two angles as would be expected since flexion/extension is controlled by different muscles than the other two motions. Flexion/extension is controlled primarily by the FP, FS and ED muscles while abduction/adduction is controlled primarily by the IO and LU muscles.

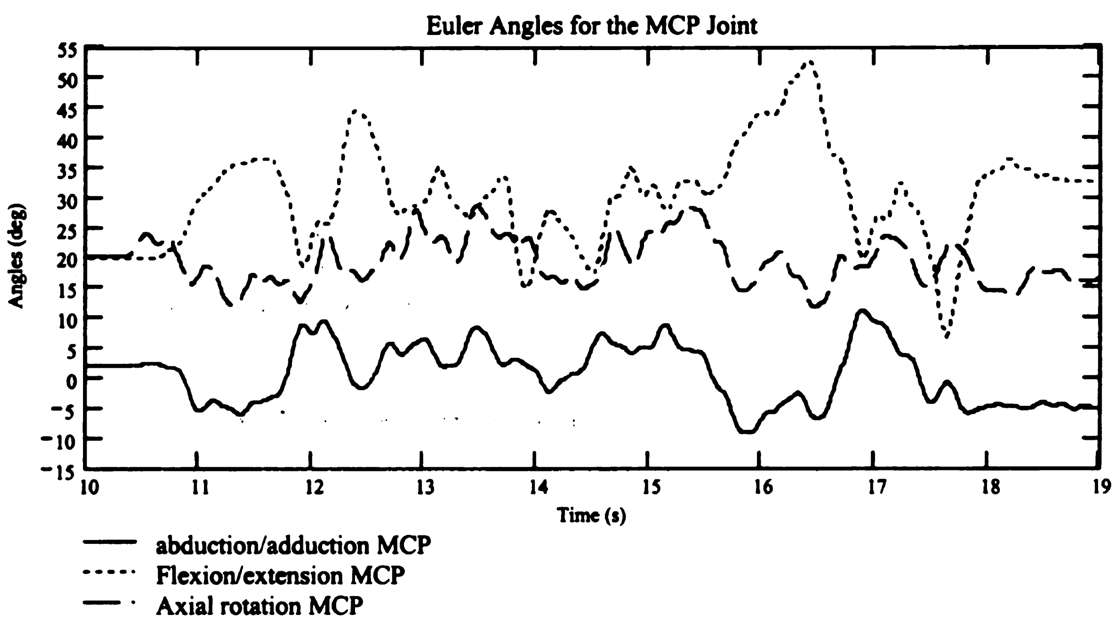

Figure 35—Euler Angles for MCP Joint

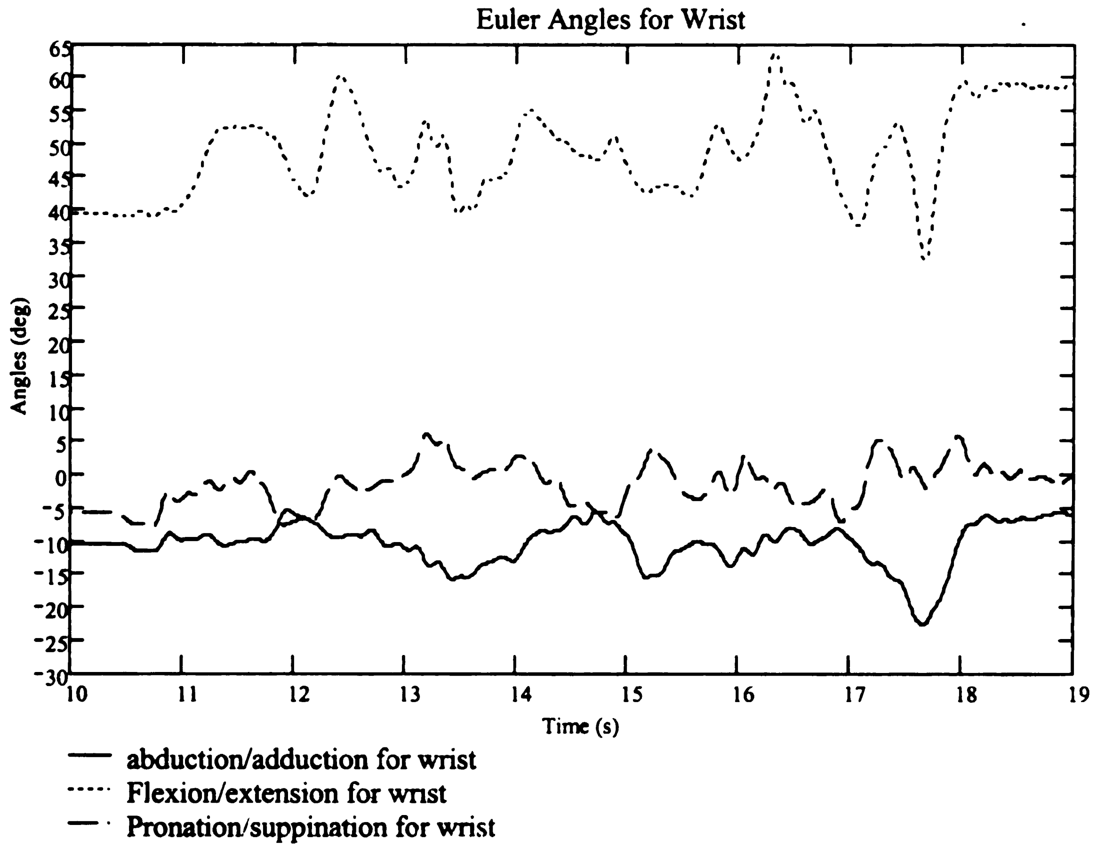

Figure 38—Euler Angles for the Wrist

Figure 38 is a graph of the Euler angles for the wrist. The range of motion for the wrist is smaller than that for any of the other joints. This is because there is very little gross motion of the wrist in typing and the fingers can accomplish most of the motion. Also, although the range of motion for abduction/adduction of the wrist is eighteen degrees, for the majority of the test, this motion was constrained to less than eleven degrees with the remaining seven only occurring when the operator used the enter key. A similar large motion would be expected in order to reach any of the keys on the outer edge of the keyboard. It is also interesting to note that each of the Euler angles for the wrist is independent as the wrist is truly capable of controlled three-dimensional motion.

In order to complete the analysis of the motion of the hand, force data must be combined with position data. Since the computers utilized in collecting the force and the position data were not synchronized, the fact that maximum key force will occur at the bottom of keystroke was utilized to synchronize the data. From Figure 37, it can be seen that there is good correlation between the peak of

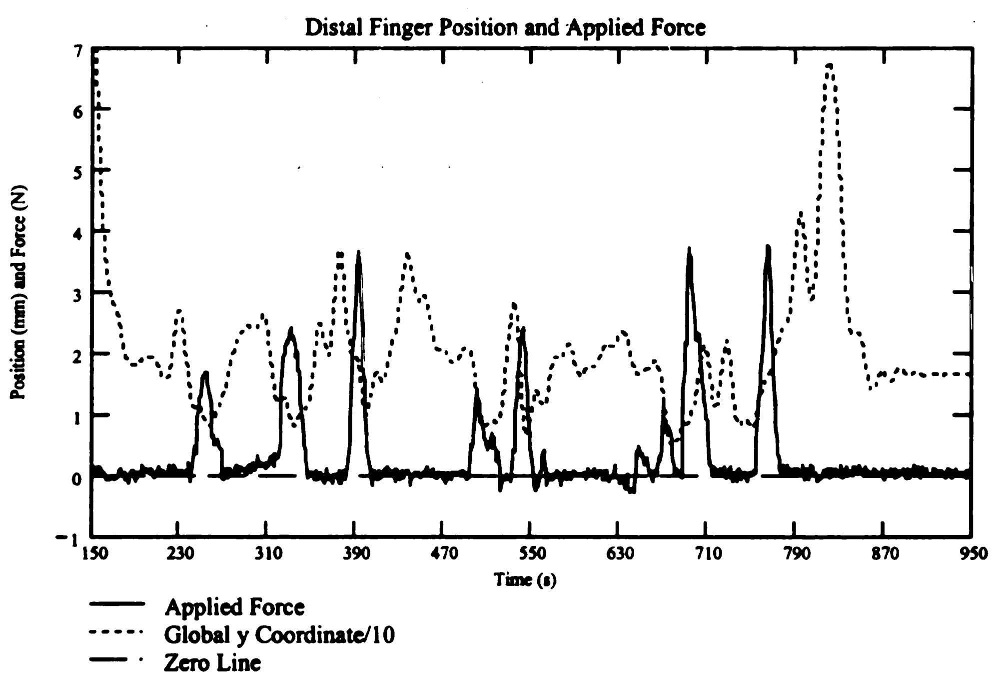

Figure 37--Position of Distal Finger Segment and Applied Force vs. Time for Determining Timing of Data

the force magnitudes and the minimum global y position of the distal segment although this correlation seems to become worse with increasing time. This declining correlation could be due to the different and unsynchronized clock speeds of the two computers taking data.

DYNAMIC VERSUS QUASI-STATIC ANALYSIS

Prior to calculating the tendon forces, the magnitudes of applied force (force between the keys and the finger) and the inertial terms in the equations of motion were compared to determine if it would be necessary to include the inertial terms in the calculation of the tendon forces. If the inertial terms are included in the analysis it is considered to be a dynamic analysis. If not, the analysis is considered to be quasi-static.

Figure 38 -

Figure 40 show the magnitudes of the inertial terms for the proximal, middle and distal segments respectively. Note that the maximum magnitude of any of the inertial terms is 0.06 N. The magnitude of this term is very low due to the low mass of the finger segments ($m_{proximal}$ = 0.014 kg, m_{middle} = 0.00554 kg and m_{distal} = 0.00377 kg).

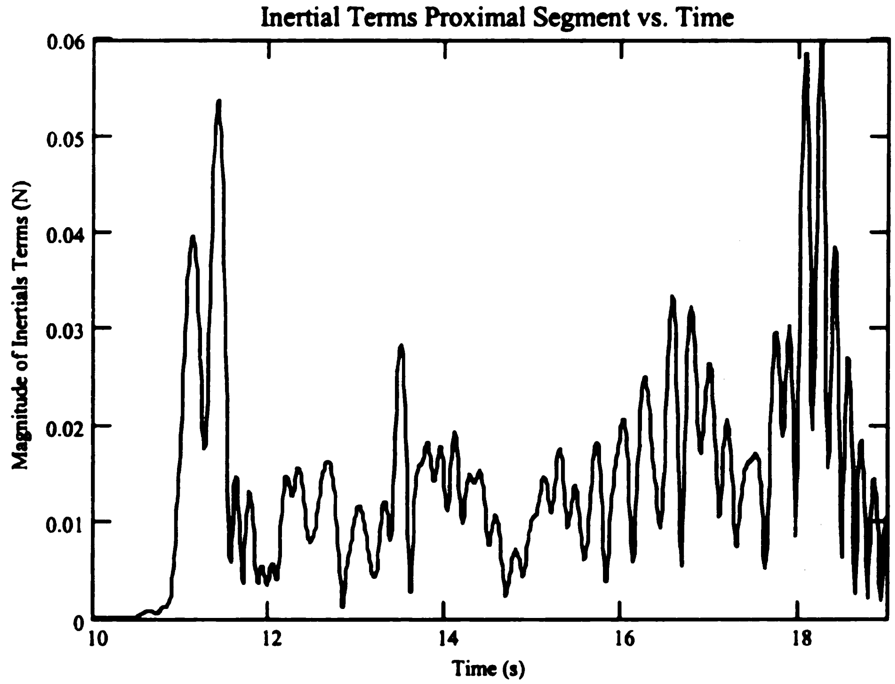

Figure 38--Magnitude of Inertial Terms on Proximal Segment Versus Time

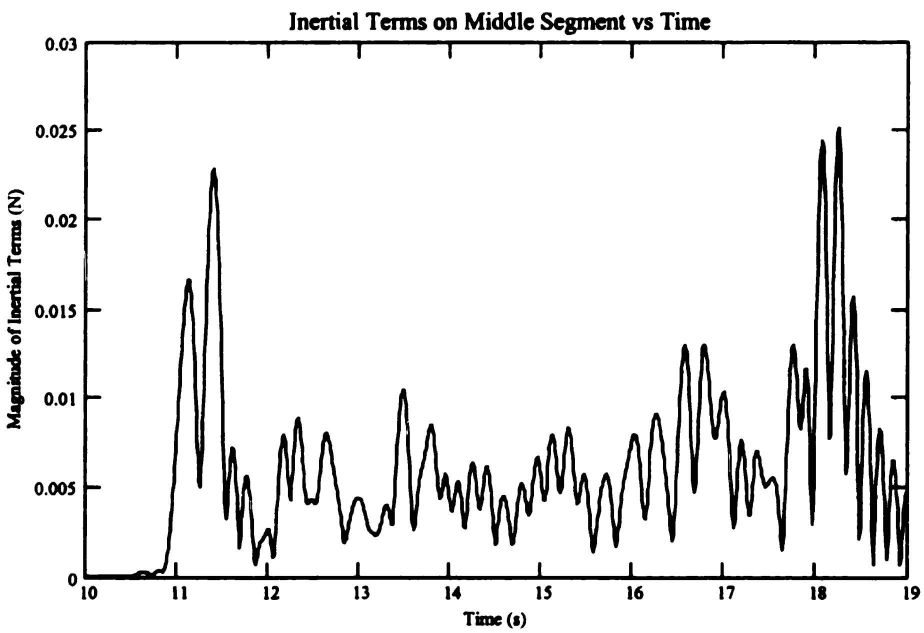

Figure 39--Magnitude of Inertial Terms on Middle Segment Versus Time

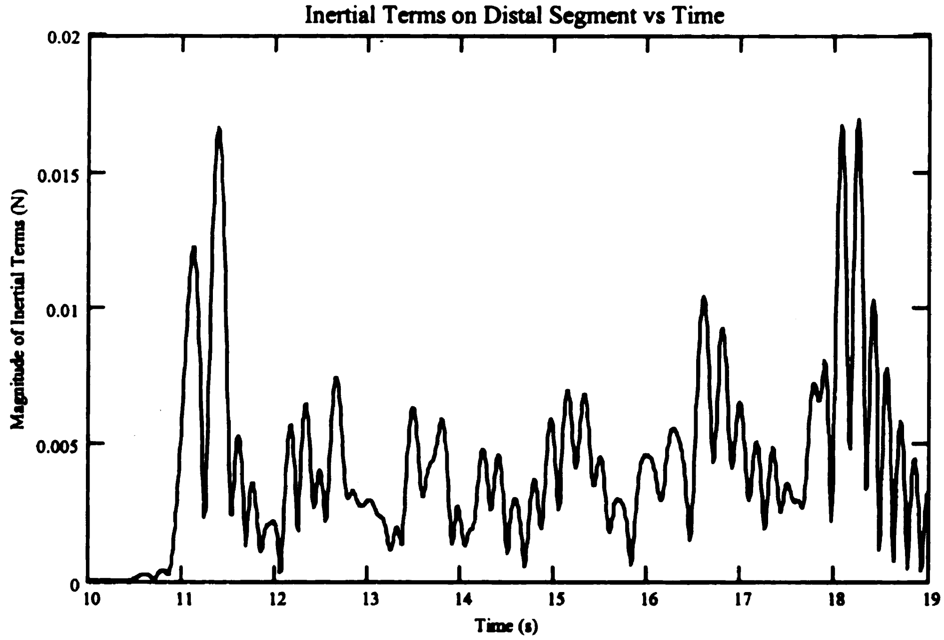

Figure 40--Magnitude of Inertial Terms on Middle Segment Versus Time

The force applied to the keys is between 0.5 N and 4 N, at least two orders of magnitude higher than the inertial forces. Because of this difference, inertial effects were neglected in determining the tendon forces.

OPTIMIZATION RESULTS

The optimization program was run to obtain the tendon forces throughout the motion. Below, the results are shown including the input forces and the results.

The input forces are shown in Figure 41 - Figure 43. These are shown for comparison with the output tendon forces.

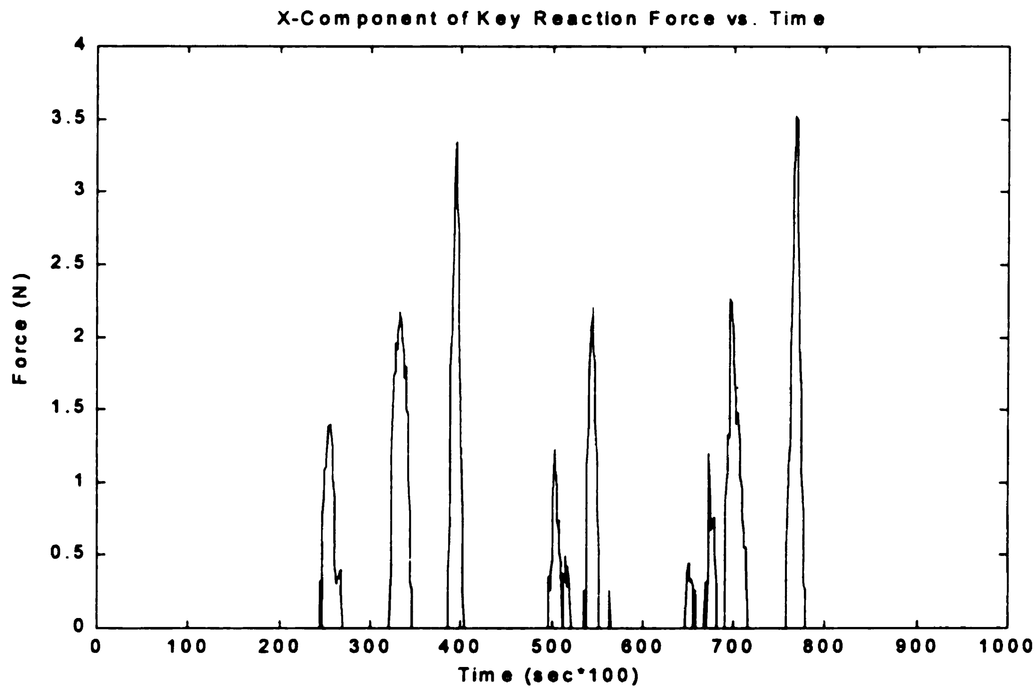

Figure 41--X-Component of Applied Force

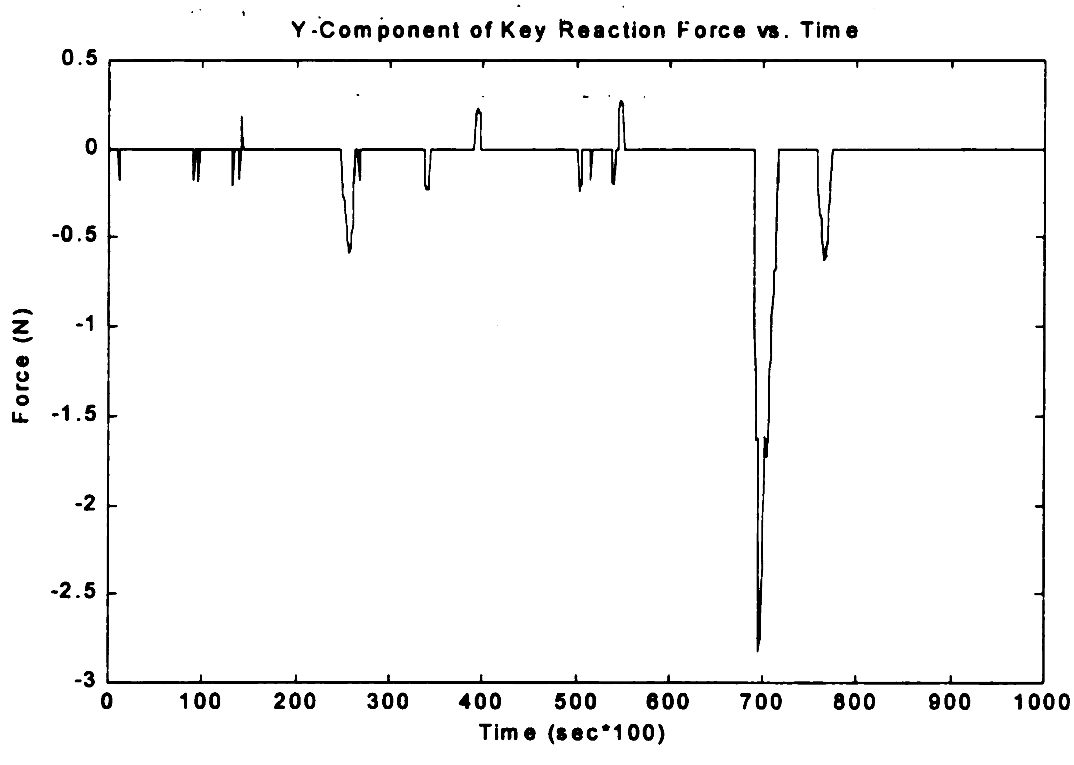

Figure 42--Y-Component of Applied Force

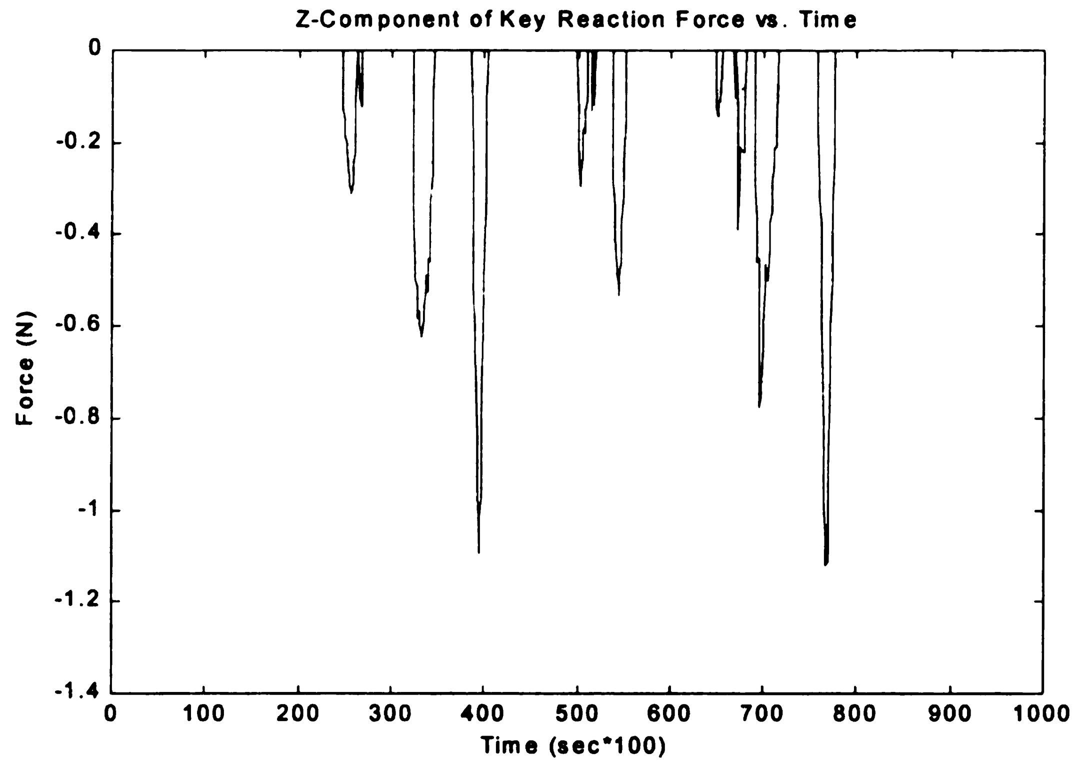

Figure 43--Z-Component of Applied Force

Although data were output for each of the tendon forces and reaction forces and moments, only the FP, FS and RB forces are discussed so the remainder of the graphs are presented in Appendix H. FP and FS are discussed because they are relevant to the completion of this work. The RB force is discussed because it is typical of the extensor forces.

Figure 44 shows the force in the FP muscle and Figure 45 shows the force in the FS muscle throughout the trial. As is expected given the constraints (all tendon forces are tensile), the forces are positive throughout the motion. In addition, their magnitudes are approximately what would be expected given the applied loads and is slightly lower than results obtained by Chao and An(An et al., 1985; Chao & An, 1978b) who predicted that the FP force should be 1.93-2.08 times the applied force for tip pinch. Comparison is made with tip pinch because of the similarity in location and direction of the applied loads in the two situations.

Although the force is positive throughout the motion, there are some points where the force is much larger than the expected value (points 695 - 700, 716). These spikes occur where a valid solution to the systems of equations was not found. This phenomena can be more clearly seen in Figure 46 which shows the force in the radial band of the extensor complex and the y-component of the applied force versus time. Both are shown to illustrate the relationship between the y-component of the applied force and those points for which the optimization technique was incapable of finding a solution to the system of equations. Note that the points where a negative value of the radial band force were points 245, 695 - 700, 716 and 778. In all cases the y-component is less than zero and therefore, the angle between the palmer surface of the distal segment of the finger and the surface of the keyboard is greater than ninety degrees. The model is capable of predicting the forces in the tendons when the y-component is negative, but small (between ninety and ninety-five degrees). However, when that angle is larger than ninety-five degrees, as is the case for points 695 - 700 and 716, the model is incapable of predicting the forces. This behavior is due to the complex nature of forces in this case.

In general, the model is capable of predicting the forces in the tendons of the finger, however, it does not predict those forces when the angle between the distal finger segment and the keyboard is large. This occurs when the typist reaches the keys on the bottom row of the keyboard.

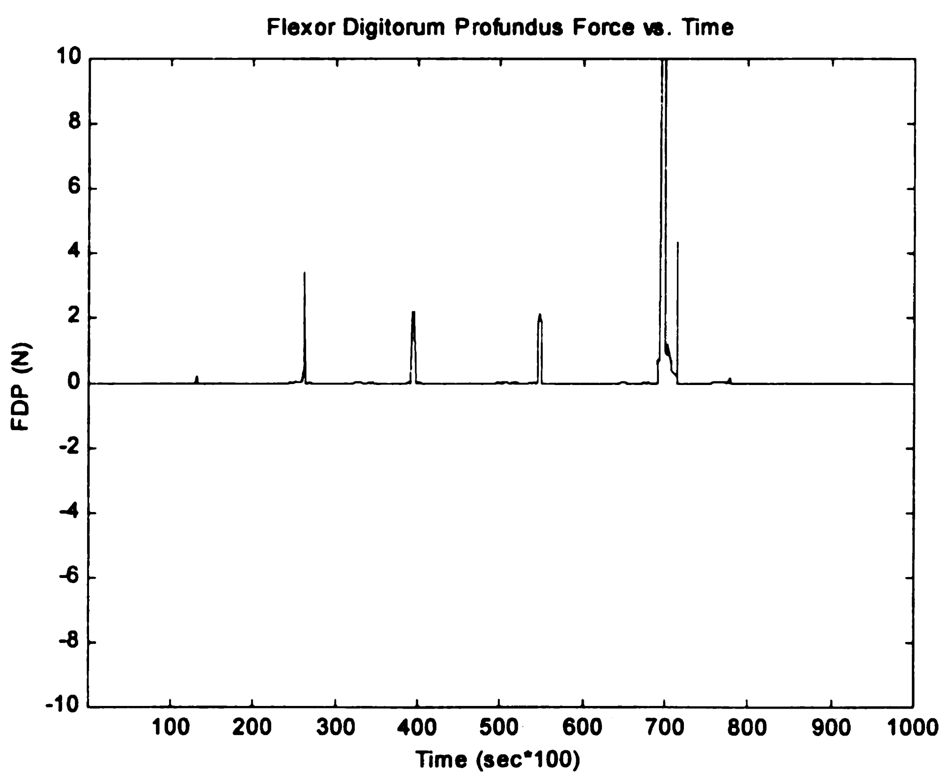

Figure 44--Graph of Flexor Digitorum Profundus for Typing Trial

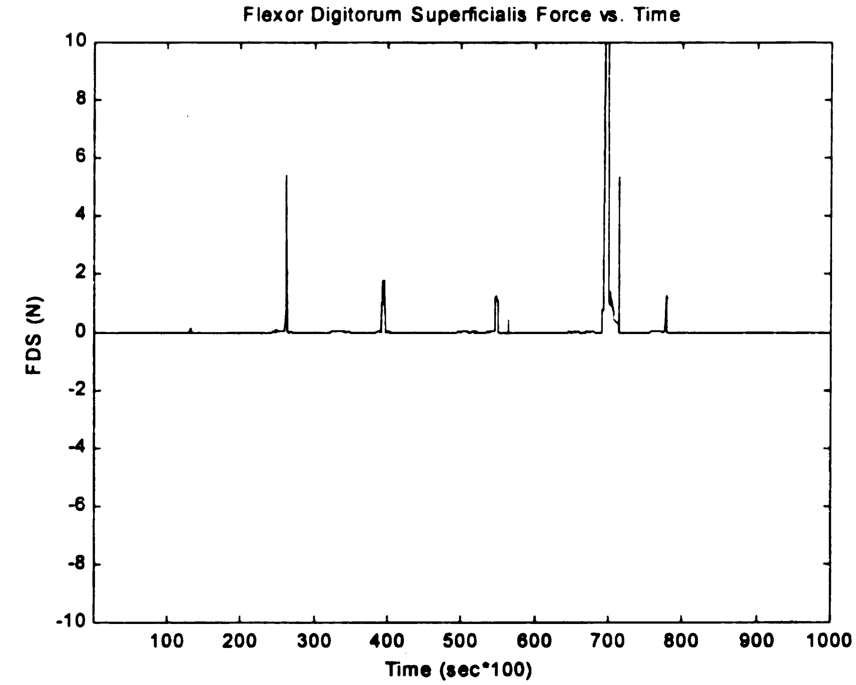

Figure 45--Graph of Flexor Digitorum Superficialis for Typing Trial

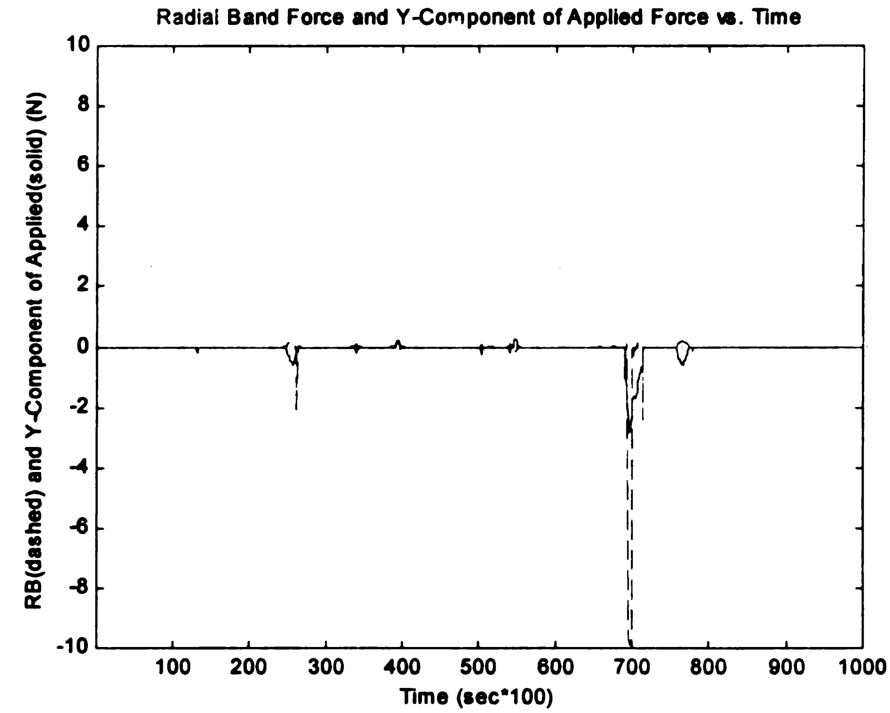

Figure 46--Graph of the Radial Band of the Extensor and the Y-component of the Applied Force for Typing Trial

ENERGY CALCULATION

The energy lost due to friction in the wrist was calculated in accordance with the procedure described in Chapter 4. It was found that 1.217×10^{-4} J per activity were lost due to the motion of the tendons of the index finger in the carpal tunnel. For this value to be useful, extensive clinical trials will need to be performed to verify that the method described herein is both accurate and repeatable. In addition, studies are needed to correlate energy values found using this method with known tendencies of activities to cause CTS. Once these studies have been performed, the true usefulness of this model will be known.

SYSTEM ACCURACY

The accuracy of the BTS system was verified as specified in the experimental procedure. The values for the mean and standard deviations for the distance between the two markers are given in Table 5 for each of the camera combinations.

Table 5—Accuracy of Calibrated Space

Cameras	Mean Distance (mm)	Standard Deviation (mm)	Minimum (mm)	Maximum (mm)	Range (mm)
1&2	17.365	0.412	16.463	19.234	2.771
3&4	17.222	0.735	14.352	21.035	6.683
1&3	17.143	0.744	14.904	19.431	4.527
2&4	17.324	0.591	11.999	19.243	7.235
1&4	17.321	0.727	12.525	20.262	7.738
2&3	17.397	0.428	16.491	19.988	2.497
W/O Errors	17.390	0.303	16.491	18.164	1.673

After careful examination, it was found that the above analysis contained some tracking errors. Due to the size and proximity of the markers, the BTS motion analysis system would not automatically track the markers. As a result, the markers needed to be identified manually in each frame of data.

In many cases, as the markers were moved through the camera space, the two markers would appear to trade positions in the camera views (in one frame, target one would be the higher target and in the next, it would be the lower target). It was very difficult to determine when this occurred and as a result, in some cases, the markers were misidentified. When this occurred, the distance between the markers was incorrect. Ninety-four of the data points had identical distance values regardless of the cameras used to track them. Due to the above-mentioned difficulties, these values were taken to be the only valid data points.

The data were reexamined and it was found that the mean distance between the points using only the ninety-four points was 17.380 mm and the standard deviation of the values was 0.303 mm. A histogram of these values is shown below in Figure 47. The marking points are given at the mean, and ± 1 thru 4 standard deviations from the mean. From this figure, it can be seen that the distribution is approximately normal about the mean.

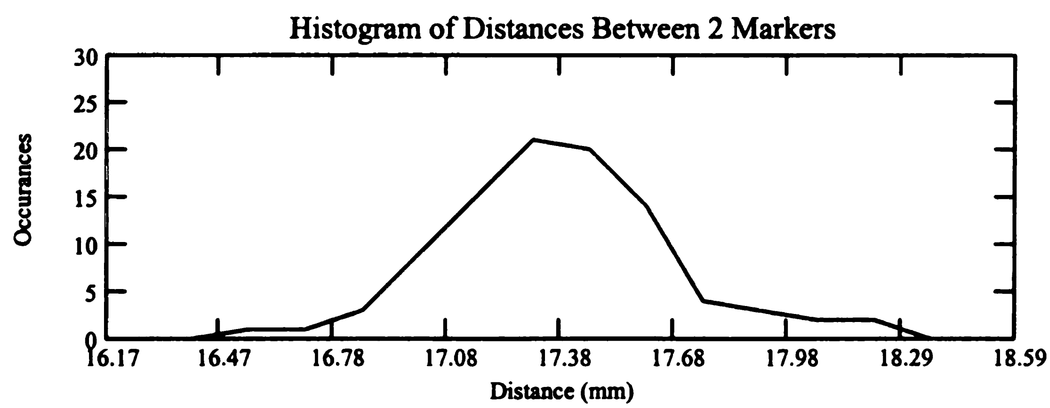

Figure 47—Accuracy of Calibrated Space Using Only Those Points Accurately Tracked

The maximum value of the distance was 18.164 mm and the minimum was 16.491 mm yielding an overall range of 1.673 mm. Given that the range of motion being studied is approximately 30 mm, this variation is acceptable. However, it does imply that a limited amount of "noise" is to be expected in the actual test data. This "noise" causes large-scale inaccuracies in the acceleration data and therefore imposes the need for filtering of the data.

In addition to determining the accuracy of the calibrated space, soft tissue motion was measured and the rigid body assumption was verified by calculating the length of each finger segment throughout the typing trials. The mean lengths and standard deviations for each of the finger segments are shown below in Table 2.

Table 6—Lengths and Standard Deviations for Index Finger Segments

Segment	Mean Length (mm)	Standard Deviation (mm)	Maximum (mm)	Minimum (mm)	Range (mm)
Proximal	54.006	1.416	57.991	49.567	8.424
Middle	29.543	1.055	31.800	27.491	4.309
Distal	23.976	0.614	25.405	22.632	2.773

Note that the soft tissue motion decreases for the more distal finger segments. This is because the range of motion and amount of soft tissue are also decreasing and is to be expected. In the above results, it is not possible to separate the inaccuracy of the BTS motion analysis system from the soft tissue motion. However, due to the relative magnitudes of the errors in the finger segment lengths and the accuracy of the calibrated space, it is reasonable to conclude that there is soft tissue motion in both the proximal and middle segments and minimal soft tissue motion in the distal segment.

In order to verify the assumption that the motion of the finger segments is planar, the dot product between the z-unit vector for the proximal and middle segments and the x-unit vector for the distal finger segment was taken and the angle between the two vectors was calculated utilizing the definition of the dot product (Equation 65). This was then graphed and the results are shown in

Figure 48.

$$\psi = \cos^{-1}(\hat{k}_p \cdot \hat{i}_d) \qquad (65)$$

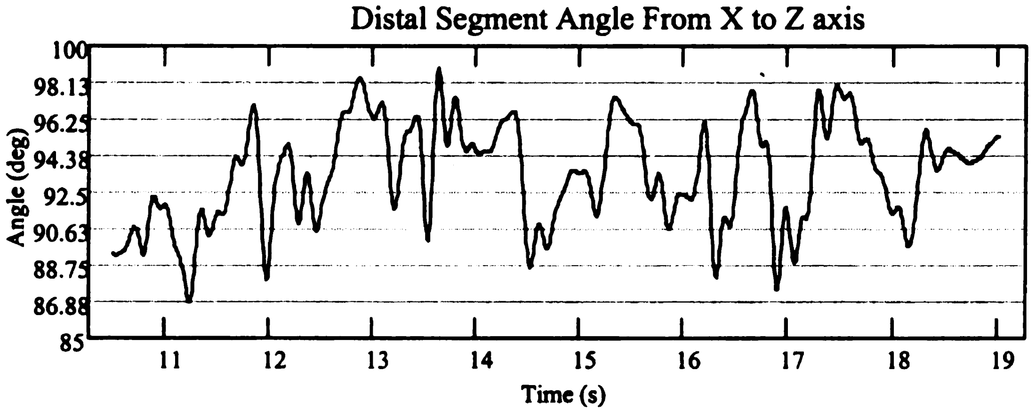

Figure 48—Graph of Angle Between the Distal X-Axis and the Finger Z-Axis

From these data, it was found that the average angle between the two vectors was 93.358° with a standard deviation of 2.615°. The angle should be 90°as the two vectors should be perpendicular if the motion of the DIP and PIP joints is purely planar, but this variation is relatively small. There are two possible causes for this variation. One is that the interphalangeal joints are not spherical, but are condoloidal in nature. The other could be inaccuracy in the marker placement for the test. Markers were aligned on the finger visually, which could introduce error. The error in the direction of the z-axis for the distal segment was corrected as described in the methods section.

CHAPTER 6--CONCLUSIONS

A model for determining a relative measure of the tendency of an activity to cause carpal tunnel syndrome was developed. For the results of this model to be used clinically, verification of the model's accuracy and repeatability must be performed. In addition, analysis should be done to attempt to correlate the results obtained from this model to known tendencies to cause carpal tunnel syndrome.

Although the analysis was performed only on the index finger for this work, the model is intended to analyze full hand motion. The results from each finger will be added together to determine the total energy for an activity. This total energy can be compared to the energy from other activities or different postures of the same activity to determine which activity will have a greater chance of causing CTS. The higher the energy dissipated, the higher the chance of causing CTS.

In the trial performed, the model predicted the tendon forces well for those finger positions where the angle between the distal finger segment and the keyboard was less than 90°. When the angle was greater than 90°, the model was incapable of predicting the forces. The angle is greater than 90° when the person reaches for keys on the bottom row of the keyboard.

For applied forces between zero and five Newtons, the resulting tendon forces were between zero and ten Newtons. These magnitudes are comparable to results found in the literature.

When analyzing the typing task, it is appropriate to utilize a quasi-static method as the influence of the inertial effects on the tendon forces is negligible when compared with the influence of the applied force. This conclusion is based upon the magnitude of the applied force being two orders of magnitude higher than the magnitude of the inertial terms. Since typing is a low force, high velocity activity, having relatively high inertial effects when compared to other activities, the quasi-static assumption can also be used when analyzing other activities.

An equation, $\phi4 = 0.9\phi3 - 0.25$, was found to relate the PIP, $\phi4$, and DIP, $\phi3$, angles. The R^2 correlation between this equation and the data from the trial is 0.952.

The standard deviation for the length of the finger segments was 0.614 mm, 1.055 mm and 1.416 mm for the proximal, middle and distal finger segments respectively. This indicates that there is soft tissue motion in the fingers. The increasing standard deviations with increasing proximity to the hand is from the greater amount of flesh on the more proximal segments of the finger.

In addition, the systems utilized to collect data for implementation in the model are adequate.

The motion analysis system was capable accurately determining the location of the targets to ± 1 mm at the six-sigma level. However, improvements should be made on the force transducers utilized to record keystroke force to ensure that force is accurately recorded and the force can be resolved into components rather than assuming that the entire applied force is in the global y-direction. In addition, before large-scale clinical use can be made of the model, motion measurement systems must be improved to facilitate easier data tracking.

Further work must be done to determine if this model is clinically valid. Clinical trials must be performed to determine if results are repeatable. Also, results must be compared with known data on incidences of CTS to determine if the model accurately predicts the tendency to cause CTS.

APPENDIX A–TENDON LOCATIONS

Tendon locations in thumb (mean value of five specimens).

		Distal Point			Proximal Point		
Joint	Tendon	X	Y	Z	X	Y	Z
	EPL	0.000	0.192	-0.057	-0.050	0.201	-0.044
IP	FPL	-0.007	-0.224	0.049	0.100	-0.318	0.034
	EPL	0.000	0.280	-0.157	-0.050	0.247	-0.224
	FPL	-0.062	-0.318	0.009	0.100	-0.521	-0.012
MP	ADD	-0.062	-0.224	-0.280	0.100	-0.575	-0.346
	EPB	0.000	0.265	0.057	-0.050	0.268	-0.019
	FPB	-0.062	-0.094	0.285	0.100	-0.416	0.435
	APB	-0.062	0.007	0.288	0.100	-0.160	0.533
	EPL	0.000	0.179	-0.385	-0.050	0.225	-0.076
	FPL	-0.067	-0.476	-0.046	0.100	-0.152	-0.276
	ADD	-0.067	-0.065	-0.395	0.100	0.269	-0.589
CMC	EPB	0.000	0.302	0.029	-0.050	0.184	0.132
	FPB	-0.067	-0.351	-0.284	0.100	0.004	-0.848
	APB	-0.067	-0.140	1.098	0.100	-0.273	0.410
	OPP	-0.067	-0.236	0.090	0.100	-0.493	-0.074
	APB	-0.067	0.346	0.212	0.100	0.136	0.239

Tendon locations in index finger (mean value of 15 specimens).

		Distal Point			Proximal Point		
Joint	Tendon	X	Y	Z	X	Y	Z
	TE	0.004	0.199	-0.010	0.000	0.196	-0.009
DIP	FP	0.004	-0.184	0.026	0.300	-0.245	0.054
	FP	-0.212	-0.308	0.009	0.400	-0.409	0.027
	RB	-0.112	0.186	0.223	0.100	0.181	0.268
PIP	UB	-0.112	0.151	-0.290	0.100	0.131	-0.312
	FS	-0.212	-0.249	0.015	0.400	-0.311	0.028
	ES	-0.038	0.278	-0.027	0.000	0.266	-0.026
	FP	-0.118	-0.386	0.031	0.300	-0.619	0.004
	FS	-0.118	-0.477	-0.074	0.300	-0.689	-0.114
	RI	-0.318	-0.033	0.443	0.400	-0.362	0.629
MCP	LU	-0.318	-0.148	0.370	0.400	-0.704	0.541
	UI	-0.318	-0.039	-0.461	0.400	-0.379	-0.442
	LE	-0.018	0.421	-0.033	0.000	0.483	-0.026

Tendon locations in middle finger (mean value of 15 specimens).

		Distal Point			Proximal Point		
Joint	Tendon	X	Y	Z	X	Y	Z
	TE	-0.036	0.157	-0.014	0.000	0.169	-0.017
DIP	FP	-0.036	-0.158	0.054	0.300	-0.239	0.050
	FP	-0.267	-0.308	0.009	0.400	-0.251	-0.007
	RB	-0.167	0.206	0.237	0.100	0.132	0.262
PIP	UB	-0.167	0.132	-0.262	0.100	0.079	-0.290
	FS	-0.267	-0.217	0.054	0.400	-0.248	0.023
	ES	-0.017	0.241	-0.019	0.000	0.234	-0.009
	FP	-0.317	-0.334	0.009	0.300	-0.522	0.001
	FS	-0.185	-0.355	0.065	0.300	-0.593	0.063
	RI	-0.185	0.011	0.340	0.400	-0.499	0.491
MCP	LU	-0.385	-0.174	0.311	0.400	-0.680	0.403
	UI	-0.385	0.011	-0.135	0.400	-0.185	-0.119
	LE	-0.085	0.352	-0.015	0.000	0.416	-0.013

Tendon locations in ring finger (mean value of 15 specimens)

		Distal Point			Proximal Point		
Joint	Tendon	X	Y	Z	X	Y	Z
	TE	-0.054	0.141	-0.016	0.000	0.154	-0.021
DIP	FP	-0.054	-0.160	0.001	0.300	-0.239	0.027
	FP	-0.276	-0.281	0.011	0.400	-0.306	-0.007
	RB	-0.176	0.142	0.176	0.100	0.092	0.256
PIP	UB	-0.176	0.141	-0.215	0.100	0.088	-0.238
	FS	-0.276	-0.218	0.048	0.400	-0.263	0.029
	ES	-0.026	0.221	0.004	0.000	0.204	0.023
	FP	-0.204	-0.302	0.022	0.300	-0.509	0.053
	FS	-0.204	-0.352	0.035	0.300	-0.567	0.057
	RI	-0.404	-0.035	0.284	0.400	-0.302	0.316
MCP	LU	-0.404	-0.112	0.186	0.400	-0.477	0.265
	UI	-0.404	0.047	-0.197	0.400	-0.240	-0.244
	LE	-0.104	0.313	0.062	0.000	0.352	0.052

Tendon locations in little finger (mean value of 15 specimens).

		Distal Point			Proximal Point		
Joint	Tendon	X	Y	Z	X	Y	Z
	TE	0.010	0.196	-0.077	0.000	0.193	-0.079
DIP	FP	0.010	-0.232	-0.041	0.300	-0.238	-0.003
	FP	-0.196	-0.333	0.040	0.400	-0.364	-0.002
	RB	-0.096	0.198	0.220	0.100	0.131	0.253
PIP	UB	-0.096	0.093	-0.317	0.100	0.120	-0.298
	FS	-0.196	-0.268	0.050	0.400	-0.345	-0.008
	ES	0.054	0.259	-0.010	0.000	0.254	0.014
	FP	-0.044	-0.427	0.080	0.300	-0.628	0.170
	FS	-0.044	-0.508	0.111	0.300	-0.708	0.170
	RI	-0.244	0.027	0.418	0.400	-0.182	0.497
MCP	LU	-0.244	-0.169	0.364	0.400	-0.553	0.469
	ADQ	-0.244	-0.023	-0.486	0.400	-0.309	-0.625
	LE	0.056	0.154	0.061	0.000	0.190	0.133

APPENDIX B—PHYSIOLOGICAL CROSS-SECTIONAL AREA FOR ALL HAND MUSCLES

PCSA for Extrinsic Muscles

Muscle	Volume (cm^3)	Fiber Length (cm)	PCSA (cm^2)	% Volume	% PCSA
BR	46.9 ± 22.0	15.8 ± 5.6	2.9 ± 0.7	8.5± 1.5	2.9 ± 0.3
ECRL	32.4 ± 10.1	8.0 ± 1.0	4.0 ± 1.0	6.2 ± 0.9	4.1 ± 0.8
ECRB	29.2 ± 11.7	5.8 ± 1.0	4.9 ± 1.6	5.3 ± 0.2	4.9 ± 0.4
SUP	24.0 ± 11.6	3.5 ± 0.8	7.3 ± 4.4	4.3 ± 1.1	6.8 ± 2.4
EDC2	6.5 ± 1.4	6.1 ± 1.4	1.1 ± 0.3	1.3 ± 0.4	1.1 ± 0.2
EDC3	12.8 ± 10.1	6.8 ± 1.7	1.7 ± 0.8	2.3 ± 1.2	1.8 ± 0.8
EDC4	8.1 ± 2.0	6.8 ± 0.8	1.2 ± 0.4	1.7 ± 0.7	1.3 ± 0.4
EDC5	3.0 ± 2.0	3.8 ± 2.6	0.5 ± 0.4	0.7 ± 0.5	0.7 ± 0.6
ECU	18.1 ± 14.6	4.8 ± 1.9	3.5± 2.1	3.4 ± 2.1	3.9 ± 2.4
APL	14.8 ± 5.6	3.9 ± 1.2	3.9 ± 2.0	2.8 ± 0.7	4.0 ± 1.5
EPB	6.0 ± 3.8	4.2 ± 0.8	1.3 ± 0.7	1.0 ± 0.4	1.3 ± 0.5
EPL	10.5 ± 5.8	5.2 ± 1.1	1.9 ± 0.8	1.8 ± 0.5	1.9 ± 0.6
EIP	6.9 ± 3.6	4.9 ± 1.0	1.3 ± 0.6	1.3 ± 0.5	1.4 ± 0.6
EDQ	8.8 ± 3.9	6.2 ± 2.8	1.5 ± 0.9	1.6 ± 0.2	1.5 ± 0.5
PT	34.2 ± 14.7	5.3 ± 1.1	6.6 ± 2.7	6.3 ± 1.2	6.5 ± 1.3
FCR	27.3 ± 11.4	5.2 ± 0.7	5.2 ± 1.9	5. 0 ± 0.5	6.0 ± 0.7
PL	6.8 ± 3.2	4.4 ± 0.9	1.5 ± 0.6	1.2 ± 0.2	1.2 ± 0.4
FCU	34.4 ± 13.6	3.3 ± 0.7	10 ± 3.0	6.2 ± 0.3	10.2 ± 1.0
FSD	10.0 ± 11.6	4.0 ± 0.5	2.4 ± 2.8	1.5 ± 1.7	2.0 ± 2.4
FS2	15.1 ± 8.1	4.2 ± 0.9	3.6 ± 2.1	2.8 ± 1.1	3.6 ± 1.6
FS3	29.5 ± 15. 9	6.5 ± 1.0	4.2 ± 1.8	5.3 ± 1.8	4.2 ± 0.7
FS4	17.8 ± 10.4	6.8 ± 1.9	2.4 ± 1.2	2.9 ± 1.4	2.2 ± 0.7
FS5	9.3 ± 5.2	4.4 ± 0.6	2.1 ± 1.4	1.7 ± 0.7	2.2 ± 1.1
FPL	23.5 ± 10.4	4.6 ± 1.2	5.1 ± 2.6	4.2 ± 0.5	5.0 ± 1.7
FP2	27.6 ± 16.1	6.7 ± 0.7	4.1 ± 2.4	4.8 ± 1.7	3.8 ± 1.2
FP3	27.8 ± 11.0	6.7 ± 0.6	4.1 ± 1.4	5.2 ± 0.9	4.1 ± 0.7
FP4	24.8 ± 9.6	6.4 ± 0.7	3.7 ± 1.1	4.7 ± 1.0	3.9 ± 0.8
FP5	14.8 ± 5.8	5.9 ± 0.8	2.5 ± 0.9	3.0 ± 1.2	2.7 ± 1.1
PQ	10.0 ± 5.2	3.1 ± 0.9	3.5 ± 2.1	1.9 ± 0.8	3.6 ± 1.7

PCSA for Intrinsic Muscles

Muscle	Volume (cm^3)	Fiber Length (cm)	PCSA (cm^2)	% Volume	%PCSA
ABP	4.8 ± 1.8	3.2 ± 0.6	1.5 ± 0.6	6.2 ± 1.4	4.4 ± 1.0
OPP	6.1 ± 3.0	2.3 ± 0.6	2.8 ± 1.3	7.3 ± 1.7	7.5 ± 2.7
ADPT	3.4 ± 1.6	3.8 ± 0.6	0.9 ± 0.4	4.2 ± 1.4	2.5 ± 1.0
ADP2	2.1 ± 2.0	1.7 ± 1.6	0.6 ± 0.6	2.4 ± 1.9	1.6 ± 1.6
ADP3	6.1 ± 3.7	3.5 ± 0.8	1.8 ± 1.2	7.8 ± 3.5	5.2 ± 2.8
ADPacc	1.6 ± 0.6	1.8 ± 0.2	0.8 ± 0.3	2.0 ± 0.3	2.4 ± 0.6
FPBsup	3.9 ± 1.2	3.1 ± 1.0	1.3 ± 0.6	5.4 ± 2.4	4.1 ± 1.6
FPBdeep	2.1 ± 1.2	2.1 ± 0.3	1.0 ± 0.5	2.8 ± 1.4	3.0 ± 1.5
DIO1R	6.0 ± 2.0	2.8 ± 0.6	2.1 ± 0.5	7.8 ± 1.6	6.5 ± 2.3
DIO1U	3.5 ± 1.5	1.7 ± 0.5	2.0 ± 0.8	4.2 ± 1.4	5.5 ± 1.6
DIO2R	1.8 ± 1.2	1.2 ± 0.2	1.4 ± 1.0	2.0 ± 0.7	3.7 ± 1.8
DIO2U	1.9 ± 0.9	1.3 ± 0.2	1.4 ± 0.8	2.5 ± 1.0	4.4 ± 2.4
DIO3R	1.4 ± 0.9	1.3 ± 0.3	1.0 ± 0.8	1.6 ± 0.8	2.7 ± 1.4
DIO3U	1.6 ± 0.8	1.3 ± 0.3	1.2 ± 0.7	2.0 ± 0.4	3.6 ± 1.3
DIO4R	1.3 ± 1.0	1.1 ± 0.2	1.1 ± 0.8	1.5 ± 0.9	2.8 ± 1.4
DIO4U	1.4 ± 0.8	1.3 ± 0.3	1.1 ± 0.7	1.7 ± 0.5	2.9 ± 1.0
ADPF2*	1.6 ± 0.6	0.0 ± 0.0	0.0 ± 0.0	2.0 ± 0.3	0.0 ± 0.0
DIO1F3*	0.3 ± 0.5	0.7 ± 0.9	0.1 ± 0.2	0.3 ± 0.5	0.4 ± 0.7
PIO1F4*	2.5 ± 0.7	1.7 ± 0.2	1.4 ± 0.4	3.3 ± 0.7	4.1 ± 0.9
DIO1F5*	1.2 ± 0.7	1.6 ± 0.2	0.7 ± 0.4	1.5 ± 0.7	2.0 ± 0.9
DIO1F6*	1.1 ± 0.4	1.6 ± 0.3	0.7 ± 0.2	1.5 ± 0.4	2.0 ± 0.6
PIO1F7*	2.2 ± 0.7	1.7 ± 0.1	1.2 ± 0.3	2.8 ± 0.4	3.5 ± 0.7
DIO1F8*	1.0 ± 0.4	1.6 ± 0.2	0.6 ± 0.2	1.3 ± 0.4	1.9 ± 0.6
PIO1F9*	2.2 ± 0.7	1.6 ± 0.1	1.3 ± 0.4	2.9 ± 0.5	4.0 ± 1.1
L2	1.7 ± 0.7	4.7 ± 0.9	0.3 ± 0.1	2.1 ± 0.4	1.0 ± 0.0
L3	1.2 ± 0.4	5.0 ± 1.4	0.2 ± 0.0	1.6 ± 0.4	0.7 ± 0.2
L4	1.0 ± 0.1	4.6 ± 1.5	0.2 ± 0.0	1.4 ± 0.4	0.7 ± 0.3
L5	0.7 ± 0.3	3.5 ± 0.8	0.2 ± 0.0	0.9 ± 0.1	0.6 ± 0.1
ADQS	3.9 ± 2.0	4.3 ± 1.0	0.8 ± 0.3	4.8 ± 1.2	2.5 ± 0.5
ADQD	3.1 ± 1.2	3.4 ± 0.9	0.9 ± 0.2	3.9 ± 0.7	2.7 ± 0.7
FDQ	1.1 ± 1.0	7.7 ± 1.2	0.4 ± 0.4	1.5 ± 1.0	1.3 ± 1.0
OPPL	3.8 ± 1.4	1.3 ± 0.2	2.9 ± 1.1	5.0 ± 1.1	8.4 ± 2.6

Appendix D--BTS Camera Calibration Constants

Subject:	Path: /data /research/hand-dyn/11-30col	Test Date: 12/1/99

BTS Calibration Setup

Calibrated By: ____________

Date: ____________ **Protocol Code:** ________

TVC Configuration: [X] MSU [ ] BTS

Current:	TVC: 4	Planes: 4	
2D Grid:	Rows: 4	Columns: 4	
3D Grid:	Rows: 4	Columns: 7	Mesh: 50 mm
	Height: 770 mm	Pl. Dist.: 150 mm	Width: 2 mm

TVC	Ω	Φ	K	x (mm)	y (mm)	z (mm)
1	-18	20	-14	330	1180	870
2	-14	-20	15	-380	1250	860
3	-12	150	0	350	1070	-510
4	-10	-160	1	-280	1090	-510

Ω: represents rotation about the X axis, tilt up and down.
Φ: represents rotation about the Y axis, panning.
K: represents rotation about the Z axis, side to side.

APPENDIX F--CALIBRATION CURVES FOR KEYS

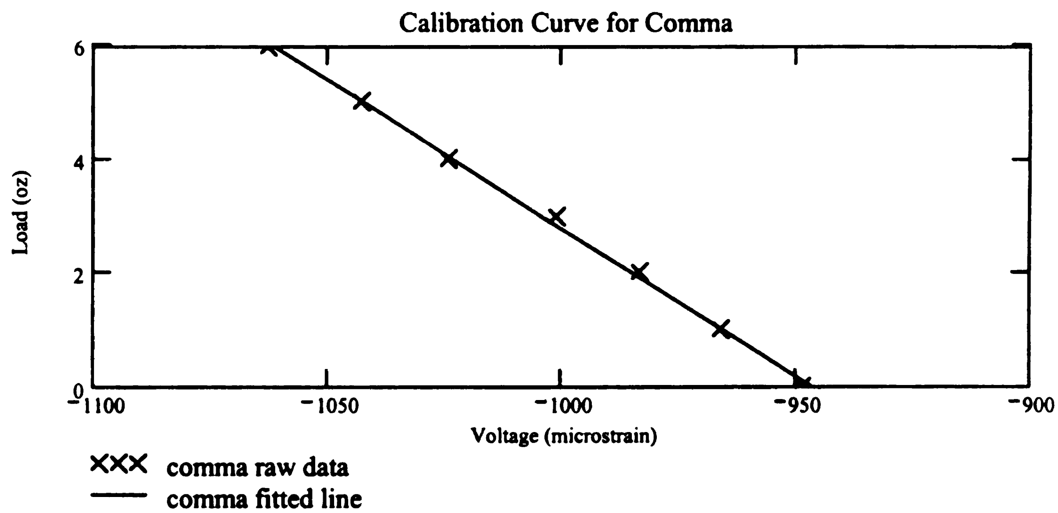

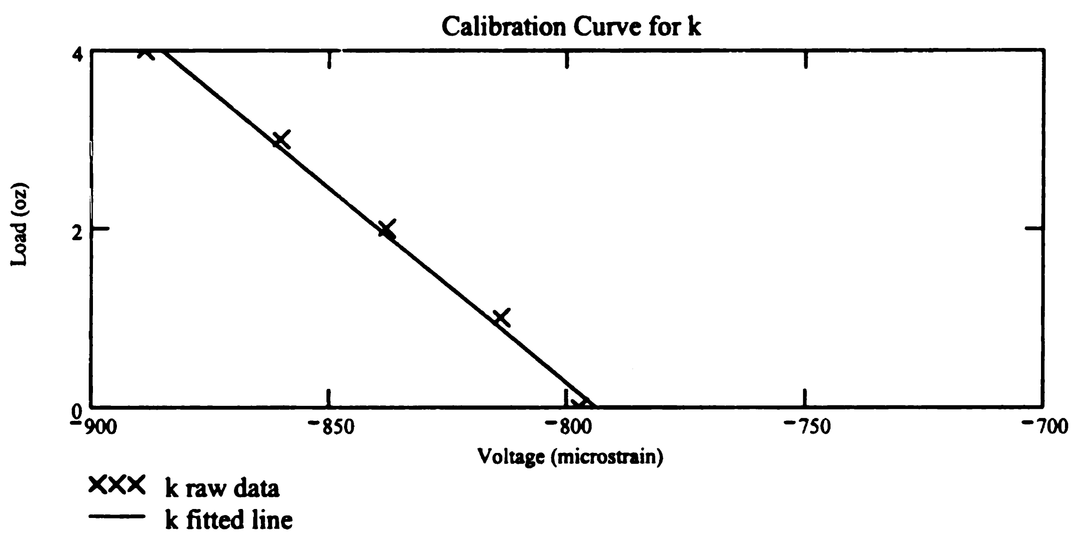

Calibration Curve for b

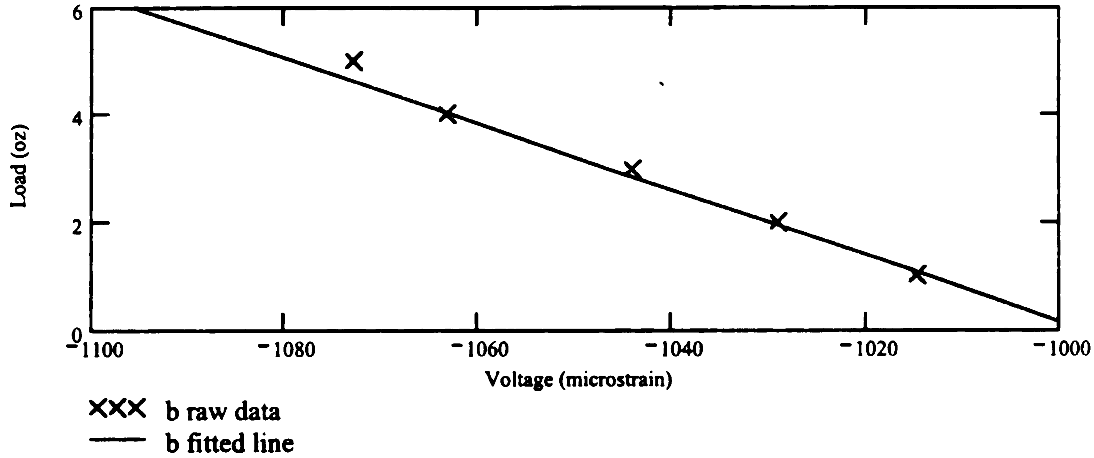

Calibration Curve for m

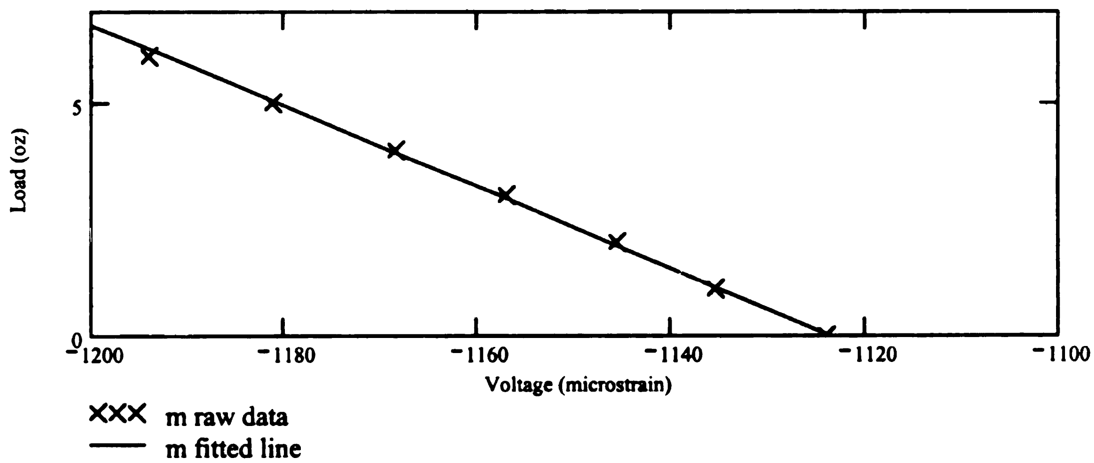

Calibration Curve for n

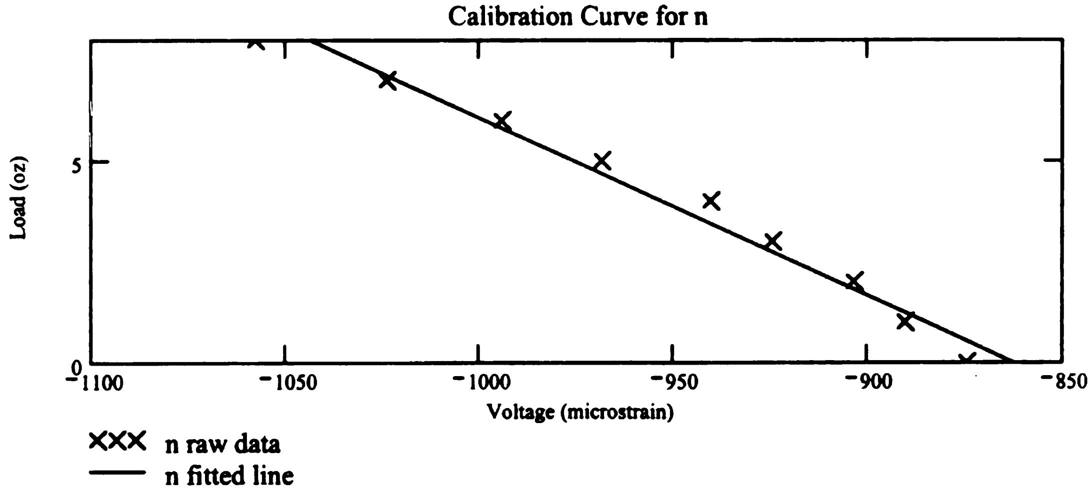

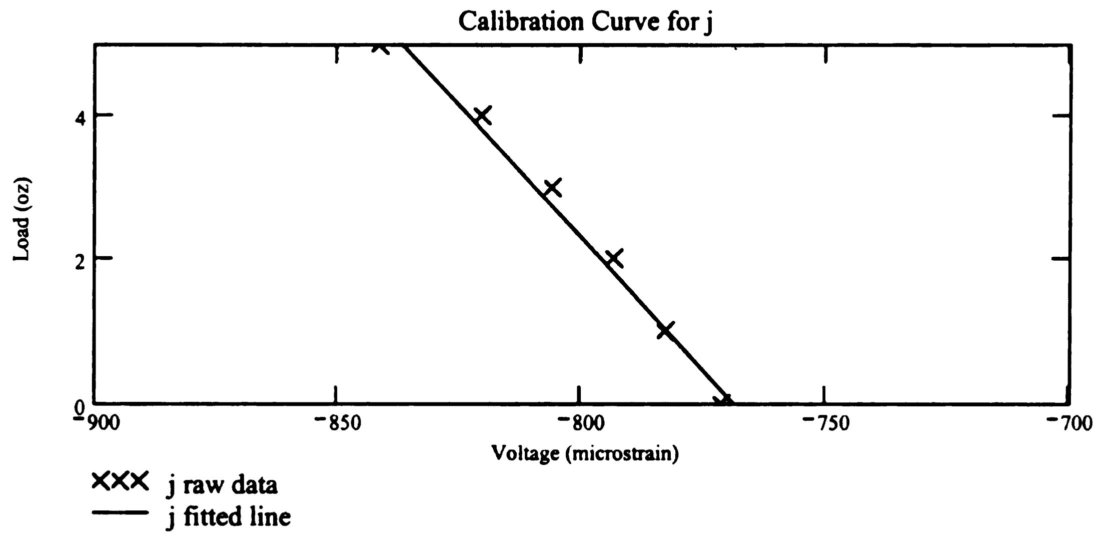

Calibration Curve for j
Load (oz)
0
2
4
-900
-850
-800
-750
-700
Voltage (microstrain)
j raw data
j fitted line

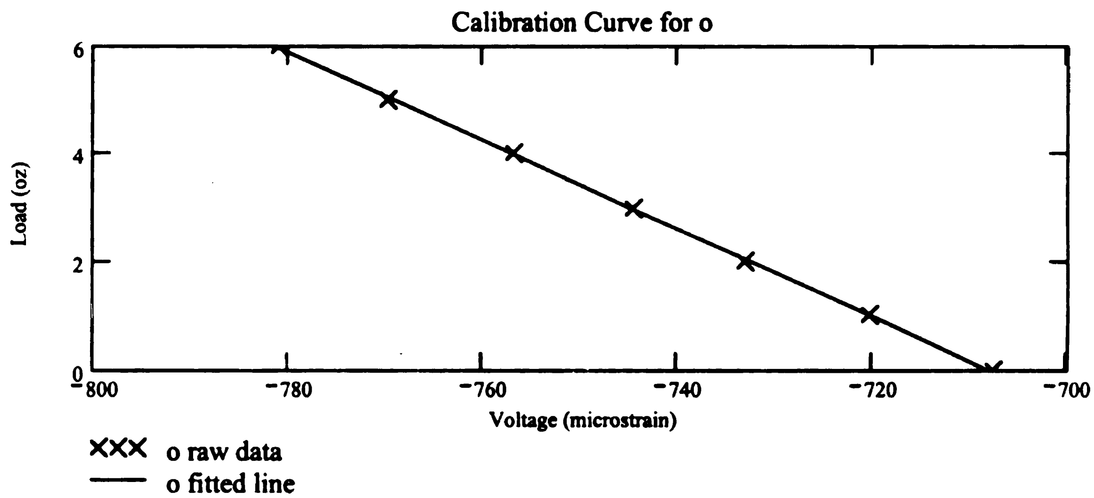

Calibration Curve for o
Load (oz)
0
2
4
6
-800
-780
-760
-740
-720
-700
Voltage (microstrain)
o raw data
o fitted line

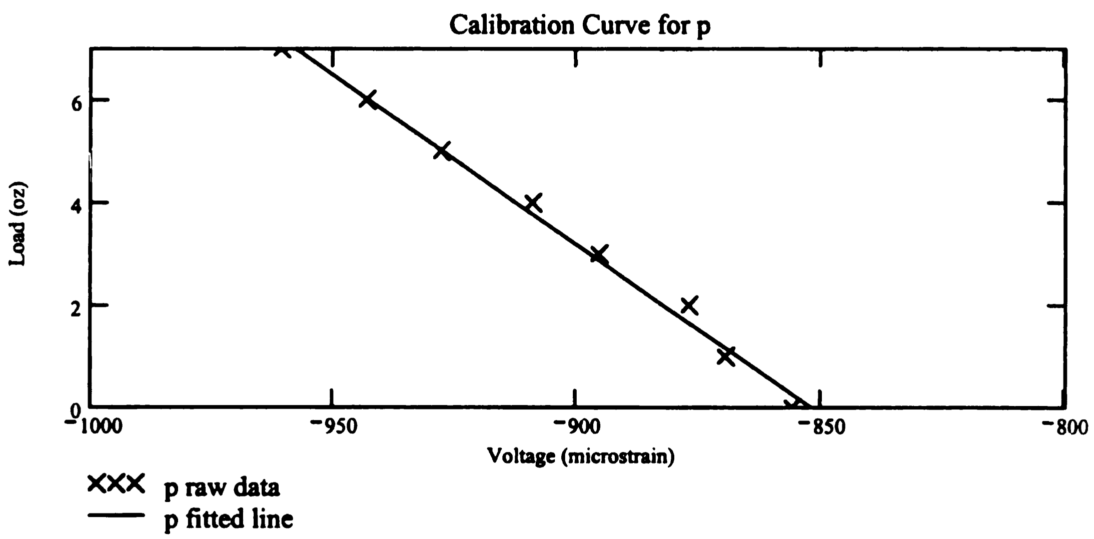

Calibration Curve for p
Load (oz)
0
2
4
6
-1000
-950
-900
-850
-800
Voltage (microstrain)
p raw data
p fitted line

Calibration Curve for period

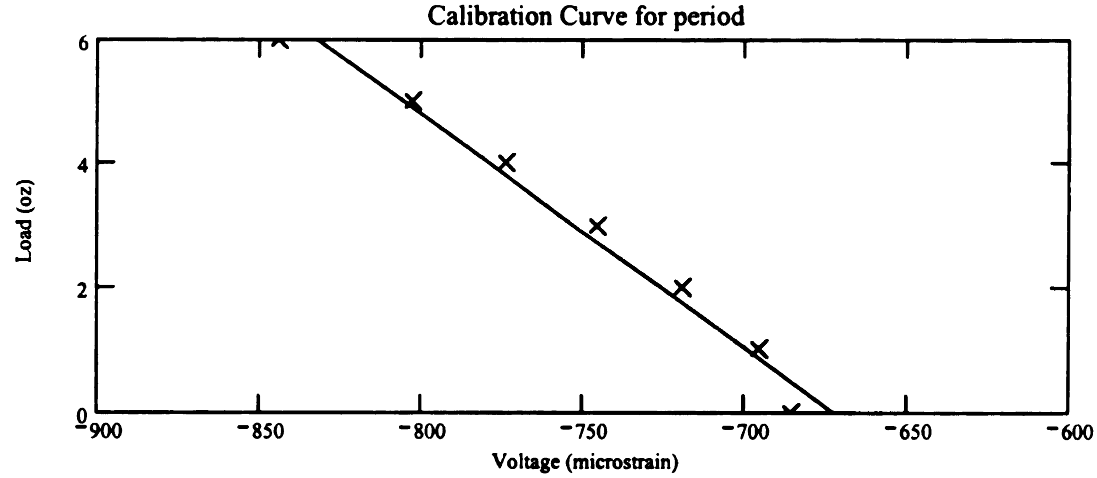

XXX period raw data
—— period fitted line

Calibration Curve for l

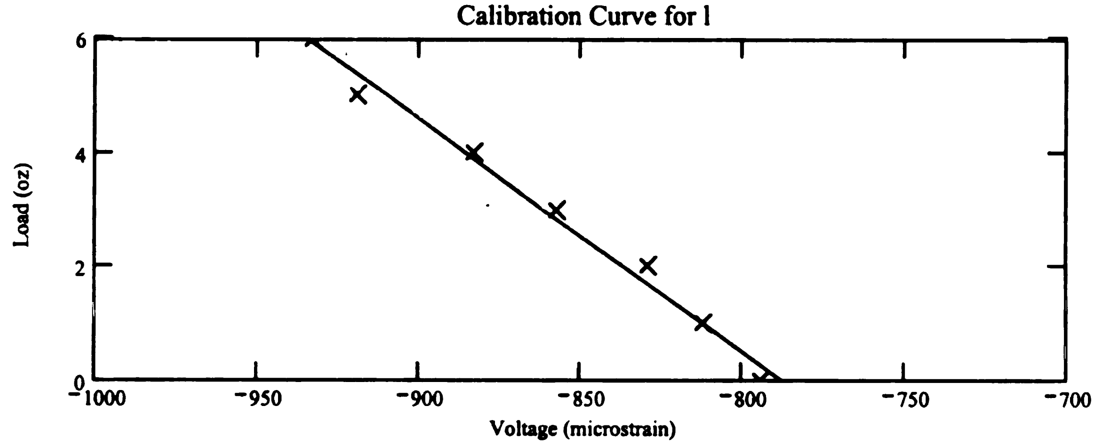

XXX l raw data
—— l fitted line

Calibration Curve for u

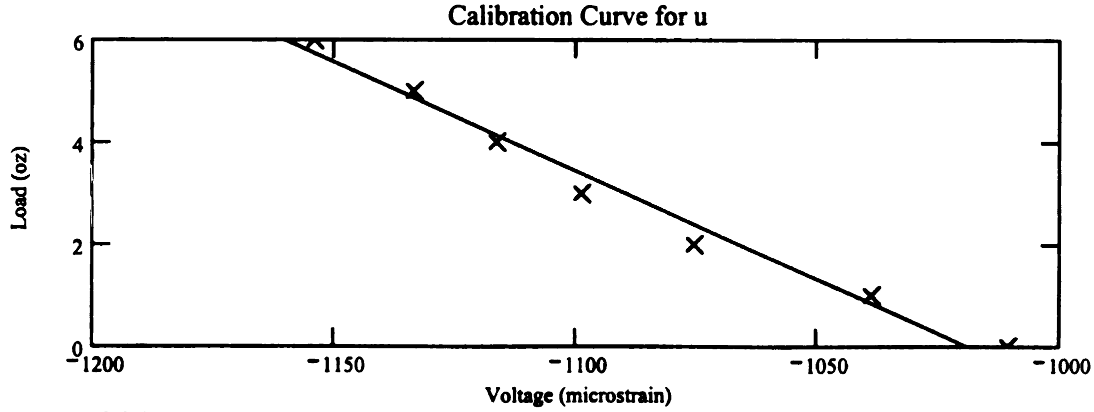

XXX u raw data
—— u fitted line

APPENDIX H--OPTIMIZATION RESULTS

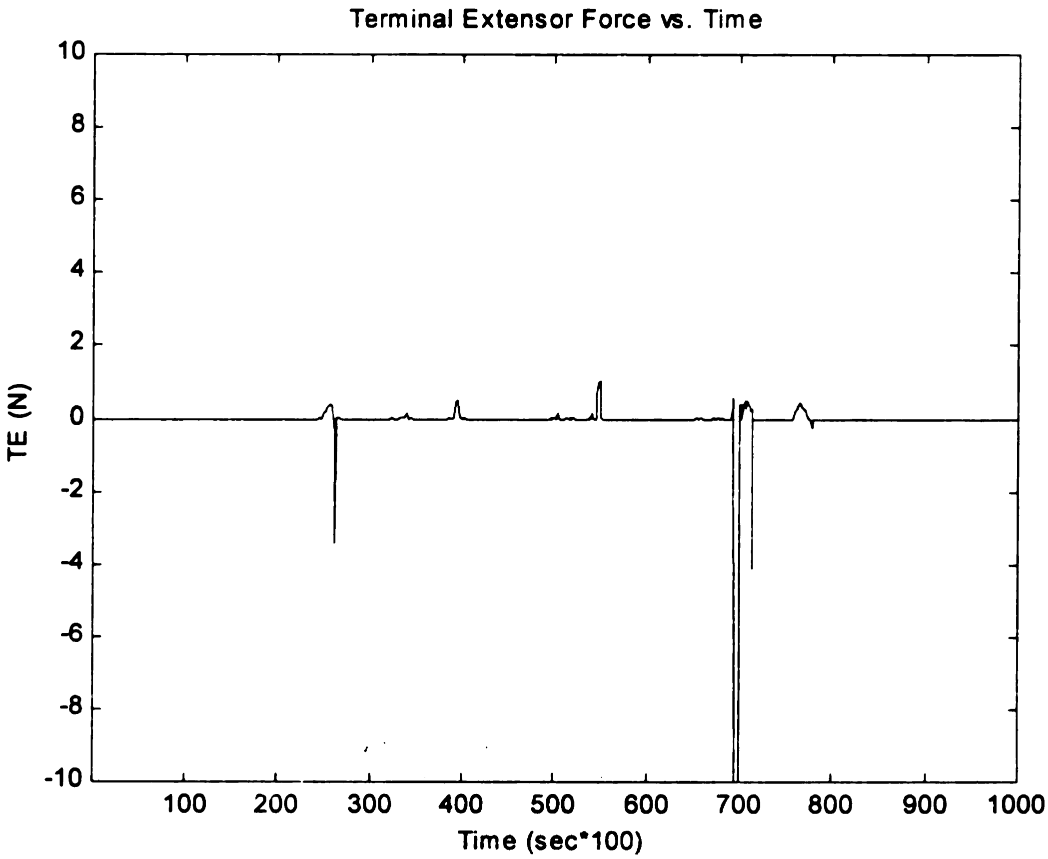

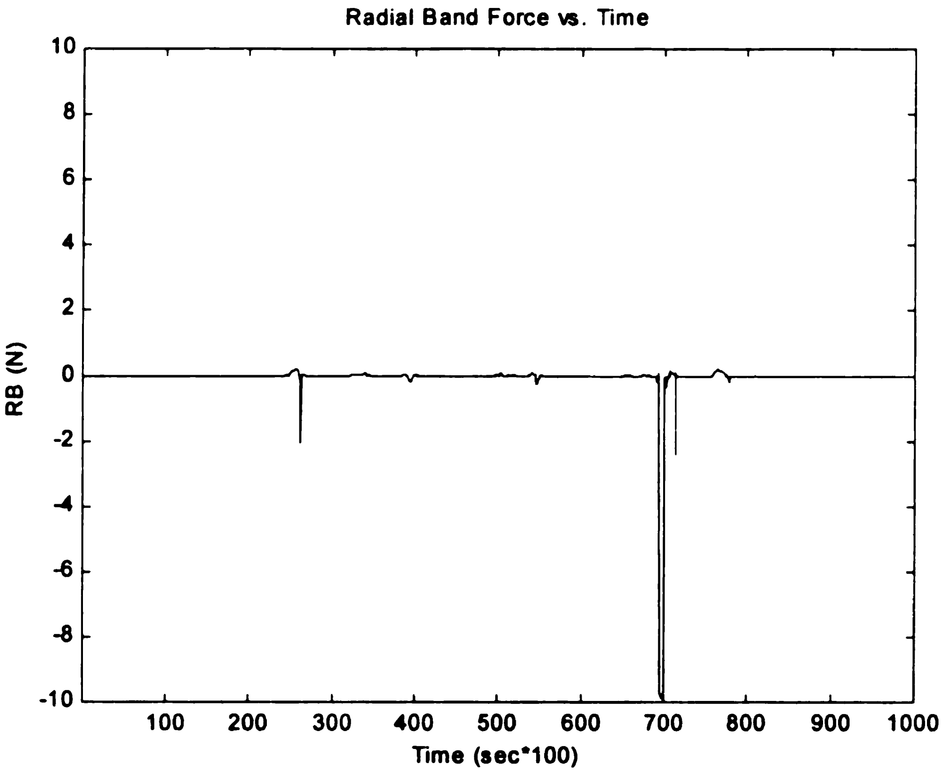

Radial Band Force vs. Time
RB (N)
10
8
6
4
2
0
-2
-4
-6
-8
-10
100
200
300
400
500
600
700
800
900
1000
Time (sec*100)

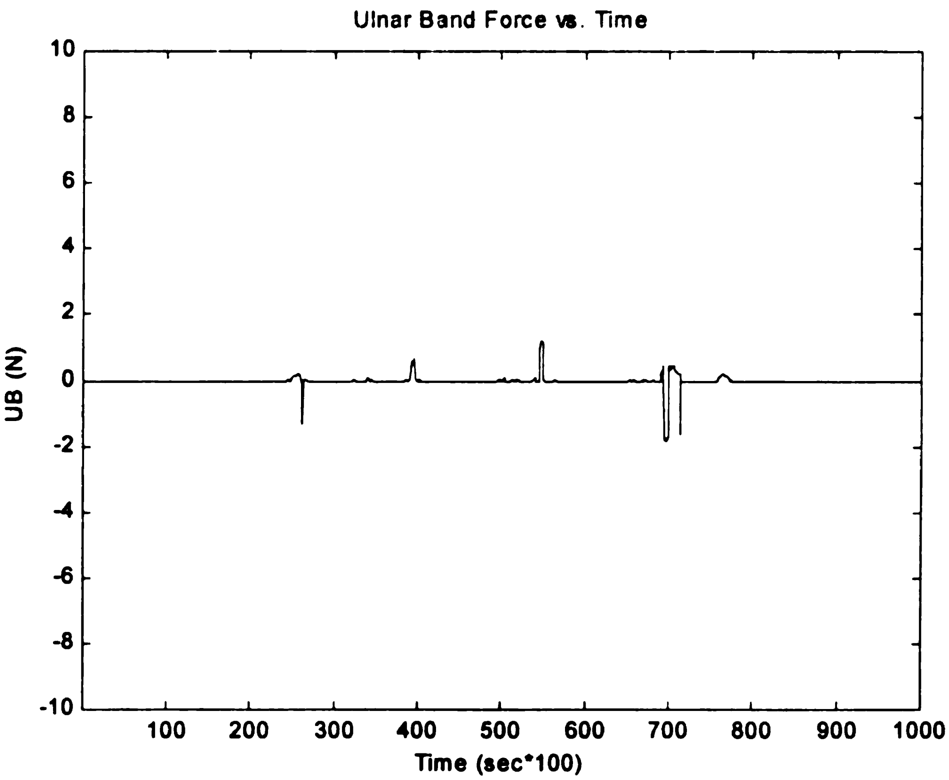

Ulnar Band Force vs. Time
UB (N)
10
8
6
4
2
0
-2
-4
-6
-8
-10
100
200
300
400
500
600
700
800
900
1000
Time (sec*100)

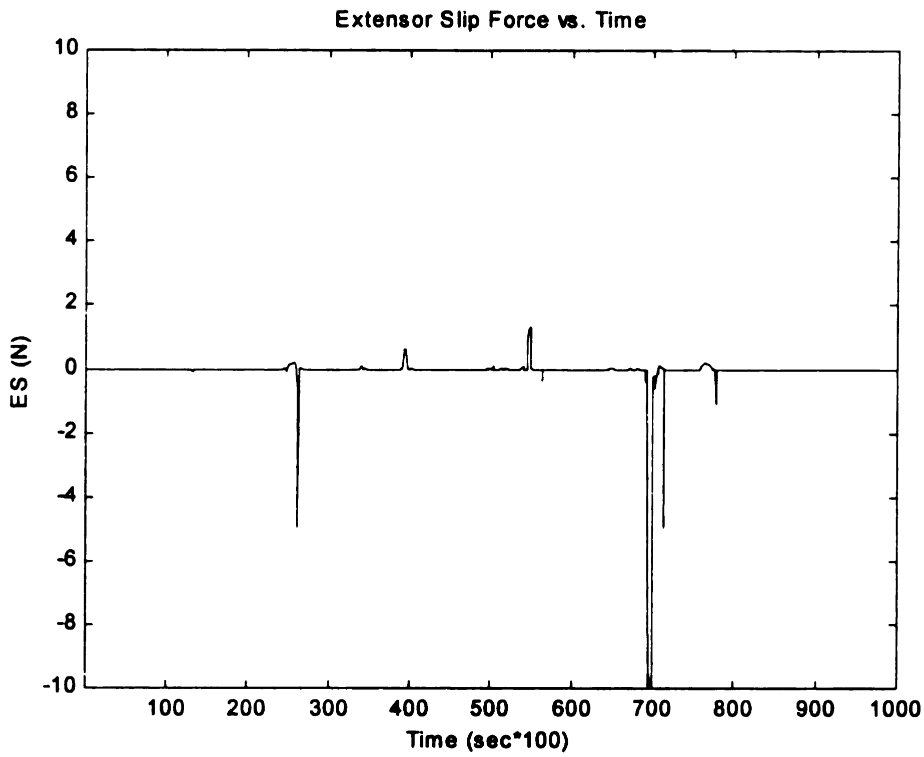
Extensor Slip Force vs. Time
ES (N)
Time (sec*100)
10
8
6
4
2
0
-2
-4
-6
-8
-10
100
200
300
400
500
600
700
800
900
1000

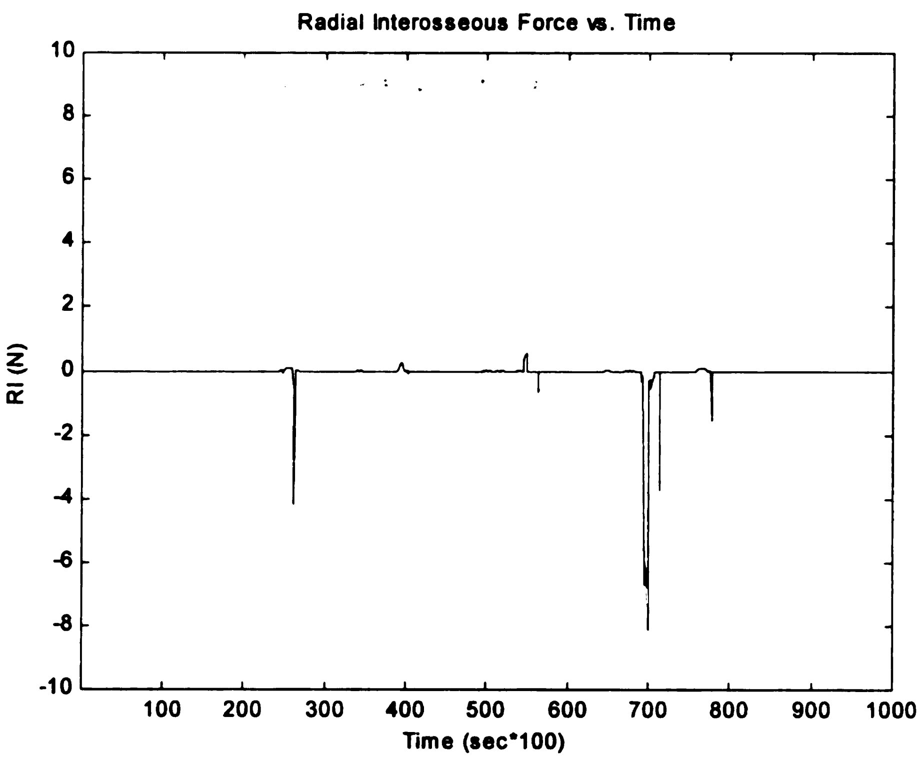
Radial Interosseous Force vs. Time
RI (N)
Time (sec*100)
10
8
6
4
2
0
-2
-4
-6
-8
-10
100
200
300
400
500
600
700
800
900
1000

Ulnar Interosseous Force vs. Time

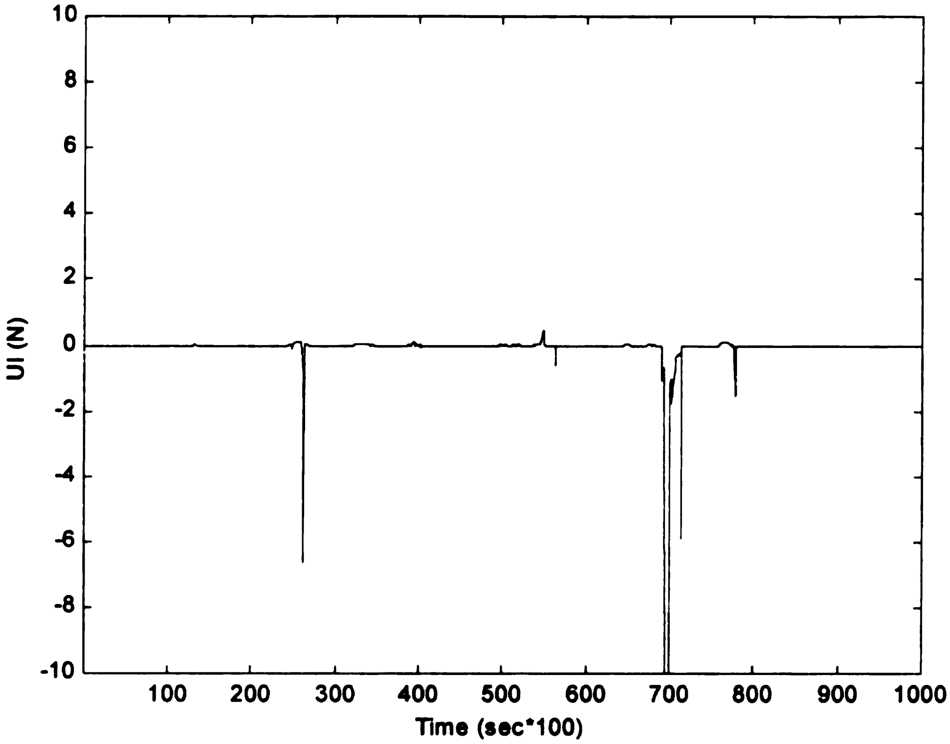

Lumbricalis Force vs. Time

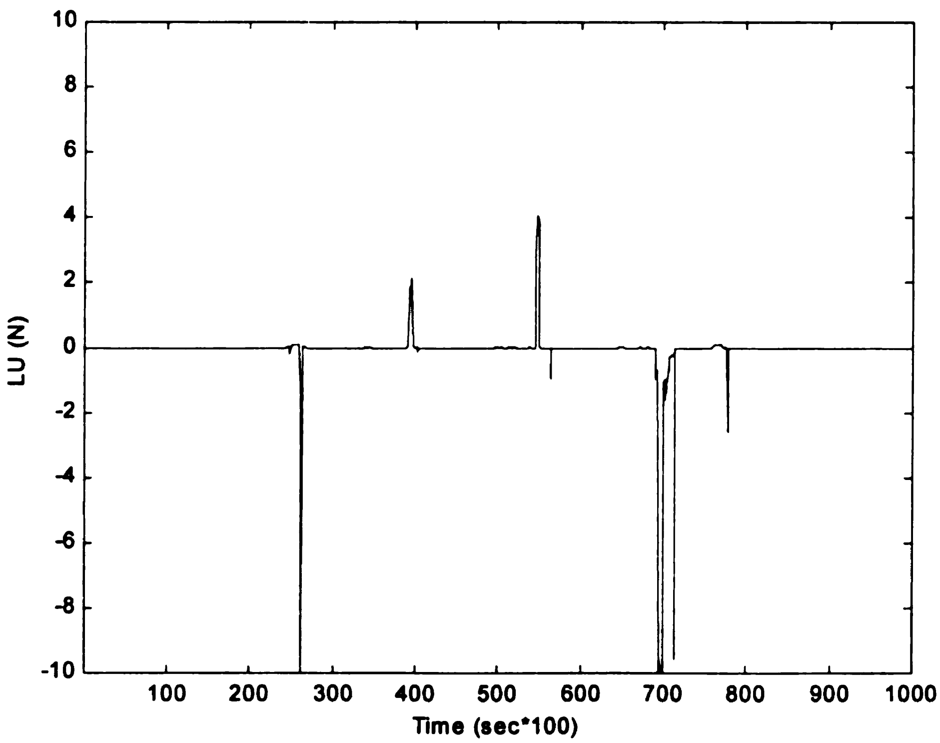

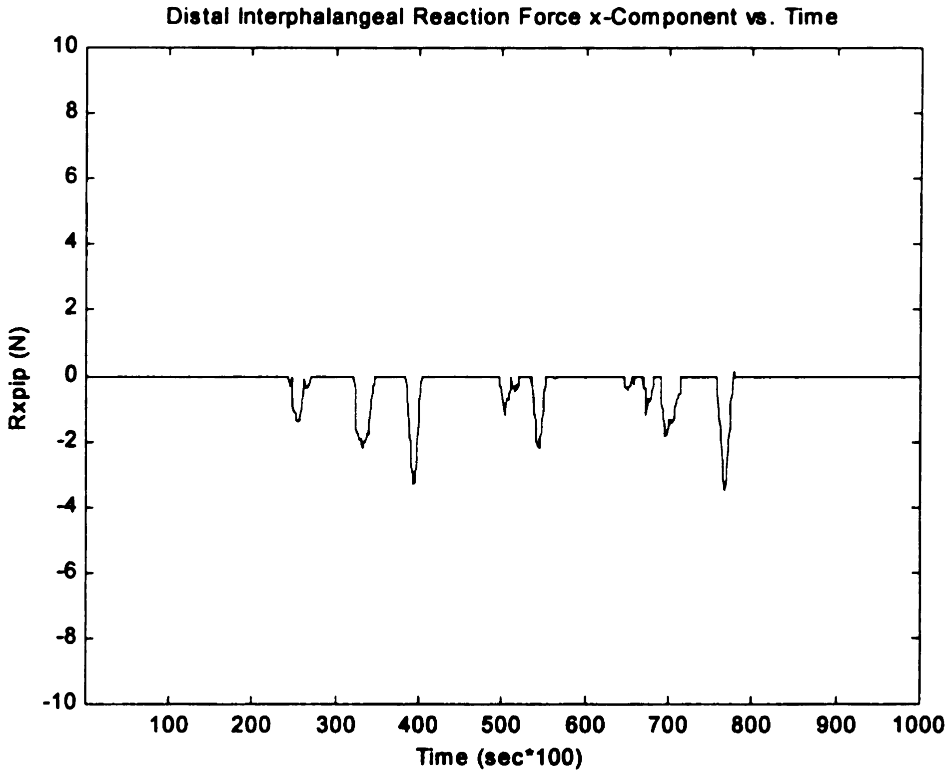

Distal Interphalangeal Reaction Force x-Component vs. Time
Rxpip (N)
10
8
6
4
2
0
-2
-4
-6
-8
-10
100
200
300
400
500
600
700
800
900
1000
Time (sec*100)

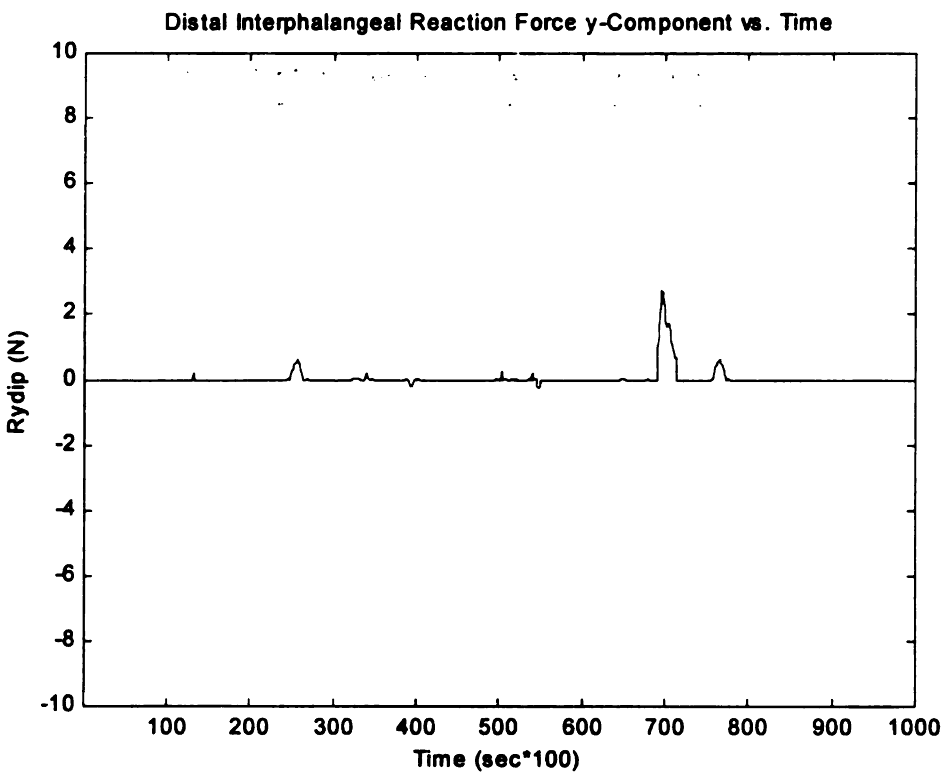

Distal Interphalangeal Reaction Force y-Component vs. Time
Rydip (N)
10
8
6
4
2
0
-2
-4
-6
-8
-10
100
200
300
400
500
600
700
800
900
1000
Time (sec*100)

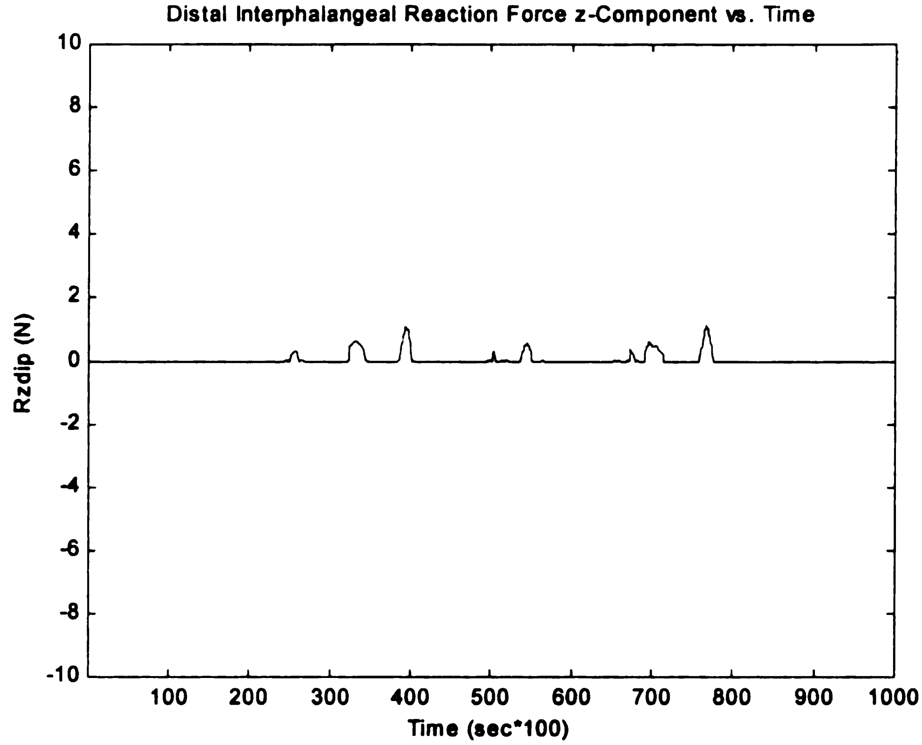

Distal Interphalangeal Reaction Force z-Component vs. Time
Rzdip (N)
10
8
6
4
2
0
-2
-4
-6
-8
-10
100
200
300
400
500
600
700
800
900
1000
Time (sec*100)

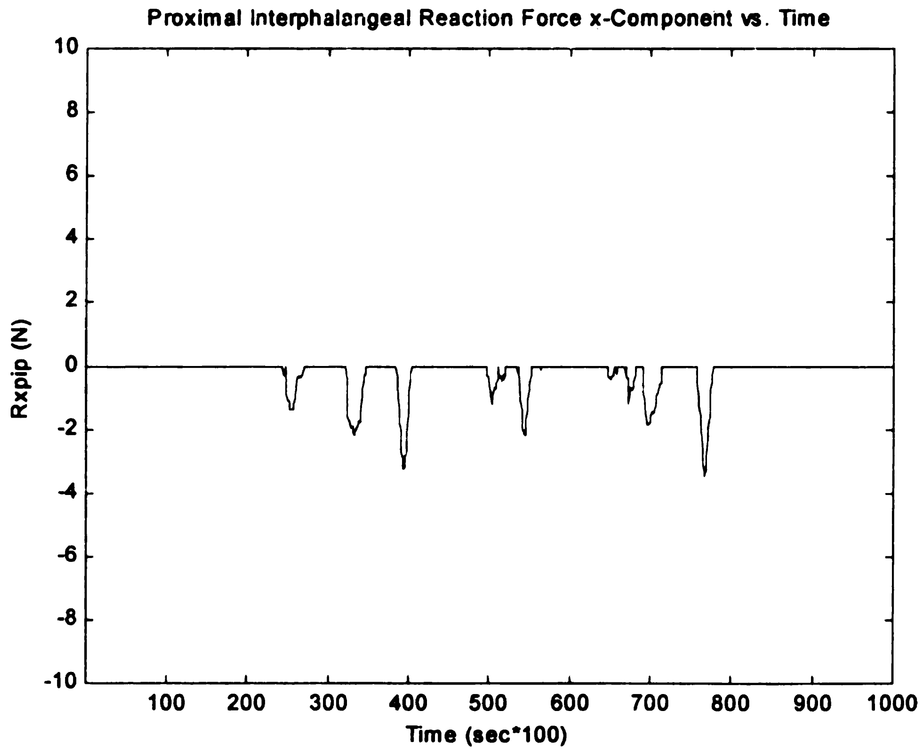

Proximal Interphalangeal Reaction Force x-Component vs. Time
Rxpip (N)
10
8
6
4
2
0
-2
-4
-6
-8
-10
100
200
300
400
500
600
700
800
900
1000
Time (sec*100)

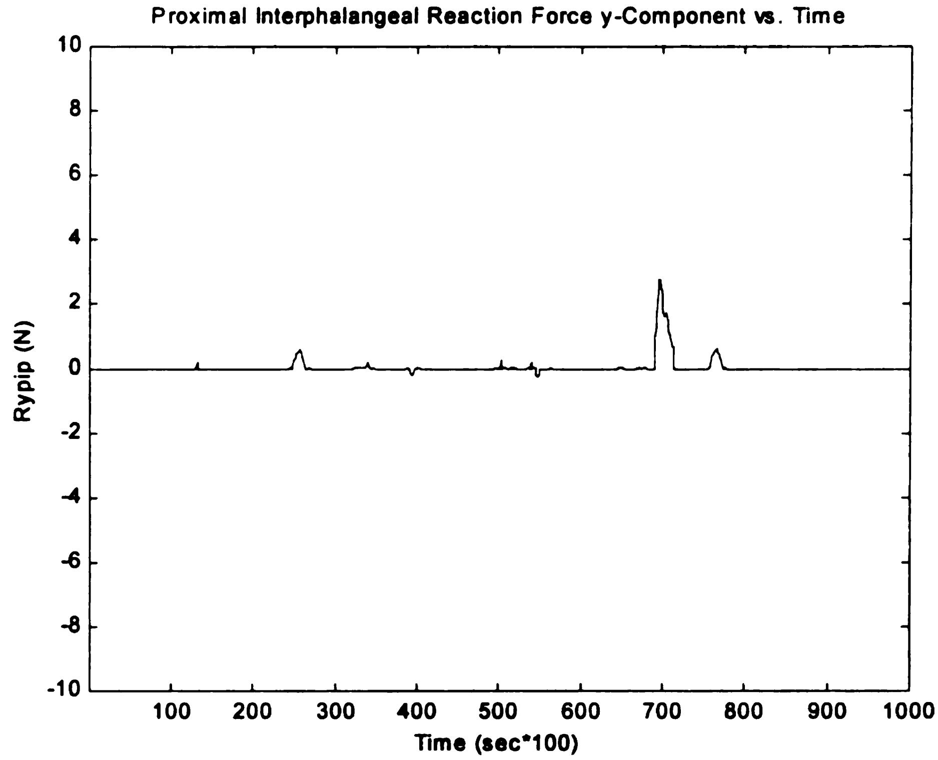
Proximal Interphalangeal Reaction Force y-Component vs. Time
10
8
6
4
2
0
-2
-4
-6
-8
-10
Rypip (N)
100 200 300 400 500 600 700 800 900 1000
Time (sec*100)

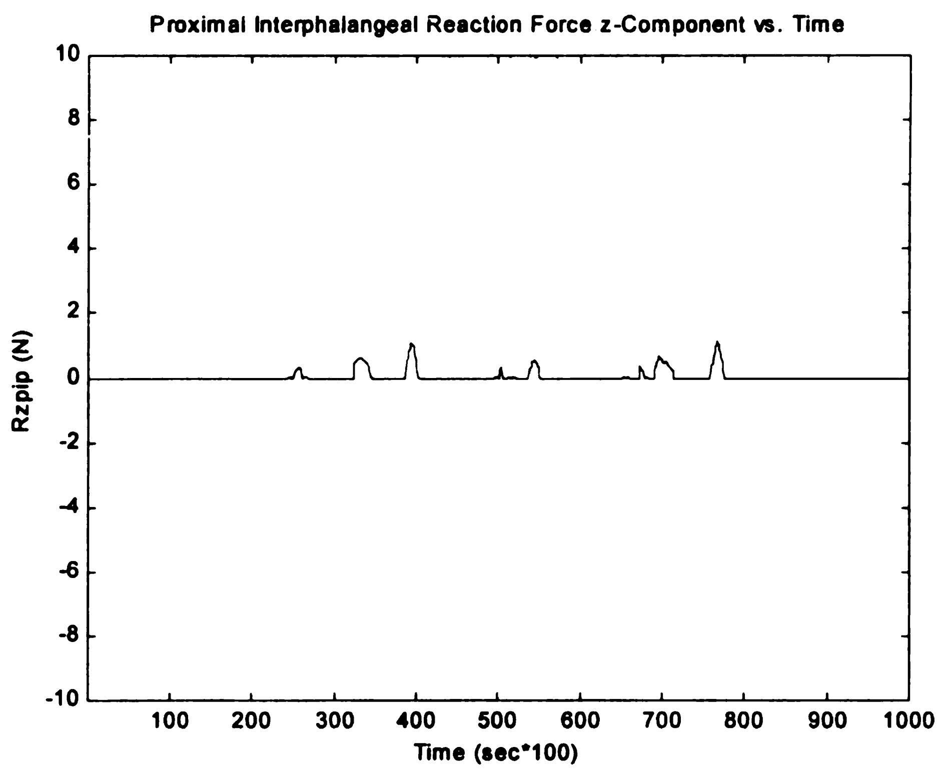
Proximal Interphalangeal Reaction Force z-Component vs. Time
10
8
6
4
2
0
-2
-4
-6
-8
-10
Rzpip (N)
100 200 300 400 500 600 700 800 900 1000
Time (sec*100)

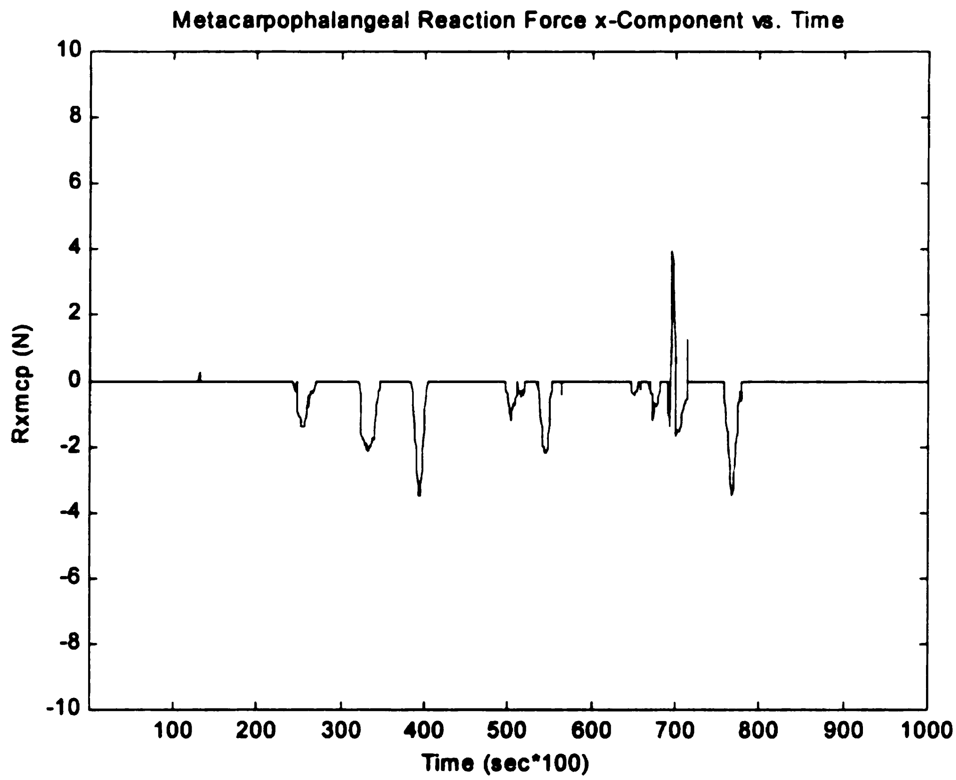
Metacarpophalangeal Reaction Force x-Component vs. Time
10
8
6
4
2
0
-2
-4
-6
-8
-10
Rxmcp (N)
100 200 300 400 500 600 700 800 900 1000
Time (sec*100)

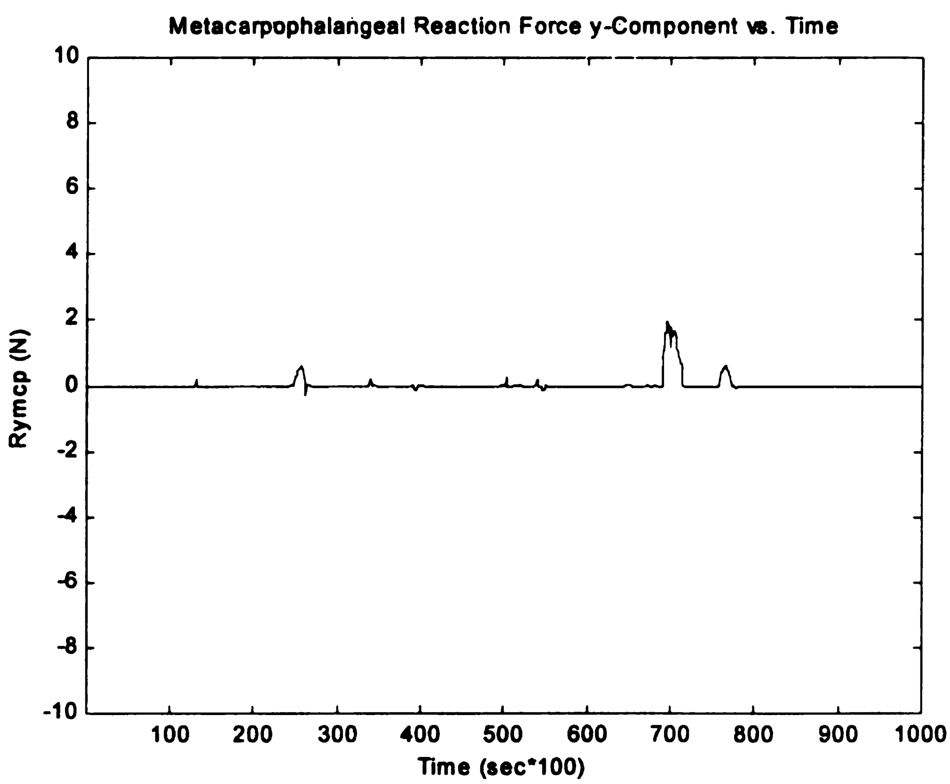
Metacarpophalangeal Reaction Force y-Component vs. Time
10
8
6
4
2
0
-2
-4
-6
-8
-10
Rymcp (N)
100 200 300 400 500 600 700 800 900 1000
Time (sec*100)

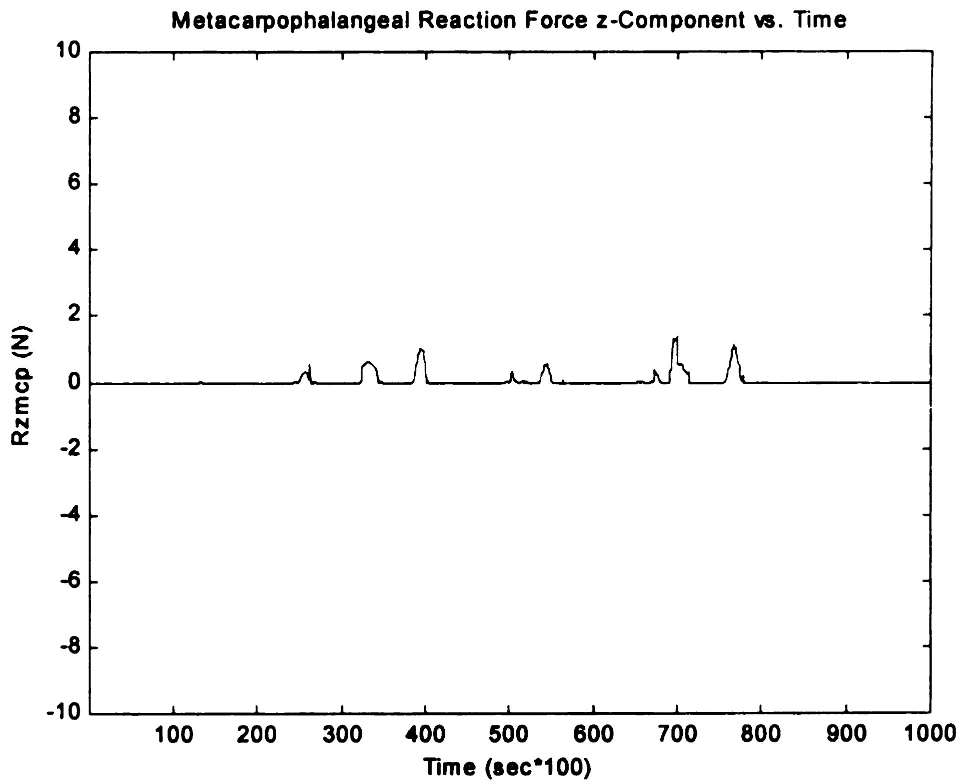
Metacarpophalangeal Reaction Force z-Component vs. Time
Rzmcp (N)
10
8
6
4
2
0
-2
-4
-6
-8
-10
100
200
300
400
500
600
700
800
900
1000
Time (sec*100)

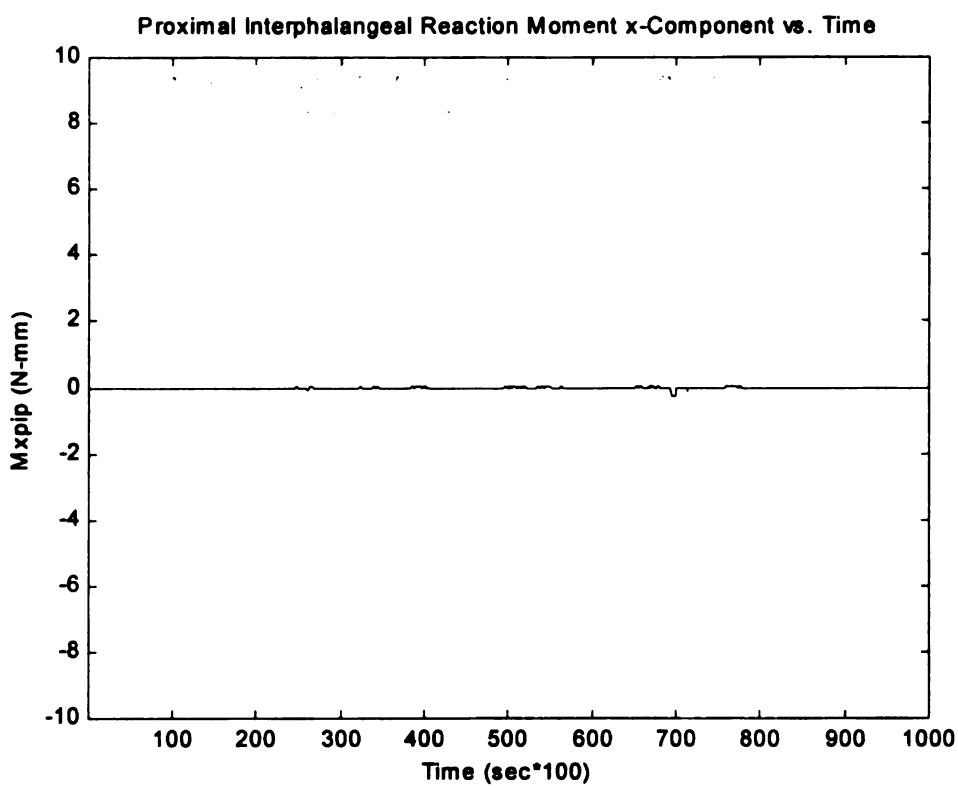
Proximal Interphalangeal Reaction Moment x-Component vs. Time
Mxpip (N-mm)
10
8
6
4
2
0
-2
-4
-6
-8
-10
100
200
300
400
500
600
700
800
900
1000
Time (sec*100)

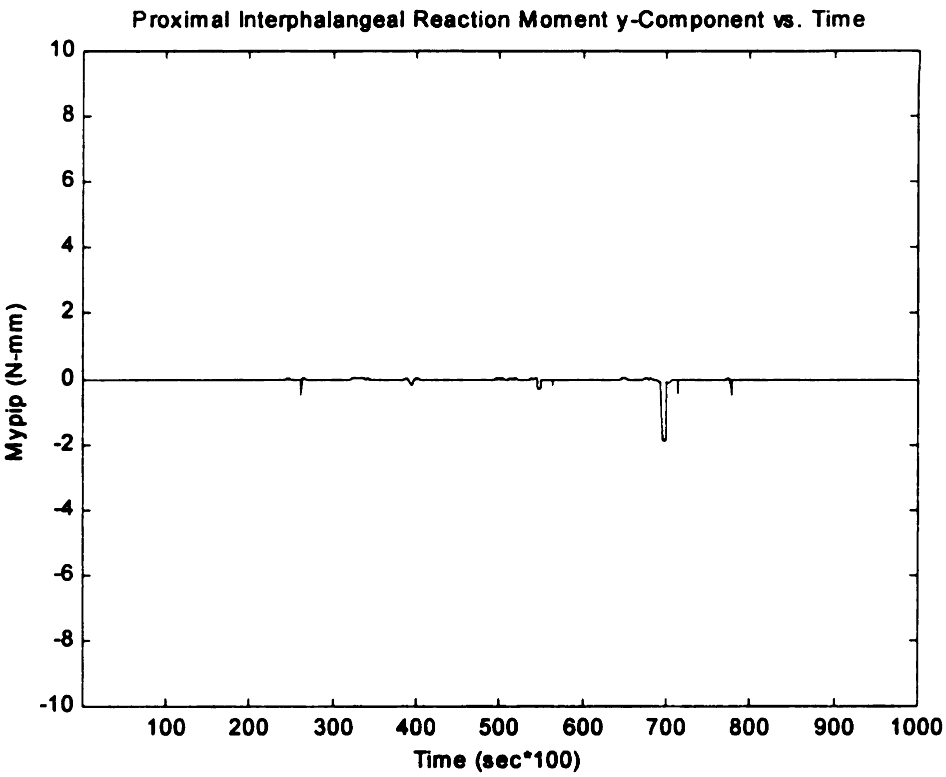
Proximal Interphalangeal Reaction Moment y-Component vs. Time
Mypip (N-mm)
10
8
6
4
2
0
-2
-4
-6
-8
-10
100
200
300
400
500
600
700
800
900
1000
Time (sec*100)

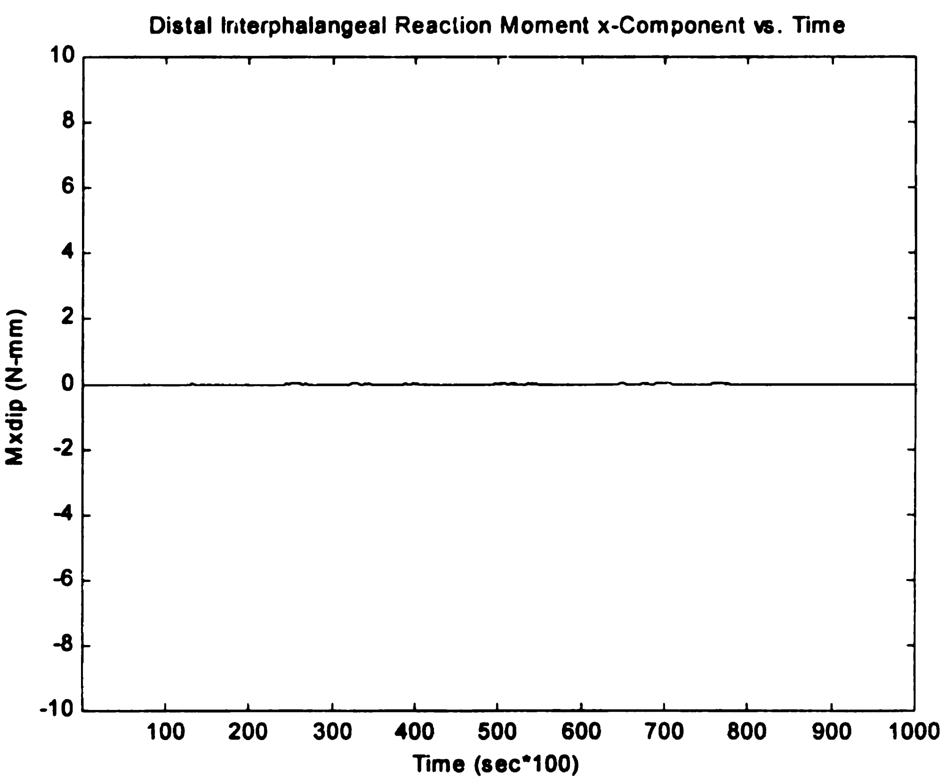
Distal Interphalangeal Reaction Moment x-Component vs. Time
Mxdip (N-mm)
10
8
6
4
2
0
-2
-4
-6
-8
-10
100
200
300
400
500
600
700
800
900
1000
Time (sec*100)

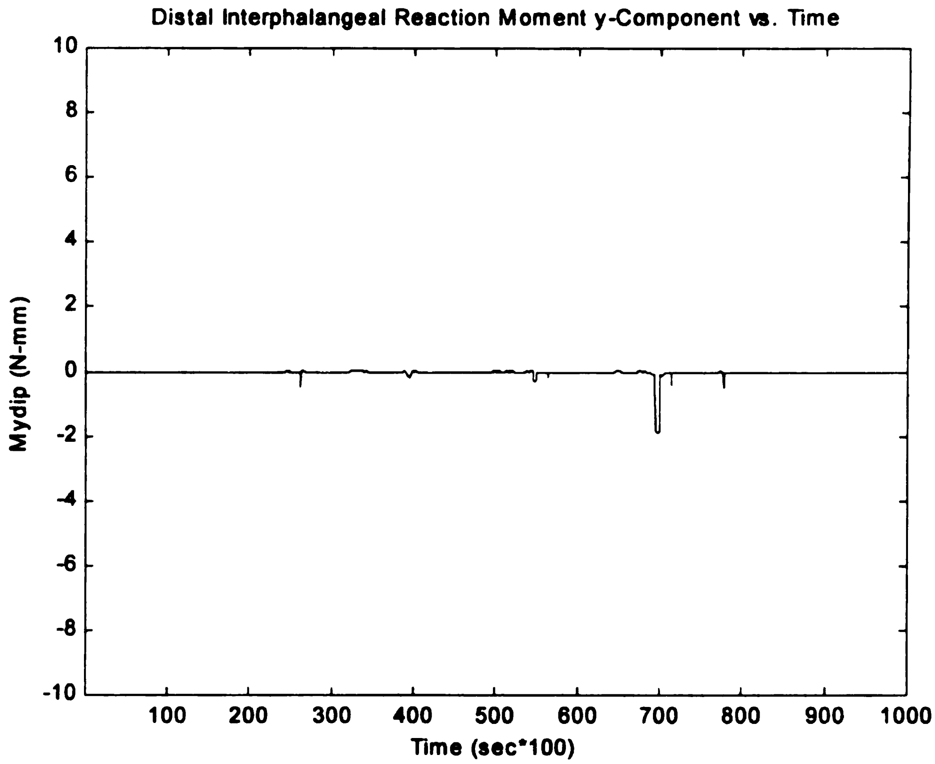
Distal Interphalangeal Reaction Moment y-Component vs. Time
10
8
6
4
2
0
-2
-4
-6
-8
-10
Mydip (N-mm)
100
200
300
400
500
600
700
800
900
1000
Time (sec*100)

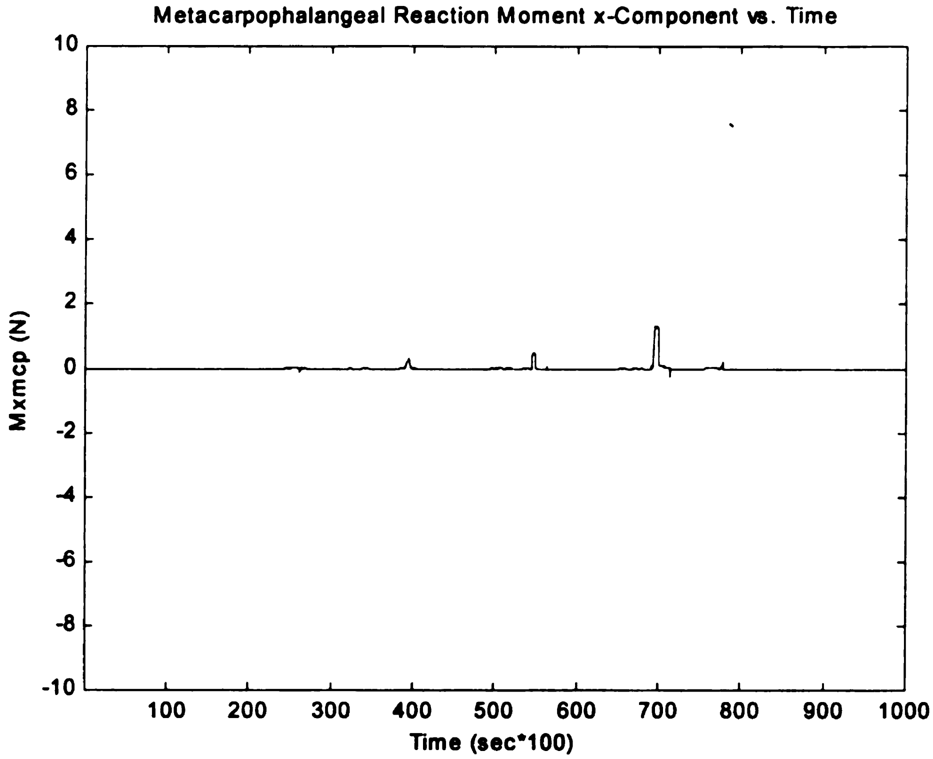

Metacarpophalangeal Reaction Moment x-Component vs. Time
Mxmcp (N)
10
8
6
4
2
0
-2
-4
-6
-8
-10
100
200
300
400
500
600
700
800
900
1000
Time (sec*100)

BIBLIOGRAPHY

Amis, A. (1987). Variation of finger forces in maximal isometric grasp tests on a range of cylinder diameters. *J. Biomed. Eng., 9*(0), 313-320.

An, K., Chao, E., Cooney, W. I., & Linscheid, R. (1979). Normative model of human hand for biomechanical analysis. *J. Biomechanics, 12*(0), 775-788.

An, K., Himeno, S., Tsumura, H., Kawai, T., & Chao, E. (1990). Pressure distribution on articular surfaces: application of joint stability evaluation. *J. Biomechanics, 23*(0), 1013-1020.

An, K., Kwak, B., Chao, E., & Morrey, B. (1984). Determination of muscle and joint forces: a new technique to solve the indeterminate problem. *J. Biomed. Eng., 106*(0), 364-367.

An, K., Ueba, Y., Chao, E., Cooney, W., & Linscheid, R. (1983). Tendon excursion and moment arm of the index finger muscles. *J. Biomechanics, 16*(0), 419-415.

An, K. N., Berglund, L., Uchiyama, S., & Coert, J. H. (1993). Measurement of friction between pulley and flexor tendon. *Biomed. Sci Instrum, 29*(0), 0.

An, K. N., Chao, E., Cooney, W. P., & Linscheid, R. L. (1985). Forces in the normal and abnormal hand. *J. Orthopedic Research, 3*(0), 202-211.

Armstrong, T. (1982). Development of a biomechanical hand model for study of manual activities. In Anthropometry and Biomechanics: Theory and Application. *?, 0*(0), 183-191.

Armstrong, T., & Chaffin, D. (1978). An investigation of the relationship between displacements of the finger and wrist joint and the extrinsic finger flexor tendon. *J. Biomechanics, 11*(0), 119-128.

Armstrong, T., & Chaffin, D. (1979). Some Biomechanical Aspects of Carpal Tunnel. *J. Biomechanics, 12*(7), 567-570.

Backhouse, K. (1968). Functional anatomy of the hand. *Physiotherapy, 54*(0), 114-117.

Backhouse, K., & Catton, W. (1954). An experimental study of the functions of the lumbrical muscles in the human hand. *J. Anat., 88*(0), 133-141.

Bay, B., Sharkey, N., & Szabo, R. (1997). Displacement and strain of the median nerve at the wrist. *Journal of Hand Surgery-American, 22*(4), 621-627.

Berme, N., Paul, J., & Purves, W. (1977). A biomechanical analysis of the metacarpophalangeal joint. *J. Biomechanics, 10*(0), 409-412.

Bigland, B., & Lippold, O. C. J. (1954). The Relation Between Force, Velocity and Integrated Electrical Activity in Human Muscle. *J.Physiol., 123*(0), 214-224.

Billi, A., Catalucci, A., Barile, A., & Masciocchi, C. (1998). Joint impingement syndrome: clinical features. *European Journal of Radiology, 27*(0), S39-S41.

Boozer, J., Sanson, M., Soutas-Little, R., Coale, E., Pierce, T., & Swanson, A. (1994). Comparison of the biomechanical motions and forces involved in high-profile versus low-profile dynamic splinting. *J. hand therapy, 7*(0), 171-182.

Brand, P. W., & Mosby, C. V. (1985). Clinical Mechanics of the Hand. *?, 0*(0), 0.

Brook, N., Mizrahi, J., Shoham, M., & Dayan, J. (1995). A biomechanical model of index finger dynamics. *Medical Engineering & Physics, 17*(1), 54-63.

Buchholz, B., & Armstrong, T. (1991). An ellipsoidal representation of human hand anthropometry. *Human Factors, 33*(4), 429-441.

Buchholz, B., & Armstrong, T. (1992). A kinematic model of the human hand to evaluate its prehensile capabilities. *J. Biomechanics, 25*(2), 149-162.

Buchner, H., Hines, M., & Hemami, H. (1985). A Mechanism for Touch Control of a Sagittal 5-linkFinger Hand. *IEEE Transactions on Systems Man and Cybernetics, 15*(1), 69-77.

Buchner, H., Hines, M., & Hooshang, H. (1988). A dynamic model for finger interphalangeal coordination. *J. Biomechanics, 21*(6), 459-468.

Buford, W., Meyers, L., & Hollister, A. (1990). Modeling and simulation system for the human hand. *J. Clinical Engineering, 15*(0), 445-451.

Burke, H. T., P. (1973). Anatomy and innervation ratios in motor units to cat gastrocnemius. *J. Physiol., 234*, 749-765.

Chao, E. (1980). Justification of the triaxial goniometer in the measurement of joint rotation. *J. Biomechanics, 13*(0), 989-1006.

Chao, E., An, KN, Cooney, WP, Linscheid, RL. (1989). *Biomechanics of the Hand--A Basic Research Study* (First ed.). Teaneck, NJ: World Scientific Publishing Co., Inc.

Chao, E., & An, K. (1978a). Graphical interpretation of the solution to the redundant problem in biomechanics. *J. Biomech. Eng., 100*(0), 159-167.

Chao, E., Opgrande, J., & Axmear, F. (1976). Three-dimensional force analysis of finger joints in selected isometric hand functions. *J. Biomechanics, 9*(0), 387-396.

Chao, E. Y., & An, K. N. (1978b). Determination of Internal Forces in Human Hand. *J. Eng. Mech., Div. ASCE, 104*(0), 255-272.

Chevallier, D., & Payandeh, S. (1998). On computation of grasping forces in dynamic manipulation using a three-fingered grasp. *Mechanism and Machine Theory, 33*(3), 225-244.

Close, J., & Kidd, C. (1969). The functions of the muscles of the thumb, the index and long fingers. *J. Bone Joint Surg., 51*(0), 1601-1620.

Cobb, T., An, K., Cooney, W., & Berger, R. (1994). Lumbrical muscle incursion into the carpal-tunnel during finger flexion. *Journal of Hand Surgery-British and European, 19*(4), 434-438.

Cobb, T., Cooney, W., & An, K. (1996). Aetiology of work-related carpal tunnel syndrome: The role of lumbrical muscles and tool size on carpal tunnel pressures. *Ergonomics, 39*(1), 103-107.

Cooney, W., An, K., Daube, J., & Askew, I. (1985). Electromyographic analysis of the thumb: a study of isometric forces in pinch and grasp. *J. Hand Surgery, 10*(0), 202-210.

Cooney, W. I., & Chao, E. (1977). Biomechanical analysis of static forces in the thumb during hand functions. *J. Bone Joint Surg., 59*(0), 27-36.

Crowninshield, R., & Brand, R. (1981). A physiologically based criterion of muscle force prediction in locomotion. *J. Biomechanics, 14*(11), 793-801.

Dennerlein, J., Diao, E., Mote, C., & Rempel, D. (1998). Tensions of the flexor digitorum superficialis are higher than a current model predicts. *J. Biomechanics, 31*(4), 295-301.

Duque, J., Masset, D., & Malchaire, J. (1995). Evaluation of handgrip force from EMG measurements. *Applied Ergonomics, 26*(1), 61-66.

Eaton, R., & Little, J. (1969). A study of the basal joint of the thumb. *J. Bone Joint Surg., 51*(0), 661-668.

Esteki, A., & Mansour, J. M. (1997). A dynamic model of the hand with application in functional neuromuscular stimulation. *Annals of Biomedical Engineering, 25*(3), 440-451.

Eyler, D., & Markee, J. (1954). The anatomy and function of the intrinsic musculature of the fingers. *J. Bone Joint Surg., 36*(0), 36169.

Fischer, G. (1969). *A treatise on the topographic anatomy of the long finger and a biomechanical investigation on its inter-joint movement.* Unpublished Ph.D. Dissertation, University of Iowa, Iowa City, IA.

Giurintano, D., Hollister, A., Buford, W., Thompson, D., & Myers, L. (1995). Virtual five-link model of the thumb. *Medical Engineering & Physics, 17*(4), 297-303.

Greenwald, D., Shumway, S., Allan, C., & Mass, D. (1994). Dynamic analysis of profundus tendon function. *Journal of Hand Surgery-American, 19*(4), 626-635.

Grosse-Lordemann, H. a. M., E.A. (1937). Der einfluss der leistung und der arbeitsgeschwindigkeit auf das arbe its maximum und den wirkungsgrad beim radfahren. *Arbeitsphysiologie, 9*, 454-475.

Harris, C., & Rutledge, A. (1972). The functional anatomy of the extensor mechanism of finger. *J. Bone Joint Surg., 57*(0), 713-726.

Hazelton, F., Smidt, G., Flatt, A., & Stephens, R. (1975). The influence of wrist position on the force produced by the finger flexors. *J. Biomechanics, 8*(0), 301-306.

Hirsch, D., Page, D., Miller, D., Dumbleton, J., & Miller, E. (1974). A biomechanical analysis of the metacarpophalangeal joint of the thumb. *J. Biomechanics, 7*(0), 343-348.

Kaplan, E. (1965). *Functional and Surgical Anatomy of the Hand* (Vol. 0).

Kaplan, E. (1966). The participation of the metacarpo-phalangeal joint of the thumb in the act of opposition. *Bull. Hosp. Joint Dis., 27*(0), 39-45.

Keir, P., Bach, J., & Rempel, D. (1998a). Effects of finger posture on carpal tunnel pressure during wrist motion. *Journal of Hand Surgery-American, 23*(6), 1004-1009.

Keir, P., Bach, J., & Rempel, D. (1998b). Fingertip loading and carpal tunnel pressure: Differences between a pinching and a pressing task. *Journal of Orthopaedic Research, 16*(1), 112-115.

Kerr, D., Griffis, M., Sanger, D., & Duffy, J. (1992). Redundand grasps, redundant manipulators, and their dual relationships. *Journal of Robotic Systems, 9*(7), 973-1000.

Landsmeer, J. (1949). The anatomy of the dorsal aponeurosis of the human finger and its functional significance. *Anat. Rec., 104*(0), 31.

Landsmeer, J. (1955). Anatomical and functional investigations on the articulation of human fingers. *Acta Anat. Suppl., 24*(0), 25204.

Landsmeer, J. (1961). Study in the anatomy of articulation. The equilibrium of the 'intercalated' bone. *Acta Morph. Neerl.-Scand., 3*(0), 287-303.

Landsmeer, J. (1962). Power grip and precision handling. *Ann. Rheum. Diss, 22*(0), 164-170.

Landsmeer, J. (1976). Atlas of Anatomy of the Hand., 349.

Leijnse, J. (1996). A graphic analysis of the biomechanics of the massless proximal biarticular chain of the human finger. *J. Biomechanics, 29*(0), 355-366.

Leijnse, J. (1997a). The controllability of the unloaded human finger with superficial or deep flexor. *J. Biomechanics, 30*(11), 1087-1093.

Leijnse, J. (1997b). Measuring force transfers in the deep flexors of the musician's hand: theoretical analysis, clinical examples. *J. Biomechanics, 30*(9), 873-882.

Leijnse, J. (1997c). Why the lumbrical muscle should not be bigger--a force model of the lumbrical in the human finger. *J. Biomechanics, 30*(11), 1107-1114.

Leijnse, J., Bonte, J., Landsmeer, J., Kalker, J., van der Meulen, J., & Snijders, C. (1992). Biomechanics of the finger with anatomical restrictions--the significance for the exercising hand of the musician. *J. Biomechanics, 25*(25), 1253-1264.

Leijnse, J., & Kalker, J. (1995). A two dimensional kinematic model of the lumbrical in the human finger. *J. Biomechanics, 28*(0), 237-249.

Leijnse, J., Snijders, C., Bonte, J., Landsmeer, J., Kalker, J., & VanDerMeulen, J. (1993). The hand of the musician: The kinematics of the bidigital finger system with anatomical restrictions. *J. Biomechanics, 26*(10), 1169-1179.

Lin, G., Amadio, P., An, K., & Cooney, W. I. (1989). Functional anatomy of the human digital flexor pulley system. *J. Hand Surgery, 14*(0), 949-956.

Linn, F. (1968). Lubrication of animal joints. *Journal of Biomechanics, 1*, 193-205.

Mathews, J. H. (1987). *Numerical Methods for Computer Science, Engineering, and Mathematics* (1 ed.). Englewood Cliffs, New Jersey: Prentice-Hall, Inc.

Micks, J., Reswick, J., & Hoger, D. (1978). The mechanism of the intrinsic-minus finger: A biomechanical study. *J. Hand Surgery, 3*(0), 333-341.

Miller, S., & Freivalds, A. (1995). A stress-strength interface model for predicting CTD probabilities. *Internal Journal of Industrial Ergonomics, 15*(6), 447-457.

Moore, A., Wells, R., & Ranney, D. (1991). Qquantifying exposure in occupational manual tasks with cumulative disorder potential. *Ergonomics, 34*(12), 1433-1453.

Nakamichi, K., & Tachibana, S. (1995). Restricted motion of the median nerve in carpal-tunnel syndrome. *Journal of Hand Surgery-British and European, 20*(4), 460-464.

Novak, C., & Mackinnon, S. (1998). Nerve injury in repetitive motion disorders. *Clinical Orthopaedics and Related Research, 351*(0), 10-20.

Nubar, Y., & Contini, R. (1961). A minimal principal in biomechanics. *Bull. Math. Biophys., 23*(0), 377-391.

Pedotti, A., Krishnan, V., & Stark, L. (1978). Optimization of muscle-force sequencing in human locomotion. *Math. Biosci., 38*(0), 57-76.

Penrod, D., Davy, D., & Singh, D. (1974). An optimization approach to tendon force analysis. *J. Biomechanics, 7*(0), 123-129.

Rash, G. S., Belliappa, P. P., Wachowiak, M. P., Somia, N. N., & Gupta, A. (1999). A demonstration of the validity of a 3-D video motion analysis method for measuring finger flexion and extension. *Journal of Biomechanics, 32*(12), 1337-1341.

Rempel, D., Dennerlein, J., Mote, C., & Armstrong, T. (1994). A method of measuring fingertip loading during keyboard use. *Journal of Biomechanics, 27*(8), 1101-1104.

Seirig, A., & Arvikar, R. (1989). *Biomechanical Analysis of the Muskuloskeletal Structure for Medicine and Sports* (Vol. 1). Philadelphia: Hemisphere Publishing Corporation.

Seradge, H., Jia, Y., & Owens, W. (1995). In-vivo measurement of carpal-tunnel pressure in the functioning hand. *Journal of Hand Surgery-American, 20*(5), 855-859.

Shewsbury, M. M., & Kuczynski, K. (1974). Flexor Digitorum Superficialis Tendon in the Fingers of the Human Hand. *The Hand, 6*(0), 121-133.

Shih, J., Ju, S., Rowlands, R., An, K., & Chao, E. (1993). Analysis of frictional joint contact. *BED, 26*(0), 51-54.

Siemienski, A. (1992). Soft saturation, an idea for load sharing between muscles. Application to the study of human locomotion. In A. M. Cappozzo, M.; Tosi, V. (Ed.), *Biolocomotion: A Centruy of Research Using Moving Prictures* (pp. 293-303). Rome: Promograph.

Small, C., Bryant, J., & Pichora, D. (1992). Rationalization of kinematic descriptors for three-dimensional hand and finger motion. *J. Biomed. Eng., 14*(0), 133-141.

Smutz, P., Serina, E., & Rempel, D. (1994a). A system for evaluating the effect of keyboard design on force, posture, comfort and productivity. *Ergonomics, 37*(10), 1649-1660.

Smutz, W., Miller, S., Eaton, C., Bloswick, D., & France, E. (1994b). Investigation of low-force high frequency activities on the development of carpal-tunnel syndrome. *Clinical Biomechanics, 9*(1), 15-20.

Sommerich, C., Marras, W., & Parnianpour, M. (1998). A method for developing biomechanical profiles of hand-intensive tasks. *Clinical Biomechanics, 13*(4), 261-271.

Spence, A. P. (1990). *Basic Human Anatomy* (Third ed.). Don Mills, Ontario: The Benjamin/Cummings Publishing Company, Inc.

Spoor, C. (1983). Balancing a force on the fingertip of a two dimensional finger model without intrinsic muscles. *J. Biomechanics, 16*(0), 497-504.

Spoor, C., & Landsmeer, J. (1976). Analysis of the zigzag movement of the human finger under influence of the extensor digitorum tendon and the deep flexor tendon. *J. Biomechanics, 9*(0), 561-566.

Srinivasan, H. (1976). Patterns of movement of totally intrinsic-minus fingers. *J. Bone Joint Surg., 58*(0), 777-785.

Stack, H. (1962). Muscle function in the finger. *J. Bone Joint Surg., 44*(0), 899.

Tamai, K., Ryu, J., An, K., Linscheid, R., Cooney, W., & Chao, E. (1988). Three-dimensional geometric analysis of the metacarpophalangeal joint. *J. Hand Surgery, 13*(0), 521-529.

Taylor, C., & Schwarz, R. (1955). The anatomy and mechanics of the human hand. *Artif. Limbs, 2*(0), 22-35.

Thomas, D., Long, C., & Landsmeer, J. (1968). Biomechanical considerations of lumbricalis behaviour in the human finger. *J. Biomechanics, 1*(0), 107-115.

Thompson, D., & Giurintano, D. (1989). A kinematic model of the flexor tendons of the hand. *J. Biomechanics, 22*(4), 327-334.

Toft, R., & Berme, N. (1980). A biomechanical analysis of the joints of the thumb. *J. Biomechanics, 13*(0), 353-360.

Tsirakos, D., Baltzopoulos, V., & Bartlett, R. (1997). Inverse optimization: Functional and physiological considerations related to the force-sharing problem. *Critical Reviews in Biomedical Engineering, 25*(4), 371-407.

Tully, E. (1995). The wrist and hand, 1: anatomy and biomechanics. *Sports Physiotherapy, 14*(0), 437-450.

Uchiyama, S., Coert, J., Berglund, L., Amadio, P., & An, K. (1995). Method for the measurement of friction between tendon and pulley. *J. Orthopedic Research, 13*(1), 83-89.

Werner, R., Armstrong, T., Bir, C., & Ayland, M. (1997a). Intracarpal canal pressures: the role of finger, hand, wrist and forearm position. *Clinical Biomechanics, 12*(1), 44-51.

Werner, R., Armstrong, T. J., Bir, C., & Aylard, M. K. (1997b). Intracarpal Canal Pressures: The Role of Finger, Hand, Wrist and Forearm Position. *Clinical Biomechanics, 12*(1), 44-51.

Winter, D. A. (1987). *The Biomechanics and Motor Control of Human Gait.* Waterloo, Ont.: University of Waterloo Press.

Zissimos, A., Szabo, R., Yinger, K., & Sharkey, N. (1994). Biomechanics of the tumb flexor pulley system. *Journal of Hand Surgery-American, 19*(3), 475-479.